

POZNAŃ UNIVERSITY OF TECHNOLOGY  
FACULTY OF COMPUTING AND TELECOMMUNICATIONS  
INSTITUTE OF MULTIMEDIA TELECOMMUNICATIONS

Doctoral dissertation

**PREDICTION TECHNIQUES  
FOR COMPRESSION OF MULTIVIEW VIDEO  
ACQUIRED USING SYSTEMS  
WITH VARIOUS CAMERA ARRANGEMENTS**

Jarosław Samelak

Supervisor: prof. dr hab. inż. Marek Domański

Auxiliary supervisor: dr inż. Damian Karwowski

Poznań 2023



POLITECHNIKA POZNAŃSKA

WYDZIAŁ INFORMATYKI I TELEKOMUNIKACJI

INSTYTUT TELEKOMUNIKACJI MULTIMEDIALNEJ

Rozprawa doktorska

**TECHNIKI PREDYKCJI  
DLA KOMPRESJI WIZJI WIELOWIDOKOWEJ  
REJESTROWANEJ ZA POMOCĄ SYSTEMÓW  
O RÓŻNYM ROZMIESZCZENIU KAMER**

Jarosław Samelak

Promotor: prof. dr hab. inż. Marek Domański

Promotor pomocniczy: dr inż. Damian Karwowski

Poznań 2023



# TABLE OF CONTENTS

|   |    |
|---|----|
| Table of contents .....   | 5  |
| Abstract .....  | 9  |
| Streszczenie.....   | 11 |
| List of symbols and abbreviations.....  | 13 |
| 1. Introduction .....   | 17 |
| 1.1. Scope of the dissertation.....   | 17 |
| 1.2. Goals and theses of the dissertation.....  | 20 |
| 1.3. Overview of the dissertation .....   | 21 |
| 2. Selected topics in the state-of-the-art of video coding .....  | 23 |
| 2.1. Introduction.....  | 23 |
| 2.2. Multiview and 3D-video coding .....  | 23 |
| 2.3. Screen Content Coding.....   | 25 |
| 2.4. Immersive Video Coding.....  | 27 |
| 3. Methodology of the experiments .....   | 31 |
| 3.1. Introduction.....  | 31 |
| 3.2. Video codec test models .....  | 31 |
| 3.3. Methodology of compression efficiency assessment.....  | 32 |
| 3.4. Test sequences.....  | 34 |
| 4. Adapting 3D-HEVC to camera arrangements other than linear.....   | 41 |
| 4.1. Introduction.....  | 41 |
| 4.2. 3D-HEVC adapted to any camera arrangement (ANY-HEVC) .....   | 43 |
| 4.2.1. Inter-view prediction for any camera arrangement .....   | 43 |
| 4.2.2. Modified Disparity Compensated Prediction.....   | 44 |
| 4.2.3. Modified inter-view prediction tools .....   | 45 |
| 4.2.4. Modified bitstream syntax .....  | 46 |
| 4.3. Evaluation of ANY-HEVC codec in compression of multiview video acquired by various camera arrangements ..... | 47 |

|   |    |
|---|----|
| 4.4. Circular rectification .....   | 51 |
| 4.4.1. Introduction .....   | 51 |
| 4.4.2. Derivation of new camera positions.....  | 53 |
| 4.4.3. Camera rotation in the ideally circular arrangement.....                         | 55 |
| 4.4.4. Modification of the intrinsic camera parameters .....                            | 56 |
| 4.4.5. Rectification of video and depth .....   | 58 |
| 4.5. 3D-HEVC adapted to rectified circular camera arrangement (ARC-HEVC) .....          | 59 |
| 4.5.1. Inter-view prediction for rectified circular camera arrangement.....             | 59 |
| 4.5.2. Modified Disparity Compensated Prediction.....                                   | 62 |
| 4.5.3. Modified inter-view prediction tools .....                                       | 62 |
| 4.5.4. Modified bitstream syntax.....   | 63 |
| 4.6. Evaluation of the proposed ARC-HEVC .....  | 65 |
| 4.6.1. Introduction .....   | 65 |
| 4.6.2. Experimental results.....  | 66 |
| 4.6.3. Conclusions .....  | 68 |
| 5. Inter-view prediction with Screen Content Coding .....                               | 71 |
| 5.1. Introduction.....  | 71 |
| 5.2. Screen Content Coding in multiview coding.....                                     | 71 |
| 5.3. The choice of view alignment for frame-compatible multiview video compression..... | 73 |
| 5.4. The choice of SCC configuration for frame-compatible multiview video compression   | 74 |
| 5.5. Screen Content Coding in stereoscopic video coding.....                            | 76 |
| 5.6. Screen Content Coding in immersive video compression.....                          | 77 |
| 5.7. Evaluation of the proposal .....   | 78 |
| 5.7.1. Goals of the experiments .....   | 78 |
| 5.7.2. Evaluation of SCC in stereoscopic video coding.....                              | 79 |
| 5.7.3. Evaluation of SCC in multiview video coding.....                                 | 81 |
| 5.7.4. Evaluation of SCC in immersive video coding.....                                 | 83 |
| 5.8. Conclusions .....  | 89 |

|  |     |
|--|-----|
| 6. Advanced Screen Content Coding.....                             | 93  |
| 6.1. Introduction.....   | 93  |
| 6.2. Improvements of SCC for multiview video compression .....     | 93  |
| 6.2.1. Frame-compatibility with specific ordering.....             | 93  |
| 6.2.2. Tile encoding.....  | 94  |
| 6.2.3. Intra Block Copy vectors precision .....                    | 95  |
| 6.2.4. Starting point for block matching in Intra Block Copy ..... | 95  |
| 6.2.5. In-loop filtering per tile .....                            | 96  |
| 6.2.6. Different Quantization Parameter for side views .....       | 97  |
| 6.2.7. Reference tile border extension.....                        | 97  |
| 6.3. Improvements of SCC for immersive video compression .....     | 98  |
| 6.3.1. Adaptation of Advanced SCC to immersive video.....          | 98  |
| 6.3.2. Using MIV metadata to control the modifications.....        | 98  |
| 6.4. Evaluation of the proposal .....                              | 99  |
| 6.4.1. Goals of the experiments .....                              | 99  |
| 6.4.2. Evaluation of Advanced SCC in multiview video coding .....  | 100 |
| 6.4.3. Evaluation of Advanced SCC in screen content coding.....    | 103 |
| 6.4.4. Evaluation of Advanced SCC in immersive video coding .....  | 104 |
| 6.5. Conclusions.....  | 110 |
| 7. Summary of the dissertation .....                               | 113 |
| 7.1. Recapitulation .....  | 113 |
| 7.2. Research work done .....                                      | 114 |
| 7.3. Original achievements of the author and conclusions .....     | 115 |
| References.....  | 117 |
| Publications of the author .....                                   | 127 |
| Appendix: Experimental results .....                               | 131 |





## ABSTRACT

The dissertation presents the author's research on novel prediction techniques for multiview video compression. The author identifies the limitations of the state-of-the-art techniques and then proposes two original solutions. The main goal is to improve the inter-view prediction in compression of multiview video acquired using systems with various camera arrangements. The proposed techniques are dedicated to modern applications of multiview video, such as virtual reality (VR), augmented reality (AR), or immersive video systems.

In the first part of the dissertation, the author adapts the state-of-the-art compression technique, 3D-HEVC, to the aforementioned applications. To achieve that, the author first proposes a novel, original rectification method for multiview video acquired by cameras distributed roughly on a circle. Then, the author modifies the inter-view prediction of 3D-HEVC to efficiently compress such rectified video. The modified codec, in the dissertation referred to as ARC-HEVC, is evaluated in terms of rate-distortion (RD) compression efficiency and coding time, and the results are compared to the state-of-the-art 3D-HEVC. According to the results, the author's proposal is both faster and more efficient.

In the second part of the dissertation, the author proposes a novel idea of using Screen Content Coding (SCC) for compression of frame-compatible multiview video. The main idea is to utilize Intra Block Copy as an inter-view prediction tool. The advantage of such a solution is that the codec does not require a complex multi-layer structure dedicated exclusively to the processing of multiview video, contrary to the state-of-the-art Multiview HEVC (MV-HEVC). Additionally, the author proposes a set of original modifications to improve the efficiency of Screen Content Coding in compression of multiview (including stereoscopic) video. Experimental evaluation shows that the author's novel approach, in the dissertation called Advanced SCC or ASCC, provides virtually the same RD compression efficiency and encoding time as MV-HEVC, both in the coding of stereoscopic and multiview video.

Both SCC and ASCC codecs are also employed by the author as the inner codecs in MPEG Immersive Video, replacing commonly used HEVC codec. Experimental evaluation of the proposed change in compression of immersive video shows a significant gain in rate-distortion compression efficiency and the quality of virtual views, at the cost of increased encoding time.



## STRESZCZENIE

Niniejsza rozprawa prezentuje przeprowadzone badania w kierunku oryginalnych technik predykcji dla kompresji wizji wielowidokowej. W rozprawie autor identyfikuje ograniczenia aktualnych technik oraz proponuje dwa oryginalne rozwiązania. Głównym celem jest poprawa predykcji międzywidokowej w kompresji wizji wielowidokowej zarejestrowanej systemami o różnym rozmieszczeniu kamer. Zaproponowane techniki są przeznaczone dla nowoczesnych zastosowań wizji wielowidokowej, takich jak wirtualna rzeczywistość (VR), rzeczywistość rozszerzona (AR), czy systemy wizji wszechogarniającej.

W pierwszej części rozprawy autor dostosowuje technikę kompresji 3D-HEVC do wspomnianych zastosowań. W pierwszej kolejności autor proponuje nowatorską, oryginalną metodę rektyfikacji wizji wielowidokowej rejestrowanej za pomocą kamer rozmieszczonych w przybliżeniu na okręgu. Następnie autor modyfikuje predykcję międzywidokową w 3D-HEVC dla efektywnej kompresji tak zrektyfikowanej wizji. Zmodyfikowany kodek, w rozprawie określany jako ARC-HEVC, jest oceniony pod kątem efektywności kompresji i czasu kodowania, a wyniki są porównane z oryginalnym 3D-HEVC. Wyniki pokazują, że proponowana metoda jest zarówno szybsza, jak i bardziej efektywna.

W drugiej części rozprawy autor proponuje oryginalną metodę polegającą na zastosowaniu techniki Screen Content Coding (SCC) w kompresji wizji wielowidokowej zgodnej ramkowo (ang. *frame-compatible*). Główną ideą jest zastosowanie Intra Block Copy jako narzędzia predykcji międzywidokowej. Zaletą takiego rozwiązania jest to, że kodek nie wymaga złożonej, wielowarstwowej struktury dedykowanej wyłącznie kodowaniu wizji wielowidokowej, w przeciwieństwie do aktualnej techniki Multiview HEVC (MV-HEVC). Dodatkowo, autor proponuje szereg modyfikacji poprawiających efektywność Screen Content Coding w kompresji wizji wielowidokowej (także stereoskopowej). Ocena eksperymentalna pokazuje, że metoda zaproponowana przez autora, w rozprawie określana jako Advanced SCC lub ASCC, jest równie efektywna jak MV-HEVC z punktu widzenia poziomu kompresji i czasu kodowania, zarówno dla kodowania wizji stereoskopowej, jak i wielowidokowej.

Kodeki SCC i ASCC zostały także zastosowane przez autora jako wewnętrzne kodeki w technice MPEG Immersive Video, zastępując powszechnie stosowany kodek HEVC. Ocena eksperymentalna dla kompresji wizji wszechogarniającej pokazuje, że zaproponowane przez autora rozwiązania są znacząco lepsze pod względem efektywności kompresji i jakości widoków wirtualnych, kosztem zwiększonego czasu kodowania.



## LIST OF SYMBOLS AND ABBREVIATIONS

|                     |   |
|---------------------|---|
| $\alpha_i$          | angle between the direction of the $i$ -th camera optical axis and $Z$ axis,<br>derived in circular rectification |
| $b$                 | bit depth of the depth sample value   |
| $c$                 | skew factor (intrinsic camera parameter)  |
| $d$                 | sample value from depth map   |
| $d_x, d_y$          | horizontal and vertical component of disparity vector   |
| $f_x, f_y$          | horizontal focal length, vertical focal length  |
| $\mathbb{K}$        | [3×3] intrinsic parameter matrix  |
| $o_x, o_y$          | coordinates of the optical center   |
| $o'_x$              | modified horizontal coordinate of optical center  |
| $\mathbb{P}$        | [4×4] projection matrix   |
| $r$                 | radius of the circle in a circular camera arrangement   |
| $\mathbb{R}$        | [3×3] rotation matrix   |
| $\mathbb{T}$        | 3-component translation vector  |
| $x, y$              | positions of a point in a view  |
| $X_{cen}, Z_{cen}$  | position of the circle center on XZ plane (parallel to the ground)  |
| $X_i, Z_i$          | position of $i$ -th camera on XZ plane  |
| $X'_i, Z'_i$        | modified position on the circle of $i$ -th camera on XZ plane   |
| $z$                 | distance between camera plane and acquired point in 3D space  |
| $Z_{near}, Z_{far}$ | depth maps normalization parameters   |

Prediction techniques for compression of multiview video acquired using systems with various camera arrangements

|          |   |
|----------|---|
| 2D       | two-dimensional                               |
| 3D       | three-dimensional                             |
| 3DTV     | three-dimensional television                  |
| ANY-HEVC | HEVC adapted to arbitrary camera arrangements |
| AR       | augmented reality                             |
| ARC-HEVC | HEVC adapted to circular camera arrangements  |
| ASCC     | Advanced Screen Content Coding                |
| AVC      | Advanced Video Coding                         |
| BD-rate  | Bjøntegaard delta rate                        |
| CTC      | common test conditions                        |
| DCP      | disparity-compensated prediction              |
| FTV      | free-viewpoint television                     |
| HEVC     | High Efficiency Video Coding                  |
| HM       | test model for HEVC                           |
| HTM      | test model for MV-HEVC and 3D-HEVC            |
| IBC      | Intra Block Copy                              |
| MIV      | MPEG Immersive Video                          |
| MPEG     | Moving Picture Experts Group                  |
| MVD      | multiview video plus depth                    |
| MV-HEVC  | Multiview High Efficiency Video Coding        |
| PSNR     | Peak Signal-to-Noise Ratio                    |
| QP       | Quantization Parameter                        |
| RD       | rate-distortion                               |
| SCC      | Screen Content Coding                         |

|      |                                     |
|------|-------------------------------------|
| TMIV | test model for MPEG Immersive Video |
| VPS  | Video Parameter Set                 |
| VR   | Virtual Reality                     |
| VVC  | Versatile Video Coding              |





# 1. INTRODUCTION

## 1.1. SCOPE OF THE DISSERTATION

**Multiview video** [Ho'07, Vetro'11B] is a set of video sequences acquired synchronously by multiple cameras. The number of cameras and their locations vary, depending on the application. Multiview video can be enriched with depth data representing the distance between the camera plane and a given point in the acquired scene [Sullivan'09]. Such representation is called Multiview Video plus Depth (MVD) [Müller'11]. Figure 1.1 presents an example of an MVD frame composed of 3 views and corresponding depth maps obtained from one of the test multiview sequences.

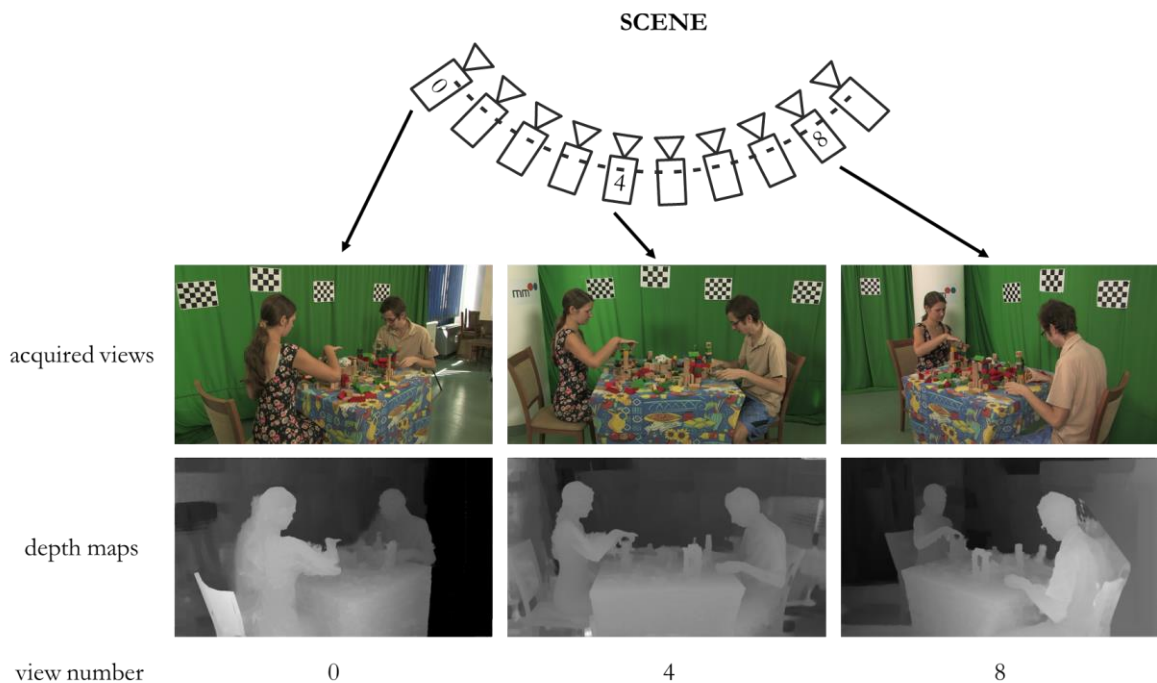


Figure 1.1. Example of a multi-camera setup and an MVD frame.

In recent years, many new applications utilizing multiview video have been developed, e.g., advanced three-dimensional television (3DTV), free-viewpoint television (FTV), virtual reality (VR), augmented reality (AR), and immersive video. Their goal is to satisfy the demand for more realistic and engaging multimedia, compared to the standard two-dimensional video.

A major challenge related to the abovementioned applications is the compression of multiview video [Domański'19]. It is estimated that video data already accounts for roughly 80% of global Internet traffic, and its share continues to grow due to (among other reasons) emerging video applications such as virtual reality or immersive video [Cisco'18, Cisco'20]. Therefore, a

vast amount of video data produced by multi-camera setups has to be efficiently compressed, preserving a high quality of the content at the same time. **This dissertation focuses on the efficient compression of multiview video.**

A straightforward way to compress multiview video is to process each view separately (simulcast encoding) using one of the existing compression techniques for monoscopic video, such as High Efficiency Video Coding (HEVC) [ISO'21, Sullivan'12] or Versatile Video Coding (VVC) [ISO'22, Bross'21]. However, this approach is inefficient as it does not utilize the similarities between the views. To address this issue, dedicated multiview video compression techniques have been developed in recent years. The most recent techniques in multiview video coding are listed below.

- Multiview HEVC (MV-HEVC) [Tech'16, Hannuksela'15]. An extension developed on top of HEVC that adds multi-layer coding with inter-view prediction, together with the required signalization.
- 3D-HEVC [Tech'16, Sullivan'13, Müller'13]. This technique is dedicated to the joint coding of camera views and depth maps. It further extends MV-HEVC, primarily by utilizing information about depth, which allows to, e.g., better predict the disparity between the views.
- MPEG Immersive Video (MIV) Coding [Boyce'21]. Dedicated to immersive video that provides playback with six degrees of freedom (6DoF) for end users. Inter-view redundancy is reduced through view synthesis and packing of the occluded parts of each view into atlases. The output images are then compressed using one of the standard compression techniques, usually HEVC.
- Versatile Video Coding (VVC) [Bross'21, ISO'22]. Although it is not its main application, the multi-layer coding functionality in VVC allows it to perform inter-view prediction in a similar manner as MV-HEVC. However, VVC lacks the capability of using depth maps to improve the compression efficiency, known from 3D-HEVC. Moreover, during the author's research, VVC was still under extensive development. **Therefore, this dissertation focuses on HEVC-based coding techniques as the state-of-the-art in multiview video compression.** Nonetheless, in the dissertation, the author takes into account future development and, whenever suitable, provides comments on the possibility of applying proposed solutions to the VVC-based codecs.

The abovementioned coding tools stem from monoscopic video compression techniques but are equipped with additional coding tools for reducing inter-view redundancy.

The coding efficiency of those techniques varies, depending on the application and the content being encoded. For instance, in the compression of video composed of 3 views, MV-HEVC is reported to provide roughly a 30% bitrate reduction compared to simulcast encoding, and 3D-HEVC reduces the bitrate by additional 20% [Tech'16]. However, this applies only when the encoded views are coplanar and arranged on a 1D line. For other view arrangements, the compression efficiency of the multiview extensions of HEVC decreases significantly, which is a major limitation of those techniques. In many modern applications, such as free-viewpoint television or immersive video, the 1D linear camera arrangement does not provide enough information about the scene to create a realistic user experience. On the other hand, non-linear camera arrangements are much more challenging to set up, and, as mentioned before, current compression techniques are not prepared to efficiently compress video data produced by them. **In this dissertation, one of the goals is to improve the rate-distortion compression efficiency for circular camera arrangement.** It is a special case of a non-linear arrangement where the cameras are distributed precisely on a circle with their optical axes directed towards its center.

Another drawback of the state-of-the-art multiview video coding techniques is that they are built on top of monoscopic (single-layer) video codecs, as special profiles dedicated exclusively to the purpose of multiview video compression. Unfortunately, such multi-layer design requires much more complex decoders, which limits their practical applications. Moreover, the development and standardization of a multiview profile require additional work, and therefore such a profile is usually prepared after the standardization of a monoscopic codec. An alternative approach to multiview video compression is to pack several views of a multiview sequence into a single frame and use a standard monoscopic video encoder for compression, with additional signalization to inform the decoder how to separate the views. Such a solution is called frame-compatible coding and is commonly used e.g. in stereoscopic video broadcasting (3D television) [Vetro'10]. The advantage of frame-compatible coding is that the decoding device does not have to be equipped with a codec supporting a dedicated multiview profile, and therefore the 3D television broadcasting signal is more accessible to the customers. On the other hand, a monoscopic video encoder is not able to utilize the similarities between the views packed into a single frame, meaning that there is no inter-view prediction. As a result, the bitstream in such cases is higher than when using dedicated multiview video encoders and comparable to simulcast encoding [Samelak'17A]. **In this dissertation, the author proposes a novel approach that introduces inter-view prediction to frame-compatible multiview video coding by the use of Screen Content Coding [Xu'16A].** Such a combination is unusual

because SCC was developed for entirely different purposes. Moreover, the idea is also applied to the compression of immersive video.

## 1.2. GOALS AND THESES OF THE DISSERTATION

There are two main goals of this dissertation. The first one is to improve the compression efficiency of rectified multiview video acquired by cameras located on a circle. In this topic, the rectification process is also proposed by the author. The second goal is to prove that Screen Content Coding, which is an extension of HEVC designed for compression of video containing a significant amount of rendered graphics, can be surprisingly used for compression of multiview video.

The theses of this dissertation are as follows:

- 1. It is possible to reduce both bitrate and encoding time of 3D-HEVC encoder in compression of rectified multiview video acquired with cameras located on a circle, compared to the state-of-the-art 3D-HEVC encoder, through adaptation of inter-view prediction to circular camera arrangements.**
- 2. It is possible to use standard-compliant HEVC Screen Content Coding for compression of stereoscopic video, frame-compatible multiview video, and immersive video. With additional improvements, the rate-distortion compression efficiency of such an approach can be comparable or even higher than the state-of-the-art dedicated techniques.**

In the dissertation, the author proposes novel, original approaches to multiview video compression. The proposed solutions are implemented on top of publicly-available implementations of HEVC encoder and its extensions: Multiview HEVC (MV-HEVC), 3D-HEVC, and Screen Content Coding (SCC). The proposed methods are evaluated experimentally through the compression of test sequences and comparing results with unmodified encoders. The adaptation of 3D-HEVC to circular camera arrangements is additionally compared with 3D-HEVC adapted to any camera arrangement, which is another proposal co-authored by the author of this dissertation [Domański'15A, Domański'16A, Samelak'16, Stankowski'15, Stankiewicz'18].

The author's idea of using Screen Content Coding as an alternative to the state-of-the-art multiview, stereoscopic, and immersive video compression techniques was published in [Samelak'17A-D, Samelak'20A-B, Samelak'21A-B] and [Samelak'22]. The paper presenting the idea of optimizing 3D-HEVC for circular camera arrangements is to be published.

### 1.3. OVERVIEW OF THE DISSERTATION

This dissertation is divided into seven chapters. Chapter 1 provides information about the scope of the dissertation, as well as its goals and theses.

Chapter 2 contains selected topics in the state-of-the-art of video coding. First, the author briefly describes the principles of video compression. Then, the author presents popular techniques for multiview, 3D, and immersive video coding, which are the dedicated solutions for compression of video acquired by multiple cameras. Finally, the author provides information about Screen Content Coding, which was designed for different applications, but in this dissertation, the author proposes to reuse it also for multiview video compression.

In Chapter 3, the methodology of conducted experiments is presented. The author provides information about test models of video encoders used for the assessment of the proposals. Moreover, the author lists test sequences and test conditions for conducted experiments. The author describes the methods used to evaluate the compression efficiency and the encoding times of the proposed solutions.

Chapter 4 presents the author's idea for adapting 3D-HEVC to circular camera arrangement. The author shows how sequences acquired with cameras located roughly on a circle can be rectified. Next, the author derives the equations for inter-view prediction between views located on a circle. Then, the test model for 3D-HEVC is adapted to make use of the new equations. Finally, the proposal is experimentally evaluated.

In Chapter 5, the author proposes new applications for Screen Content Coding. After explaining the idea, the author shows how to apply SCC to stereoscopic, multiview, and immersive video coding. The goal of this work is to keep the codec standard-compliant, meaning that the bitstream produced by the encoder could be decoded by the state-of-the-art HEVC SCC decoder. The resulting encoders are compared experimentally with the state-of-the-art solutions.

In Chapter 6, the author introduces several customized improvements to the codecs from Chapter 5 to make them more efficient for the new applications. The description of the author's improvements is followed by more experimental results.

In Chapter 7, the author comments on his achievements and summarizes the results with regard to the goals of the dissertation.



## 2. SELECTED TOPICS IN THE STATE-OF-THE-ART OF VIDEO CODING

### 2.1. INTRODUCTION

In this chapter, the author briefly describes some aspects of the state-of-the-art of video coding. The main focus is put on multiview, 3D, and immersive video compression. The author also describes selected techniques of Screen Content Coding related to the author's proposal of using SCC for multiview video compression.

As mentioned in Chapter 1, the author's research is based on HEVC and its extensions, nonetheless it should be noted that multiview profiles are also present in previous generations of video coding standards, i.e., multiview profile in MPEG-2 [Chen'97, Ohm'99, ISO'12] and Multiview Video Coding (multiview extension of AVC) [ISO'14, Vetro'11A]. Regardless of the standard, the principle in multiview video compression is to exploit the similarities between the coded views.

### 2.2. MULTIVIEW AND 3D-VIDEO CODING

Multiview HEVC (MV-HEVC) and 3D-HEVC extensions were developed by the ITU-T/ISO/IEC Joint Collaborative Team on 3D Video Coding Extension Development (JCT-3V) and included in the second and third edition of the HEVC standard [ISO'21, Sullivan'12, Sullivan'13], respectively. They introduce a multilayer coding design, i.e., joint coding of multiple views. Compared to simulcast coding, the main benefit of such design is the encoder's ability to perform inter-view prediction that exploits the similarities between the views. In MV-HEVC and 3D-HEVC, inter-view prediction is performed through block-based matching between the picture being encoded and the previously encoded reference picture of another view and within the same time instance. This approach is analogous to the inter-frame prediction, where the reference picture belongs to the same view but a different time instance.

One of the coding tools that utilize inter-view prediction is Disparity Compensated Prediction (DCP), which estimates disparity vectors and calculates prediction residuals [Müller'13]. A disparity vector points to the best-matching block of samples in the reference view. In 3D-HEVC, disparity vector  $(d_x, d_y)$  is also predicted by the use of depth maps, according to Equation (2.1):

$$\begin{aligned} d_x &= \frac{f_{x1}(t_2 - t_1)}{z} - o_{x2} + o_{x1} , \\ d_y &= 0 \end{aligned} \quad (2.1)$$

where:

$d_x, d_y$  – horizontal and vertical component of disparity vector,

$f_{x1}$  – horizontal focal length of the source camera,

$t_1, t_2$  – positions of the source and target camera along the horizontal axis,

$o_{x1}, o_{x2}$  – horizontal optical centers of the source and target camera,

$z$  – distance between the image plane and acquired point in 3D space, i.e., depth.

In Equation (2.1), all the components except for  $z$  are camera parameters, which are assumed to be constant for a given pair of source and target cameras. The distance  $z$  is calculated from the depth map sample value using the following Formula (2.2):

$$z = \left( \frac{d}{2^b} \left( \frac{1}{Z_{near}} - \frac{1}{Z_{far}} \right) + \frac{1}{Z_{far}} \right)^{-1} , \quad (2.2)$$

where:

$Z_{near}, Z_{far}$  – the smallest and the biggest value of  $z$ ,

$b$  – bit depth of sample values of the depth map,

$d$  – normalized disparity (sample value in depth map).

To avoid confusion, it should be stressed that depth maps are usually represented as greyscale images, where bigger sample values indicate lower depth (a point is closer to the image plane), and sample values closer to 0 indicate greater depth (Figure 1.1). Therefore, the horizontal component of disparity vector ( $d_x$ ) in MV-HEVC and 3D-HEVC is inversely proportional to depth  $z$  and proportional to the value of depth map sample  $d$  (i.e., normalized disparity). The bigger the value of the depth map sample (the object is closer to the camera), the bigger the horizontal disparity. Regarding the vertical component of the disparity vector, 3D-HEVC assumes it is always equal to 0, i.e., the views are vertically aligned. On the one hand, 3D-HEVC encoder benefits from those assumptions through significant simplification of the disparity-compensated prediction (DCP). For example, for each pair of cameras, 3D-HEVC prepares dedicated look-up tables that map each possible depth sample value onto disparity; for a typical case of 8-bit depth, such a table contains 256 values. This allows the encoder to significantly reduce the time required to perform inter-view prediction. On the other hand, the



aforementioned assumptions limit the use of 3D-HEVC to multiview video acquired by cameras located on a line, aligned vertically and with optical axes in parallel. Even though a great deal of effort was put into building multi-camera systems that would meet those requirements, it is not possible to position the cameras ideally. Therefore, before compression, multiview video is usually rectified, which corresponds to correcting the positions of cameras and suppressing the results of differences in their properties (Figure 2.1) [Hartley'99, Kang'08, Stankowski'10].

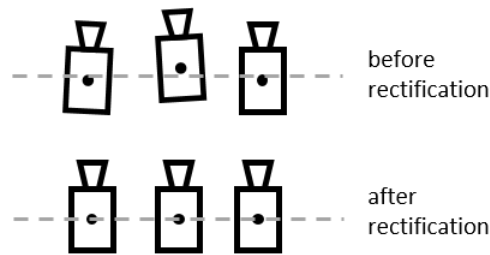


Figure 2.1. Linear camera setup before and after rectification.

It should be stressed that rectification does not correct the real positions of cameras but transforms the views obtained from the cameras into video virtually obtained from an ideally positioned set of cameras [Ho'12, Choi'12]. This improves the accuracy of the inter-view prediction, thus also the overall compression efficiency.

## 2.3. SCREEN CONTENT CODING

Screen Content Coding (SCC) is an extension added to the fourth version of the HEVC standard [ISO'21, Xu'16A]. Contrary to the main profile of HEVC dedicated to camera-captured content, the SCC was developed to improve the compression efficiency of video containing a significant portion of rendered graphics, text, or animations (Figure 2.2).

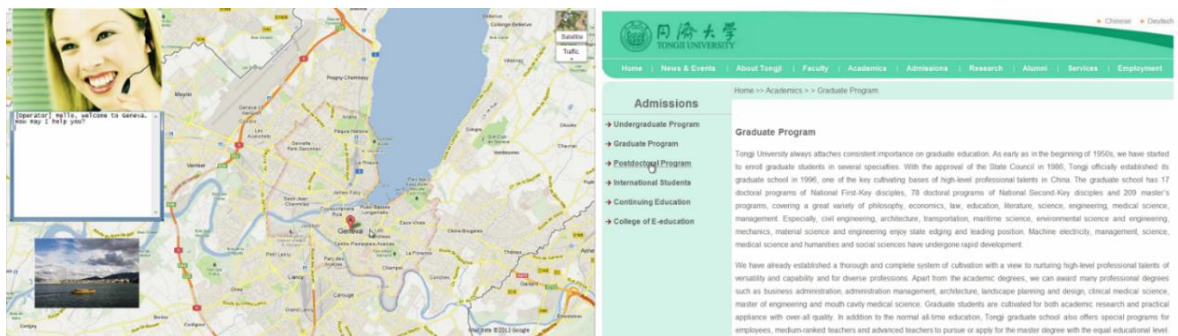


Figure 2.2. Examples of frames from test sequences containing screen content: sc\_map (left) and sc\_web\_browsing (right).

Applications of SCC include but are not limited to: screen sharing, wireless displays, remote desktop access, streaming e-sports, or cloud gaming. Screen Content Coding profile

improves the compression efficiency of computer-generated content by leveraging its characteristics, such as the presence of repeatable patterns, sharp edges, plain monochromatic areas, limited palette of colors, or lack of noise. It is done through a set of dedicated coding tools, from which the most important ones are listed below.

**Intra Block Copy (IBC)** [Xu'16B], also known as Current Picture Referencing [Xu'19], predicts the content by searching for the most similar block of samples in the currently processed picture. The position of the best matching block of samples is indicated by the IBC vector, similarly to the standard inter-frame prediction. However, since the reference picture is also the current picture, the search area for IBC is restricted to the previously encoded part of the picture (Figure 2.3). Moreover, the search in IBC is performed at full-pel accuracy, contrary to the standard sub-pel inter-frame prediction. Intra Block Copy is a very effective technique for compression of fonts and other repetitive patterns.

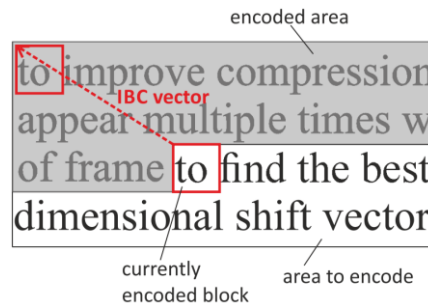


Figure 2.3. Example of using Intra Block Copy.

**Palette Mode** [Pu'16, Sun'19] – screen content is often composed of a small number of distinct colors, especially at the level of a single coding unit (CU). SCC encoder can decide to enumerate them, prepare palettes and transmit indices to colors from palettes rather than applying standard prediction.

**Adaptive Motion Vector Resolution** [Xu'16A] allows for dynamic modification of the accuracy of motion-compensated prediction. In the compression of screen content, it is often beneficial to represent motion vectors at full-pel resolution because the cost of spending more bits on sub-pel motion vectors can exceed the profit of more accurate motion estimation.

**Adaptive Color Transform** [Zhang'15, Jhu'20] allows the encoder to choose between RGB and YCbCr color space for each CU.

It should be noted that Screen Content Coding is not related to multiview video coding, especially when the multiview video is captured with cameras. Nevertheless, in the dissertation, the author proposes the usage of SCC as a novel approach to the compression of camera-

captured multiview video and immersive video. Chapter 5 describes the process of adaptation of the unmodified SCC to the new application, whereas in Chapter 6 the author presents how SCC can be modified to achieve rate-distortion compression efficiency similar to that of the dedicated multiview compression techniques. It should also be mentioned that Screen Content Coding was included in the most recent video coding standard – Versatile Video Coding [Xu’22] – and therefore, the author’s propositions remain valid.

## 2.4. IMMERSIVE VIDEO CODING

In recent years, virtual reality (VR), augmented reality (AR), and mixed reality systems are gaining importance. They provide a new type of experience where the user is immersed in the scene and, depending on the number of degrees of freedom provided by the system, can control the viewing position and orientation of the content [Domański’17]. Video content processed by such systems is often referred to as immersive video. It may be computer-generated or captured by a set of cameras, planar (2D), or omnidirectional (360-degree). Immersive video is usually represented as Multiview Video plus Depth (MVD), however other representations, such as point clouds, are also being researched [Hu’23, Li’20, Schwarz’19, Cui’19]. Nevertheless, in the dissertation, the author focuses only on the MVD representation.

One of the critical factors that influence the overall quality of a VR system is the quality of virtual views presented to the user. Therefore, in recent years, a lot of effort has been put into improving virtual view synthesis [Bonatto’21, Ceulemans’18, Fachada’18, Rahaman’18, Dziembowski’17A]. It has been proven that the efficiency of view synthesis strongly depends on the quality of depth maps, hence the research on depth map estimation also attains a lot of interest [Mieloch’21, Rogge’19, Dziembowski’17B, Mieloch’17A, Mieloch’17B, Mieloch’17C]. Another technical challenge for the development of immersive video is the amount of data required to fully represent a scene. On the one hand, the more input views are used, the better the quality of the virtual view synthesis can be achieved. On the other hand, such a vast amount of data may be impractical for transmission and storage, even when compressed using modern multiview video encoders. Therefore, in order to cope with the task of efficient representation of multiview video data, a new type of video codec called MPEG Immersive Video (MIV) was recently developed by the ISO/IEC MPEG group [Boyce’21].

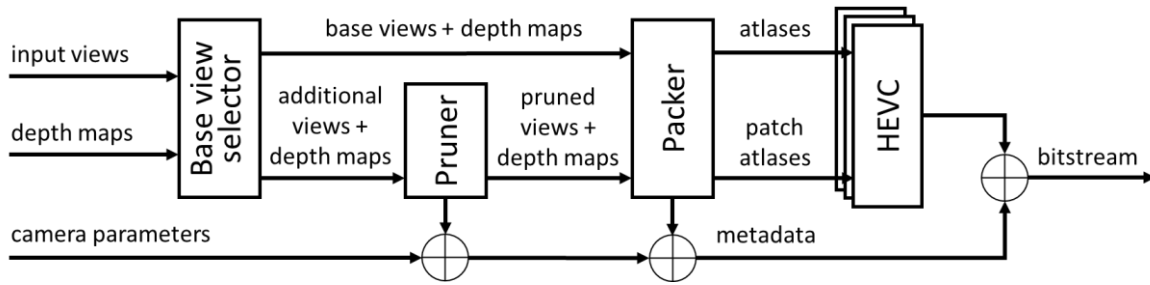


Figure 2.4. Block diagram of MIV encoder.

The goal of a MIV encoder is to reduce the spatial redundancy from the input multiview video, which is composed of multiple input views, corresponding depth maps, and parameters of corresponding cameras (Figure 2.4). In the first step, the encoder chooses a subset of input views (base views) and corresponding depth maps. The base views and their depth maps are merged into frame-compatible structures called atlases. Then, using view synthesis, the areas of additional views that can be synthesized from base views are removed in a process called pruning. The remaining parts (patches), i.e., areas occluded in the base views and present only in the additional views, are packed into several views called patch atlases (Figure 2.5). Pruning also applies to depth maps. An example of the output data after MIV pruning and packing, composed of atlases of base views and patches, is presented in Figure 2.6.

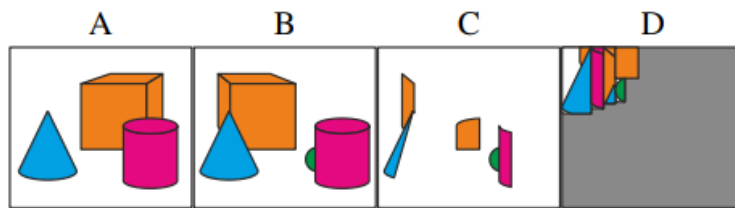


Figure 2.5. The process of preparing a patch atlas.  
A – base view, B – additional view, C – pruned additional view, D – patch atlas.

Apart from atlases containing video data and depth maps, a MIV encoder outputs metadata about pruning and packing. This allows MIV decoder to properly unpack and position the patches in the reconstructed views. The metadata is put directly into the bitstream, while the output video and depth atlases are compressed using simulcast HEVC encoders. The choice of HEVC as the internal codec was motivated by HEVC being commonly used in products. Nevertheless, MIV provides flexibility in choosing the video codec for compression of atlases to ensure the possibility of replacing it with VVC and other video coding techniques [Boyce'21].

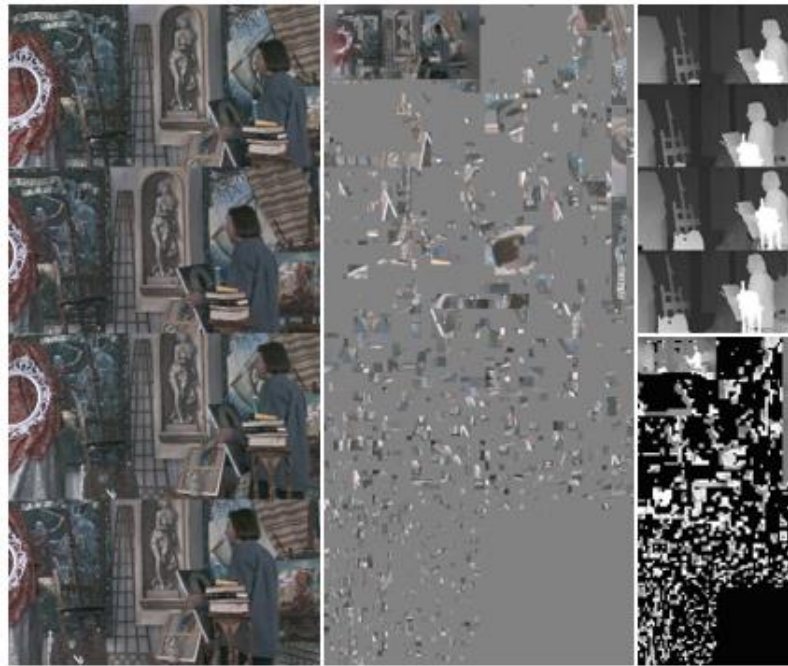


Figure 2.6. Example of MIV output atlases: atlas with packed input base views (left), patch atlas for views (middle), atlas with packed depth maps of corresponding base views (top-right), patch atlas for depth maps (bottom-right).



### 3. METHODOLOGY OF THE EXPERIMENTS

#### 3.1. INTRODUCTION

In the dissertation, the author presents several proposals for inter-view prediction and multiview video compression, dedicated to various applications. The author implemented the proposed techniques on top of appropriate test models and then evaluated them experimentally through the compression of multiple commonly used test sequences. The results were compared to the state-of-the-art solutions.

In this chapter, the common part of the methodology of performed experiments is described, which includes information about test models and their configurations, test sequences, and metrics used to compare the results. Details that are specific to a given evaluation are described separately in sections dedicated to each of the experiments.

#### 3.2. VIDEO CODEC TEST MODELS

In the previous chapter (Chapter 2), multiple HEVC-based video codecs are described: HEVC Screen Content Coding, Multiview HEVC, 3D-HEVC, and MPEG Immersive Video with HEVC as the inner codec. Each of these codecs is provided with the respective test model, which is a publicly available software implementation commonly used as a reference in experimental research. Versions of test models for each video codec used in the author's research are presented in Table 3.1. All the test models are based on the same HEVC core, HM-16.9. This assures fair comparison in the evaluation because the results are not affected by the changes between different versions of test models. Moreover, each codec is provided with a dedicated Common Test Conditions (CTC) – a document that specifies, e.g., default configurations of test model software to be used in the experiments. Those recommendations are meant to ensure reliable comparison between tested codecs. In the conducted experiments, unless stated otherwise, the configuration of the codecs follows appropriate CTC.

In some of the conducted experiments, the author considers two coding scenarios defined in CTCs: All Intra and Random Access. All Intra disables temporal prediction, i.e., all the frames are coded as I-frames [Sullivan'12].

Table 3.1. Test Models used in the experiments.

| Video coding technique     | Test Model                     | CTC         |
|----------------------------|--------------------------------|-------------|
| HEVC Main                  | HM-16.9 [HM]                   | [Bossen'13] |
| HEVC Screen Content Coding | HM-16.9+SCM-8.0 [HM+SCM]       | [Yu'15]     |
| Multiview HEVC             | HTM-16.2 [HTM]                 | [Müller'14] |
| 3D-HEVC                    | HTM-16.2 [HTM]                 | [Müller'14] |
| MPEG Immersive Video       | TMIV v.8 [TMIV] + HM-16.9 [HM] | [CTC MIV]   |

The compression techniques proposed in the dissertation are implemented by the author on top of the aforementioned test models. It should be noted that software implementation of a test model for a video codec is very complex, e.g., the source code of HTM (test model for 3D-HEVC) contains roughly 120 thousand lines of code in C++. Such source code of the test model is called the reference software. It is a result of the collaboration of many research teams and software engineers, and it requires many man-years of work to develop such an advanced video codec. As the evolution of video codecs progresses, achieving significant improvement in compression efficiency becomes more difficult and usually is attained at the cost of increased complexity and longer encoding times.

### 3.3. METHODOLOGY OF COMPRESSION EFFICIENCY ASSESSMENT

This section is dedicated to the description of the methodology used for the evaluation of the author's ideas for improving the compression efficiency of multiview video. The term "rate-distortion compression efficiency" (or simply "compression efficiency") used in the dissertation should be understood as the relation between the quality of the reconstructed video (after compression and decompression of the original video) and the bitrate of the compressed video stream produced by the encoder. Better compression efficiency indicates that the tested codec, compared to the reference one, provides better quality of reconstructed video at a given bitrate or lower bitrate at a given quality level.

In the dissertation, the quality is usually measured as PSNR (Peak Signal-to-Noise Ratio) of luma samples between original and reconstructed video, which is a common approach in the assessment of lossy compression [Wang'04] and is calculated according to Equation (3.1):



$$PSNR = 10 \log_{10} \left( \frac{(2^b - 1)^2}{MSE} \right), \quad (3.1)$$

where:

$b$  – bit depth of sample values of the depth map,

$MSE$  – mean squared error, calculated according to Equation (3.2):

$$MSE = \frac{1}{H \cdot W} \sum_{y=0}^{H-1} \sum_{x=0}^{W-1} [V_D(x, y) - V_R(x, y)]^2, \quad (3.2)$$

where:

$W, H$  – width and height of the coded view,

$V_D(x, y), V_R(x, y)$  – luma sample value at position  $(x, y)$  in the decoded and reference (before compression) views, respectively.

It should be stressed that PSNR (expressed in dB), when used as a quality metric of video compression techniques, is usually calculated only for the luma component of the input views, ignoring chroma components as well as depth maps. In the dissertation, unless stated otherwise, the author follows the commonly used approach for quality assessment.

As mentioned in Section 2.4, in immersive video applications, the overall quality of a system mostly depends on the quality of synthesized virtual views rather than decoded views. Some artifacts of view synthesis that do not influence the subjective quality, such as slightly shifted edges or minor changes in luminance sample values, may cause a significant decrease in PSNR. Other artifacts may not impact PSNR, but they significantly deteriorate virtual view quality when assessed by end users. Therefore, in the experiments related to immersive video (Section 5.7.4 and Section 6.4.4), the quality is additionally measured for the virtual views using other metrics:

- WS-PSNR – Weighted-to-Spherically-Uniform PSNR [Sun'17],
- VIF – Visual Information Fidelity [Sheikh'06],
- VMAF – Video Multimethod Assessment Fusion [Li'16],
- MS-SSIM – Multi-Scale SSIM [Wang'04],
- IV-PSNR – ISO/IEC MPEG metric for immersive video [Dziembowski'22, ISO'19].

The abovementioned alternative metrics are more resilient to view synthesis artifacts and, therefore, better correlated with the subjective quality assessment.

According to Common Test Conditions, the evaluation of video encoders should be performed at multiple rate points. The parameter that is responsible for controlling the bitrate of a modern video encoder, such as AVC, HEVC (including MV-HEVC and 3D-HEVC), or VVC, is called Quantization Parameter (QP) [Ma'05, Sullivan'12, Bross'21]. Encoding at small values of QP results in a higher bitrate but better quality. Higher QP values reduce the bitrate at the cost of lower quality of reconstructed video and visible compression artifacts. The experiments presented in the dissertation are performed at 4 different values of QP (defined separately in the description of each experiment). If an experiment includes compression of depth map images, their QP sets may differ from the values used for input views. Experimental compression results, i.e., 4 bitrate and quality pairs for each tested encoder, can be used to interpolate the rate-distortion curves using a third-order polynomial. Averaged bitrate reduction at a given quality (alternatively, averaged quality improvement at a given bitrate) is often calculated by MPEG research teams using the Bjøntegaard metric [Bjøntegaard'01]. That metric is also used in the experiments conducted by the author for the compression efficiency assessment.

In the experiments, the author of the dissertation also compares the encoding time. It is calculated as the mean coding time of 4 compression cycles, one per each QP. In order to ensure a fair comparison of the results, all the processing is performed on the same desktop computer equipped with an Intel Core i7 3.4 GHz CPU unit, 64 GB RAM, and Microsoft Windows 10 Pro operating system.

### 3.4. TEST SEQUENCES

In the evaluation of compression techniques proposed in the dissertation, multiple test sequences are used. The test set contains the following types of sequences:

- Multiview sequences acquired with dense linear camera setups (Table 3.2). The cameras are coplanar, located on a line with their optical axes in parallel. The provided content is already rectified to an ideal linear camera arrangement (Figure 2.1).
- Multiview sequences acquired with nearly-circular camera setups (Table 3.3). The cameras are located roughly in a circle. Acquired sequences are not rectified.
- Multiview sequences acquired with two-dimensional linear camera setups – cameras are coplanar and distributed in the form of two-dimensional matrices (Table 3.4)
- Multiview sequences acquired with omnidirectional cameras (Table 3.5). Such sequences are dedicated to immersive video applications.

- Single-view sequences containing screen content (Table 3.6). These are recommended for the assessment of compression techniques related to screen content.

Table 3.2. Multiview sequences acquired with dense linear camera setups.

| Test sequence name | Luma frame size | Frame rate | Content type | Sequence source  |
|--------------------|-----------------|------------|--------------|------------------|
| Balloons           | 1024×768        | 30 fps     | NC           | [Tanimoto'09]    |
| Kendo              | 1024×768        | 30 fps     | NC           | [Tanimoto'09]    |
| Newspaper          | 1024×768        | 30 fps     | NC           | [Ho'08]          |
| Poznan_Hall2       | 1920×1088       | 25 fps     | NC           | [Domański'09]    |
| Poznan_Street      | 1920×1088       | 25 fps     | NC           | [Domański'09]    |
| Poznan_Carpark     | 1920×1088       | 25 fps     | NC           | [Domański'09]    |
| IntelFrog          | 1920×1080       | 30 fps     | NC           | [Salahieh'19]    |
| GT_Fly             | 1920×1088       | 25 fps     | CG           | [Zhang'11]       |
| Dancer             | 1920×1080       | 25 fps     | CG           | [Rusanovskyy'11] |
| Shark              | 1920×1080       | 60 fps     | CG           | [Senoh'14]       |

Table 3.3. multiview sequences acquired with nearly-circular camera setups.

| Test sequence name | Luma frame size | Frame rate | Content type | Sequence source |
|--------------------|-----------------|------------|--------------|-----------------|
| Ballet             | 1024×768        | 25 fps     | NC           | [Zitnick'04]    |
| Breakdancers       | 1024×768        | 25 fps     | NC           | [Zitnick'04]    |
| BBB_Flowers        | 1280×768        | 24 fps     | CG           | [Kovacs'15]     |
| Poznan_Blocks      | 1920×1080       | 25 fps     | NC           | [Wegner'14]     |
| BBB_Butterfly      | 1280×768        | 24 fps     | CG           | [Kovacs'15]     |
| Poznan_Fencing2    | 1920×1080       | 25 fps     | NC           | [Domański'16B]  |

Table 3.4. Multiview sequences acquired with omnidirectional cameras.

| Test sequence name | Luma frame size | Frame rate | Content type | Sequence source |
|--------------------|-----------------|------------|--------------|-----------------|
| ClassroomVideo     | 4096×2048       | 30 fps     | CG           | [Kroon'18]      |
| TechnicolorMuseum  | 2048×2048       | 30 fps     | CG           | [Doré'18]       |
| TechnicolorHijack  | 4096×4096       | 30 fps     | CG           | [Doré'18]       |
| Chess              | 2048×2048       | 30 fps     | CG           | [Ilola'19]      |
| Group              | 1920×1080       | 30 fps     | CG           | [Doré'20B]      |
| ChessPieces        | 1920×1080       | 30 fps     | NC           | [Guillo'18]     |

Table 3.5. Multiview sequences acquired with cameras located on a 2D matrix.

| Test sequence name | Luma frame size | Frame rate | Content type | Sequence source |
|--------------------|-----------------|------------|--------------|-----------------|
| OrangeKitchen      | 1920×1080       | 30 fps     | CG           | [Boissonade'18] |
| TechnicolorPainter | 2048×1088       | 30 fps     | NC           | [Doyen'17]      |
| Fan                | 1920×1080       | 30 fps     | CG           | [Doré'20A]      |
| Mirror             | 1920×1080       | 30 fps     | CG           | [Doré'21]       |

Table 3.6. Single-view sequences containing screen content.

| Test sequence name  | Luma frame size | Frame rate | Sequence source |
|---------------------|-----------------|------------|-----------------|
| Basketball_Screen   | 2560×1440       | 60 fps     | [Suzuki'14]     |
| ChinaSpeed          | 1024×768        | 30 fps     |                 |
| ChineseEditing      | 1920×1080       | 60 fps     |                 |
| MissionControlClip2 | 2560×1440       | 60 fps     |                 |
| MissionControlClip3 | 1920×1080       | 60 fps     |                 |
| sc_console          | 1920×1080       | 60 fps     |                 |
| sc_desktop          | 1920×1080       | 60 fps     |                 |
| sc_flyingGraphics   | 1920×1080       | 60 fps     |                 |
| sc_map              | 1280×720        | 60 fps     |                 |
| sc_programming      | 1280×720        | 60 fps     |                 |
| sc_robot            | 1280×720        | 30 fps     |                 |
| sc_web_browsing     | 1280×720        | 30 fps     |                 |
| SlideShow           | 1280×720        | 20 fps     |                 |

All of the sequences are publicly available and recommended by the appropriate common test conditions for the evaluation of video coding techniques. They all have the same bit depth of samples, equal to 8 bits, and the chroma format is 4:2:0. It is assumed that geometric distortions of camera lenses are corrected, i.e., the cameras are calibrated [Collins'99, Lucchese'03].

The content of used test sequences is very diverse to ensure that the results of experiments reflect the compression efficiency of video encoders when used in practice. Test sequences can be divided by content into two groups: computer-generated (CG) and natural content (NC). Examples of frames from test sequences are presented in Figures 3.1–3.5.

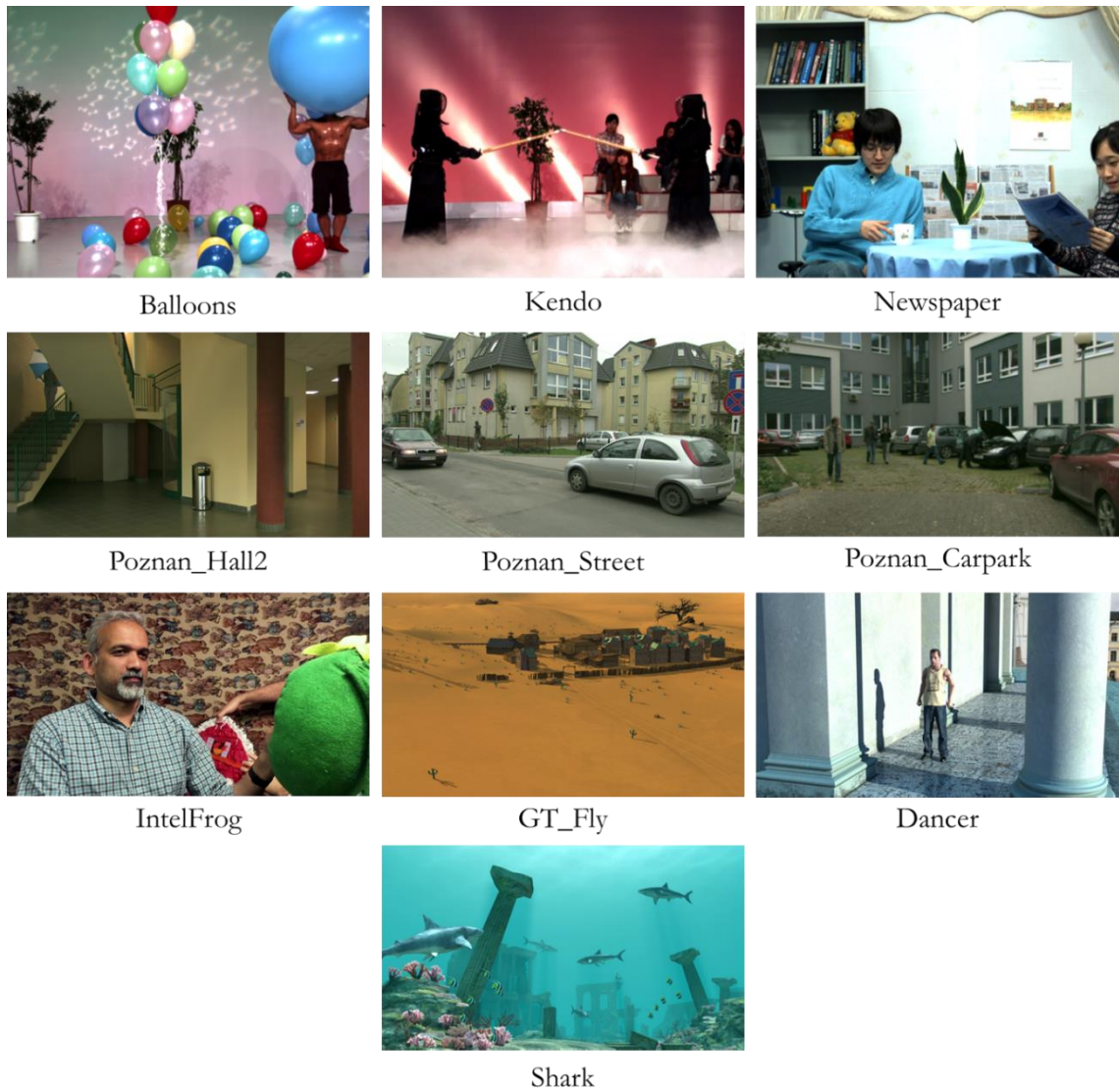


Figure 3.1. Examples of frames from multiview test sequences acquired with dense linear camera setups.

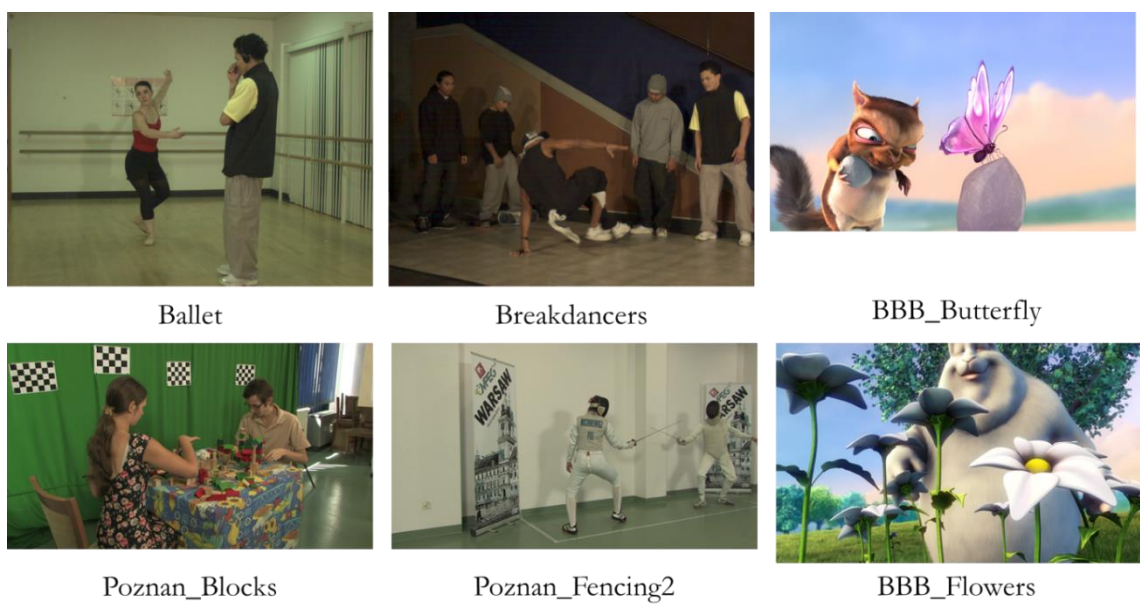


Figure 3.2. Examples of frames from multiview test sequences acquired with nearly-circular camera setups.

Prediction techniques for compression of multiview video acquired using systems with various camera arrangements

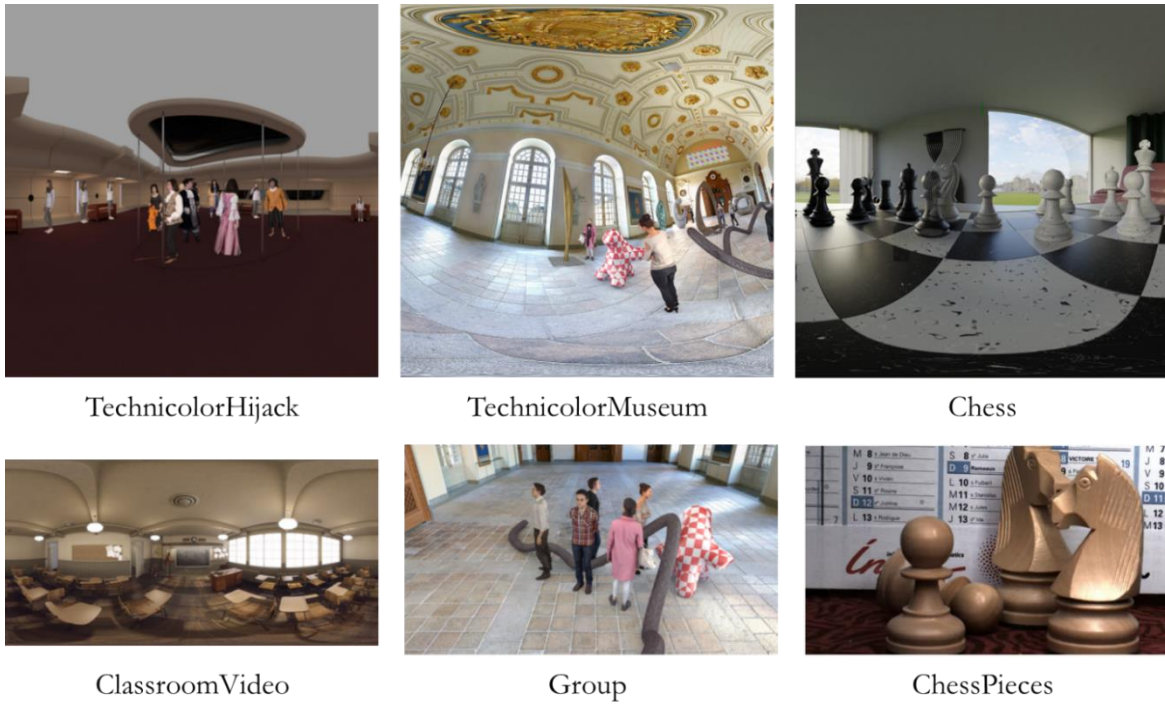


Figure 3.3. Examples of frames from multiview test sequences acquired with omnidirectional cameras.



Figure 3.4. Examples of frames from multiview test sequences acquired with rectangular camera setups.

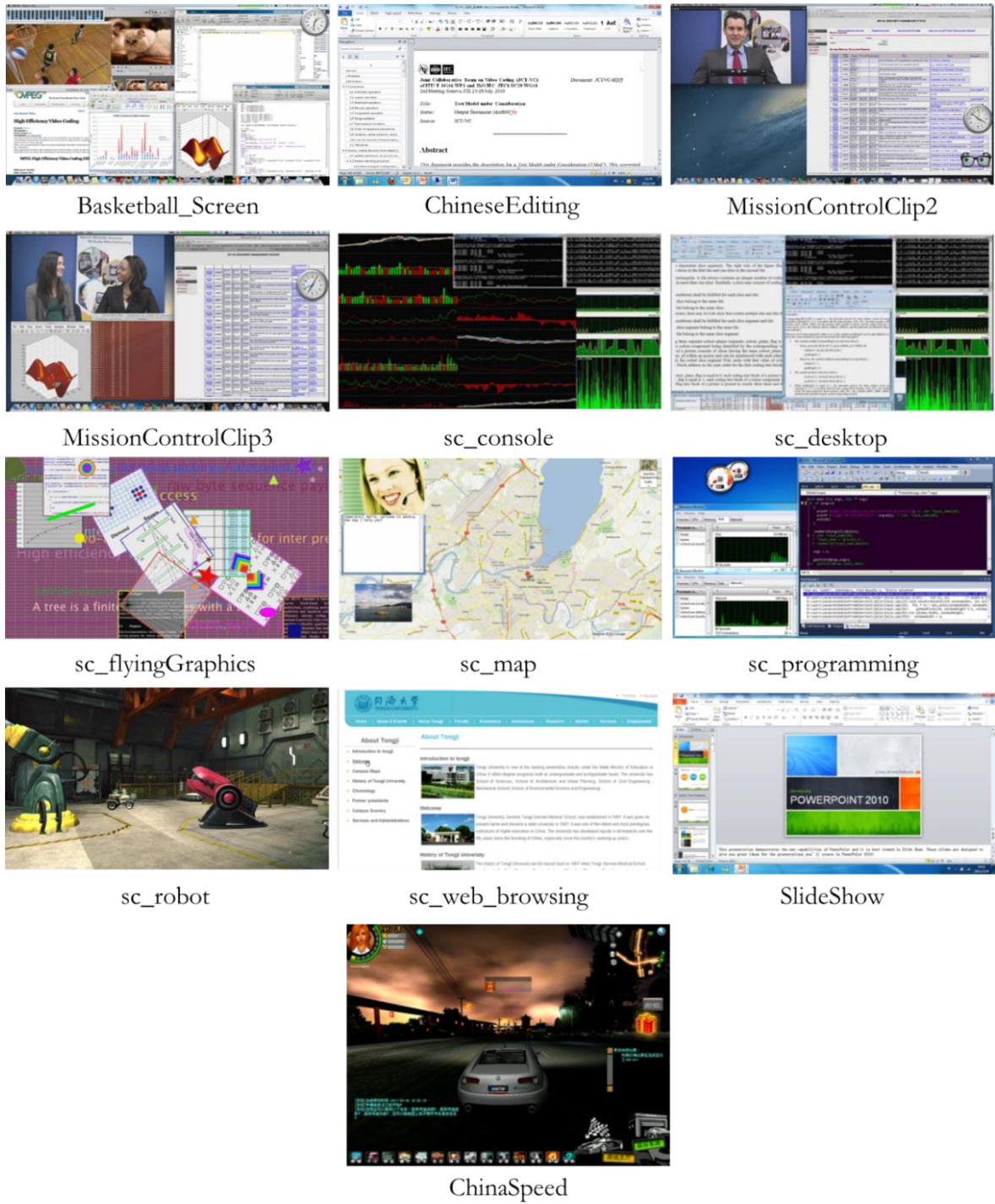


Figure 3.5. Examples of frames from single-view sequences containing screen content.





## 4. ADAPTING 3D-HEVC TO CAMERA ARRANGEMENTS OTHER THAN LINEAR

### 4.1. INTRODUCTION

As mentioned in Section 2.2, both MV-HEVC and 3D-HEVC assume that the input video is captured by multiple cameras distributed densely on a line. Such camera arrangement is used mainly for the purpose of displaying multiview content on autostereoscopic displays, which allow users to watch a stereoscopic video without wearing special glasses or other headgear, and even shift the viewer's position horizontally in a limited range. This technology, however, still has not become popular. On the contrary, other multiview applications such as free-viewpoint television (FTV), virtual reality, or immersive video systems are recently gaining more attention. Unfortunately, the aforementioned applications require video content that is captured from different perspectives using sparsely distributed cameras. Even though it is possible to use 3D-HEVC for compression of multiview video obtained from camera arrangements other than linear, the compression gain is significantly smaller than for linear camera arrangements [Stankowski'15, Samelak'16, Tech'16] due to inaccurate inter-view prediction. For that reason, 3D-HEVC and other state-of-the-art multiview profiles are not suitable for modern multiview applications.

The aforementioned problem was addressed by adapting the inter-view prediction of 3D-HEVC to arbitrary camera arrangements by the use of point mapping in 3D space. **The author of the dissertation participated in this research, implementation, and evaluation of the proposed modifications in the reference software, and co-authored several papers on that topic** [Stankowski'15, Domański'16A, Samelak'16, Stankiewicz'18]. A detailed description of this technique is presented in Section 4.2. In the dissertation, this solution is referred to as **ANY-HEVC**.

The main drawback of 3D point mapping is that it significantly increases the complexity of the inter-view prediction compared to standard 3D-HEVC. For instance, it is not possible to prepare look-up tables mapping depth to disparity (as described in Section 2.2) because the position of corresponding points in two views depends on multiple variables. Therefore, even though the proposed technique improves the compression efficiency in the case of camera arrangements other than linear, it also significantly increases the encoding time.

Among other multiview camera arrangements, much attention is paid to 2D arrays of cameras and circular arrangements [Tanimoto'12, Domański'15C, Cserkaszky'18]. In the case of circular arrangements, the cameras surround a scene and acquire it from different perspectives. The advantage of such an approach is that a few sparsely distributed cameras allow capturing the scene from various angles, which is an essential feature in the context of, e.g., FTV or immersive video applications [Domański'15A, Boyce'21].

In this chapter, the author of the dissertation presents **a novel idea of adapting 3D-HEVC for the compression of multiview video captured with cameras located roughly on a circle** and rectified to the views located ideally on a circle with optical axes directed towards its center. Such an approach is dual to 3D-HEVC, where video rectification and the assumption of linear camera arrangement allow to simplify inter-view prediction of the codec. The proposal, in the dissertation called **ARC-HEVC**, is a third way of dealing with the compression of MVD, and it should be considered as a trade-off between simple but with limited applications standard 3D-HEVC and flexible but more complex ANY-HEVC (Figure 4.1).

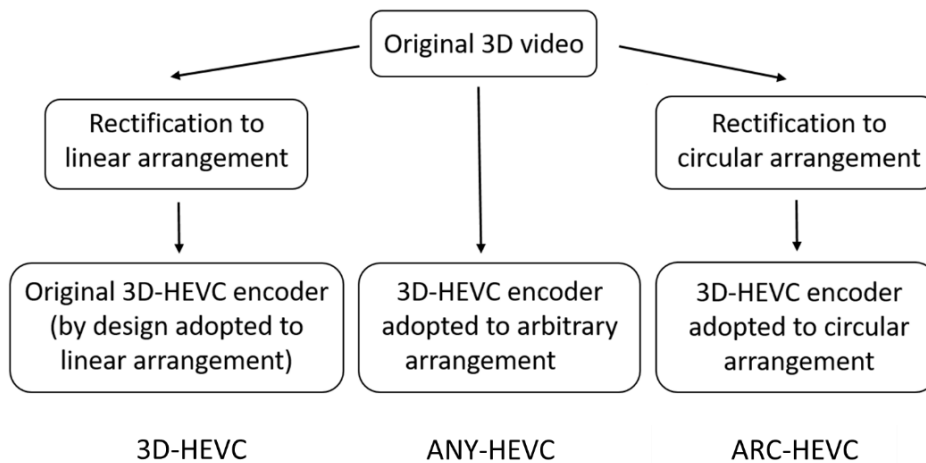


Figure 4.1. Three approaches to compression of 3D video: state-of-the-art 3D-HEVC dedicated for linear camera arrangements (3D-HEVC), modified 3D-HEVC for compression of arbitrary camera arrangements (ANY-HEVC, Sections 4.2-4.3), and the proposed codec for circularly rectified views (ARC-HEVC, Sections 4.4-4.6).

Along with the new codec, the author proposes **a novel procedure for circular rectification of a multiview video acquired by nearly-circular camera arrangements**. This rectification process and the adaptation of 3D-HEVC inter-view prediction are presented in Sections 4.4 and 4.5, respectively.

## 4.2. 3D-HEVC ADAPTED TO ANY CAMERA ARRANGEMENT (ANY-HEVC)

### 4.2.1. INTER-VIEW PREDICTION FOR ANY CAMERA ARRANGEMENT

This section describes the modified inter-view prediction by the use of 3D point mapping, which is the core of the ANY-HEVC codec. It is assumed that all camera parameters are known and represented by intrinsic parameters gathered in matrix  $\mathbb{K}$  (4.1), and extrinsic parameters, i.e., rotation matrix  $[3 \times 3]$   $\mathbb{R}$  and 3-component translation vector  $[3 \times 1]$   $\mathbb{T}$ . The derivation of the camera parameters is out of the scope of the dissertation and can be found in [Hartley'03, Cyganek'09, LaValle'20].

$$\mathbb{K} = \begin{bmatrix} f_x & c & o_x \\ 0 & f_y & o_y \\ 0 & 0 & 1 \end{bmatrix}, \quad (4.1)$$

where:

$f_x, f_y$  – focal lengths,

$o_x, o_y$  – coordinates of the optical center,

$c$  – skew factor.

The abovementioned intrinsic and extrinsic camera parameters can be used to calculate the projection matrix  $[4 \times 4]$   $\mathbb{P}$  for each camera using Equation (4.2) [Hartley'03]:

$$\mathbb{P} = \begin{bmatrix} \mathbb{K} & 0 \\ 0^T & 1 \end{bmatrix} \begin{bmatrix} \mathbb{R} & -\mathbb{R} \cdot \mathbb{T} \\ 0^T & 1 \end{bmatrix}. \quad (4.2)$$

Then, the positions of the corresponding points in two camera views (denoted by indices 1 and 2) can be derived according to Formula (4.3) [Hartley'03]

$$\begin{bmatrix} z_2 \cdot x_2 \\ z_2 \cdot y_2 \\ z_2 \\ 1 \end{bmatrix} = \mathbb{P}_2 \cdot \mathbb{P}_1^{-1} \begin{bmatrix} z_1 \cdot x_1 \\ z_1 \cdot y_1 \\ z_1 \\ 1 \end{bmatrix}, \quad (4.3)$$

where:

$(x_1, y_1), (x_2, y_2)$  – positions of corresponding points in Views 1 and 2,

$z_1, z_2$  – distances between the acquired point in 3D space and the planes of Camera 1 and 2, respectively, calculated from depth map sample values using Formula (2.2),

$\mathbb{P}_1, \mathbb{P}_2$  – projection matrices for Views 1 and 2.

The Formula (4.3) allows to project any point  $(x_1, y_1, z_1)$  from the plane of Camera 1 directly onto the plane of Camera 2, resulting in point  $(x_2, y_2, z_2)$ . This operation, in the dissertation referred to as 3D point mapping, is used in the ANY-HEVC codec instead of simple depth-to-disparity mapping from 3D-HEVC. The description of the modifications is presented in Sections 4.2.2 – 4.2.4, and their evaluation is presented in Section 4.3.

#### 4.2.2. MODIFIED DISPARITY COMPENSATED PREDICTION

This section describes the modification of Disparity Compensated Prediction (DCP) in ANY-HEVC. As mentioned in Section 2.2, in 3D-HEVC, a disparity vector has only one (horizontal) component derived directly from camera parameters and a given depth map sample through Equation (2.1). In ANY-HEVC, modified DCP uses 3D point mapping to project the position  $(x_1, y_1)$  of the coded block of samples onto the reference view, resulting in a new position  $(x_2, y_2)$ , as presented in Figure 4.2.

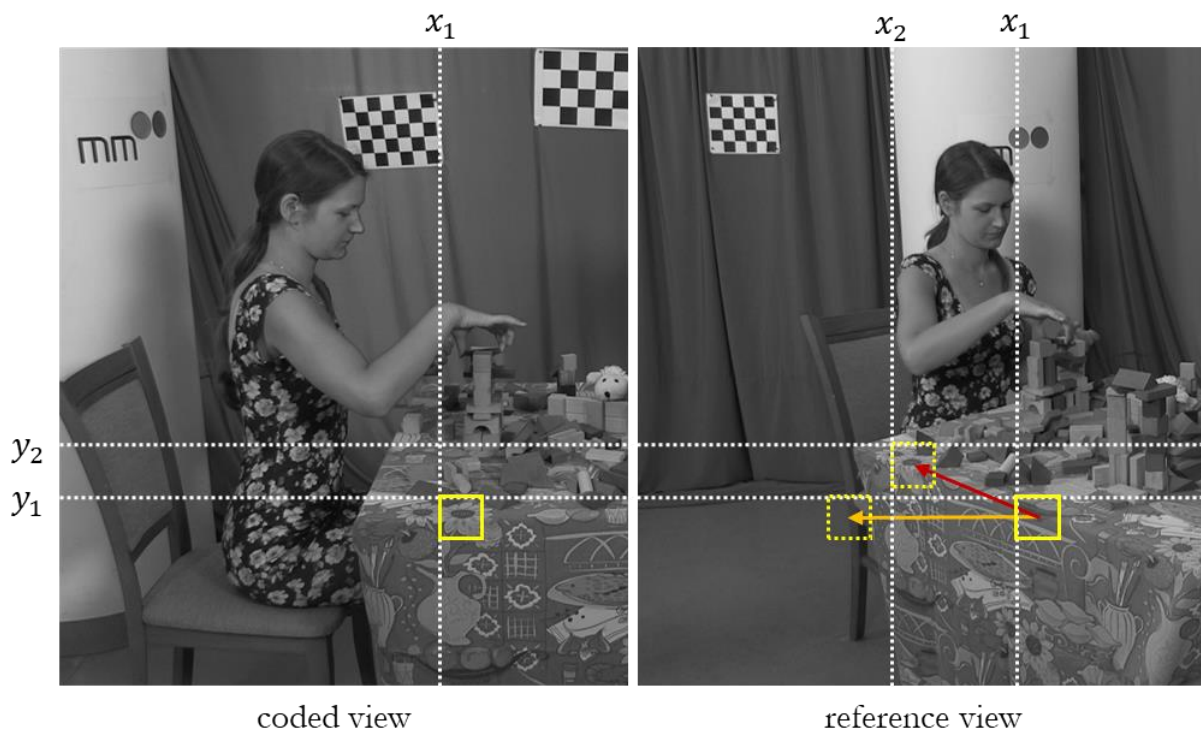


Figure 4.2. Visualization of disparity vectors in 3D-HEVC (orange) and ANY-HEVC (red) and the corresponding predicted blocks of samples (yellow dotted squares) in a multiview video acquired by nearly-circular camera arrangement, Poznan\_Blocks sequence.

The difference in the position of the corresponding points in Views 1 and 2 is then used to find the 2-dimensional disparity vector  $(d_x, d_y)$  according to Equation (4.4):

$$\begin{aligned} d_x &= x_2 - x_1, \\ d_y &= y_2 - y_1. \end{aligned} \tag{4.4}$$

The example presented in Figure 4.2 shows that the unmodified DCP from 3D-HEVC can be highly inaccurate when applied to nearly-circular multiview video. First, it is caused by the lack of a vertical component of disparity vector. Secondly, the 3D-HEVC codec does not take into account camera rotation, so the length of the horizontal component of disparity vector can also be incorrect.

On the other hand, adding the vertical component of disparity vector, as proposed in ANY-HEVC, requires more bits to be transmitted in the bitstream. Therefore, to be beneficial, the more accurate DCP should compensate for the overhead caused by 2D disparity vectors. Naturally, this may decrease the rate-distortion compression efficiency when using ANY-HEVC to compress multiview video acquired by linear camera arrangements. The evaluation of such a case is presented in Section 4.3.

### 4.2.3. MODIFIED INTER-VIEW PREDICTION TOOLS

As a consequence of introducing in ANY-HEVC a non-zero vertical component of disparity vector, several inter-view prediction tools have to be adapted to make use of 2D disparity vectors.

One of the tools to be updated is Inter-View Motion Prediction. In 3D-HEVC, motion vectors can be predicted from the reference view, from the position of the collocated block shifted by disparity. In the proposal, the disparity is a two-dimensional vector, therefore the derivation of the position of the collocated block needs to be changed. Moreover, 3D-HEVC assumes that the cameras capturing the scene are densely distributed on a line with parallel optical axes, hence the motion appears to be the same in each view. However, when the cameras are distributed arbitrarily, the motion direction may be different for each view (Figure 4.3).

In order to correctly predict motion in the case of non-linear camera arrangements, motion vectors predicted from the reference view have to be distorted according to the change of perspective between the cameras. In the proposed solution, both points  $a_1$  and  $b_1$  that indicate the motion vector are projected onto corresponding points  $a_2$  and  $b_2$  in the target view, and the difference  $b_2 - a_2$  results in the new motion vector.

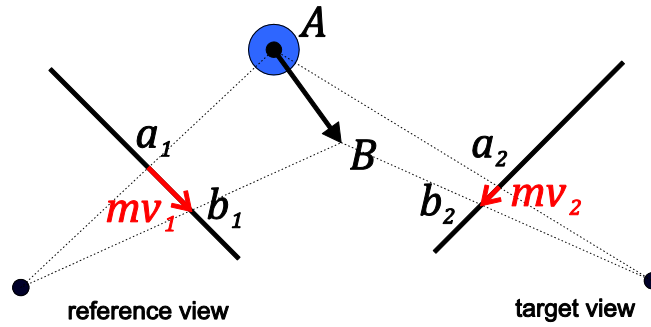


Figure 4.3. Different motion vectors representing the same motion in the reference and target views.

Other tools that are updated to make use of two-dimensional disparity vectors are View Synthesis Prediction, Neighboring Block Disparity Vector, Depth-oriented Neighboring Block Disparity Vector, and Illumination Compensation. In all of the aforementioned tools, the standard approach of mapping depth to disparity is replaced with the projection of depth sample value at a given position in the view, using the 3D point mapping presented in Section 4.2.1.

#### 4.2.4. MODIFIED BITSTREAM SYNTAX

As mentioned in Section 4.2.1, inter-view prediction through 3D point mapping requires all camera parameters, and they also have to be available for the decoder. Therefore, ANY-HEVC encoder has to include them in the bitstream. However, floating point numbers have to be transmitted in the bitstream at finite precision. Therefore, each camera parameter would suffer from rounding errors that would accumulate when calculating projection matrices for 3D point mapping. To avoid that, ANY-HEVC codec transmits the components of projection matrices for each view instead of raw camera parameters [Samelak'16]. Additionally, the precision of the aforementioned components is adjusted dynamically in such a way that the rounding errors do not exceed 0.05%. Precision coefficients are also added to the bitstream.

Depending on whether the parameters change in time or not, ANY-HEVC transmits the projection matrices either in Video Parameter Set or Slice Header [ISO'21]. The updated syntax for both cases is presented in Table 4.1 and Table 4.2.

The presence of additional parameters in the bitstream results in an increased bitrate after ANY-HEVC compression compared to the state-of-the-art 3D-HEVC. In the case of camera arrangements other than linear, this overhead may be reduced by better prediction. However, for linear camera arrangements, such representation is redundant and leads to decreased RD compression efficiency (see Section 4.3).

Table 4.1. ANY-HEVC modified syntax for transmission of camera parameters in Video Parameter Set (VPS).

|  | Value |
|--|-------|
| vps_3d_extension() {                       |       |
| <b>cp_precision</b>                        | ue(v) |
| for (n = 0; n < NumViews; n++) {           |       |
| i = ViewOIdxList[n]                        |       |
| <b>cp_in_slice_segment_header_flag[i]</b>  | u(1)  |
| if (!cp_in_slice_segment_header_flag[i]) { |       |
| <b>vps_cp_znear[i]</b>                     | se(v) |
| <b>vps_cp_zfar[i]</b>                      | se(v) |
| for (j=0; j<12; j++)                       |       |
| <b>vps_cp_projection_matrix[i][j]</b>      | se(v) |
| for (j=0; j<12; j++)                       |       |
| <b>vps_cp_projection_matrix_prec[i][j]</b> | ue(v) |
| }  |       |
| }  |       |
| }  |       |

Table 4.2. ANY-HEVC modified syntax for transmission of camera parameters in Slice Header.

|  | Value |
|--|-------|
| if( cp_in_slice_segment_header_flag[ ViewIdx ] ) { |       |
| for ( i=0; i<num_cp[ ViewIdx ]; i++) {             |       |
| <b>cp_znear[i]</b>                                 | se(v) |
| <b>cp_zfar[i]</b>                                  | se(v) |
| for (j=0; j<12; j++)                               |       |
| <b>cp_projection_matrix[i][j]</b>                  | se(v) |
| for (j=0; j<12; j++)                               |       |
| <b>cp_projection_matrix_prec[i][j]</b>             | ue(v) |
| }  |       |
| }  |       |
| }  |       |

### 4.3. EVALUATION OF ANY-HEVC CODEC IN COMPRESSION OF MULTIVIEW VIDEO ACQUIRED BY VARIOUS CAMERA ARRANGEMENTS

In the previous section, it is stated that using full 3D point mapping in ANY-HEVC provides an accurate inter-view prediction, regardless of the arrangement of the cameras used to capture the scene. On the other hand, the disparity vector in DCP becomes a two-dimensional vector, which requires transmission of the additional component in the bitstream. Moreover, such complex inter-view prediction requires additional camera parameters to be also added to the bitstream. This section presents an experimental comparison of rate-distortion compression efficiency between ANY-HEVC and the standard techniques: HEVC simulcast, MV-HEVC, and 3D-HEVC. The goal is to verify how the camera arrangement and the number of views influence the bitrate at a given quality.

The experiments are performed on 7 linear and 4 nearly-circular sequences. Details for the used sequences can be found in Chapter 3. It should be stressed that nearly-circular

sequences are not rectified to an ideal circle – that case is considered later in the chapter in Sections 4.4 – 4.6. The experiments are performed in Random Access configuration, according to the appropriate Common Test Conditions, as described in Chapter 3. Detailed configuration is presented in Table 4.3.

Table 4.3. Configuration details used for the experiments.

| Parameter   | Value              |
|---|--------------------|
| Number of coded frames                            | 50                 |
| QP for views                                      | 25, 30, 35, 40     |
| QP for depth maps                                 | 34, 39, 42, 45     |
| Sample Adaptive Offset                            | on                 |
| View Synthesis Prediction                         | on (if applicable) |
| View Synthesis Optimization                       | off                |
| Inter-view Motion Prediction                      | on (if applicable) |
| Neighboring Block Disparity Vector                | on (if applicable) |
| Depth-oriented Neighboring Block Disparity Vector | on (if applicable) |

The results for linear camera arrangements are presented in Table 4.4, whereas Table 4.5 gathers the results for nearly-circular camera arrangements. In both cases, HEVC simulcast encoding is used as the reference. Bitrate reduction is expressed as BD-rate for luma samples, as described in Chapter 3.

Table 4.4. Bitrate reduction for compression of 3 views acquired by linear camera arrangements, compared to simulcast HEVC. Negative values indicate lower bitrates at the same quality.

| Sequence       | MV-HEVC        | 3D-HEVC        | ANY-HEVC       |
|----------------|----------------|----------------|----------------|
| Poznan_Hall2   | -30.60%        | -36.44%        | -36.36%        |
| Poznan_Street  | -43.24%        | -46.20%        | -46.19%        |
| Dancer         | -49.27%        | -52.20%        | -52.19%        |
| Kendo          | -32.99%        | -41.75%        | -41.68%        |
| Ballons        | -32.19%        | -39.30%        | -39.26%        |
| Newspaper      | -35.12%        | -38.66%        | -38.59%        |
| <b>Average</b> | <b>-37.23%</b> | <b>-42.43%</b> | <b>-42.38%</b> |



Table 4.5. Bitrate reduction for nearly-circular camera arrangements, compared to simulcast HEVC. Negative values indicate lower bitrates at the same quality.

| Sequence       | 3 views        |                |                | 5 views        |                |                | 7 views        |                |                |
|----------------|----------------|----------------|----------------|----------------|----------------|----------------|----------------|----------------|----------------|
|                | MV-HEVC        | 3D-HEVC        | ANY-HEVC       | MV-HEVC        | 3D-HEVC        | ANY-HEVC       | MV-HEVC        | 3D-HEVC        | ANY-HEVC       |
| Ballet         | -19.72%        | -21.78%        | -26.35%        | -23.64%        | -26.16%        | -31.80%        | -24.32%        | -27.58%        | -33.52%        |
| Breakdancers   | -21.84%        | -25.87%        | -30.00%        | -29.72%        | -33.15%        | -38.65%        | -31.21%        | -34.43%        | -40.36%        |
| BBB_Flowers    | -5.59%         | -5.69%         | -8.00%         | -7.33%         | -7.20%         | -9.79%         | -8.47%         | -8.22%         | -10.74%        |
| Poznan_Blocks  | -13.65%        | -12.77%        | -16.72%        | -15.95%        | -14.53%        | -19.23%        | -16.45%        | -14.51%        | -19.64%        |
| <b>Average</b> | <b>-15.20%</b> | <b>-16.53%</b> | <b>-20.27%</b> | <b>-19.16%</b> | <b>-20.26%</b> | <b>-24.86%</b> | <b>-20.11%</b> | <b>-21.19%</b> | <b>-26.06%</b> |

The results for linear camera arrangements (Table 4.4) prove that the dedicated techniques for multiview video compression provide significant gain compared to independent compression of each view. As expected, the smallest gain of roughly 37% is reported for MV-HEVC as it does not utilize the information about depth to improve inter-view prediction. The most significant reduction in the bitrate is achieved for the state-of-the-art 3D-HEVC, which is dedicated to linear camera arrangements. In the case of ANY-HEVC, it is nearly as effective as the standard 3D-HEVC. The slight difference in favor of 3D-HEVC is caused by the increased number of camera parameters used in ANY-HEVC.

Regarding nearly-circular camera arrangements (Table 4.5), the bitrate reduction is noticeably smaller than in the case of linear arrangements. This is caused by the sparse distribution of cameras and the relatively significant perspective difference between the views, which leads to less accurate inter-view prediction. Similarly to the compression of linear sequences, MV-HEVC reports the smallest bitrate reduction compared to the HEVC simulcast. 3D-HEVC is a more efficient technique, however, the difference is not outstanding. This indicates that due to the assumption of linear camera arrangement, 3D-HEVC is inefficient for compression of multiview video captured with camera arrangements other than linear. A more significant gain is observed for ANY-HEVC at the cost of complex inter-view prediction using 3D point mapping.

Another conclusion from the results presented in Table 4.5 is that the more views are coded, the bigger the bitrate reduction is. This is caused by the increasing contribution of inter-view prediction in the coding process. Depending on the sequence, the gain can be as high as 40% for the compression of 7 views using ANY-HEVC. Therefore, multiview video acquired

using camera arrangements other than linear can also be efficiently compressed using advanced inter-view prediction techniques.

Table 4.6 presents the comparison of the encoding times for different multiview codecs in reference to the HEVC simulcast. The encoding in all cases was performed on the same number of views, i.e., the depth maps were also encoded using HEVC simulcast and MV-HEVC, even though they are not required for compression of views acquired by cameras.

Table 4.6. Encoding time change for compression of 7 views acquired by nearly-circular camera arrangements, compared to simulcast HEVC. Positive values indicate longer encoding.

| Sequence       | MV-HEVC       | 3D-HEVC        | ANY-HEVC       |
|----------------|---------------|----------------|----------------|
| Ballet         | 113.51%       | 168.27%        | 191.52%        |
| Breakdancers   | 85.95%        | 209.89%        | 216.17%        |
| BBB_Flowers    | 98.35%        | 190.97%        | 225.61%        |
| Poznan_Blocks  | 59.69%        | 95.10%         | 106.22%        |
| <b>Average</b> | <b>89.38%</b> | <b>166.06%</b> | <b>184.88%</b> |

The results in Table 4.6 show that the processing time of the dedicated multiview video encoders is much longer than when using simulcast encoding. This is caused by the inter-view prediction techniques that incorporate complex algorithms to improve the rate-distortion compression efficiency at the cost of longer computational time. For example, MV-HEVC provides roughly 20% bitrate reduction (Table 4.5) at the cost of encoding time increased by, on average, 90%.

In the case of nearly-circular camera arrangements, ANY-HEVC provides the biggest bitrate reduction, but on the other hand, this encoder is also the slowest due to the complex 3D point mapping. However, the author observed that if the cameras were distributed ideally on a circle, i.e., the acquired views were circularly rectified, the inter-view prediction could be simplified, and thus the encoding time could be reduced. This idea is presented in the following sections of this chapter.

## 4.4. CIRCULAR RECTIFICATION

### 4.4.1. INTRODUCTION

In the dissertation, the author proposes an efficient modification of the 3D-HEVC codec for processing circularly rectified 3D video (multiview video with depth, MVD) and the procedure for circular rectification. Acquisition systems with multiple cameras sparsely distributed around the scene have already been successfully set up and used to record some of the publicly available 3D video test sequences [Suzuki'09, Stankiewicz'18, Domański'15B, Domański'16B]. Setting up such a multi-camera system is even more challenging than in the case of linear camera arrangements. In practice, the cameras are never located ideally in a circle. The goal of the author's circular rectification is to correct the imperfections of camera positioning in a nearly-circular camera arrangement. This allows preparing an original codec (ARC-HEVC) with simplified inter-view prediction (compared to ANY-HEVC), dedicated to compression of circularly rectified multiview video (Figure 4.4). Such an approach is dual to 3D-HEVC, however the assumption of circular camera arrangement instead of linear is more useful in various applications, as described in Section 4.1.

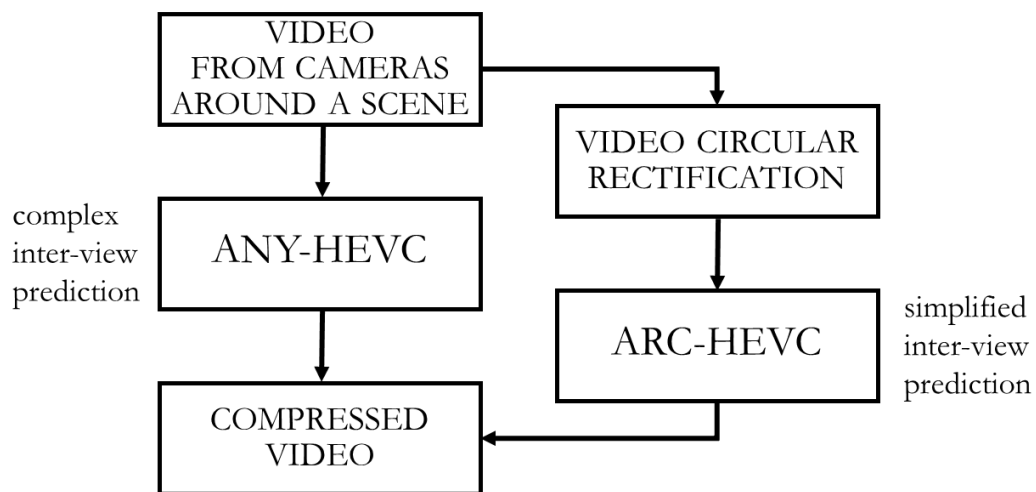


Figure 4.4. Two approaches to compression of multiview video acquired using systems with nearly-circular camera arrangements.

In the dissertation, circular rectification is not considered as a part of ARC-HEVC, but rather as a post-processing phase after capturing multiview video. It is in line with 3D-HEVC where the input video is expected to already be rectified. Therefore, the performance of the proposed circular rectification is not taken into account when comparing ARC-HEVC with other compression techniques.

The proposed circular rectification transforms the original MVD data and results in the multiview video with depth maps virtually obtained from cameras located on an ideal circle and with optical axes collocated on a single plane and intersecting in the center of the circle (Figure 4.5).

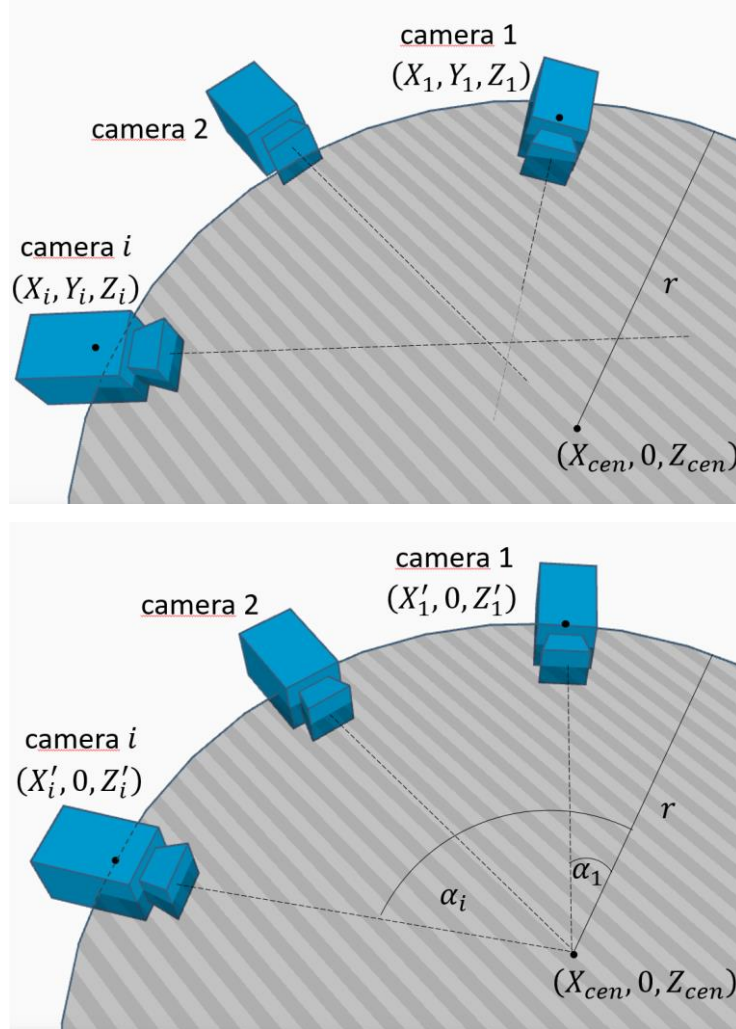


Figure 4.5. Circular camera setup before (top) and after (bottom) the proposed rectification.

The procedure for the proposed circular rectification of the multiview video is based on the equation for 3D point mapping (Equation (4.3)) between the original and the rectified view and is defined as follows:

$$\forall \left\{ \begin{array}{l} x \in \mathbb{Z} : 0 \leq x < W, \\ y \in \mathbb{Z} : 0 \leq y < H \end{array} \right\}, \quad \begin{bmatrix} z_{x',y'} \cdot x' \\ z_{x',y'} \cdot y' \\ z_{x',y'} \\ 1 \end{bmatrix} = \mathbb{P}_{circle} \cdot \mathbb{P}_{org}^{-1} \begin{bmatrix} z_{x,y} \cdot x \\ z_{x,y} \cdot y \\ z_{x,y} \\ 1 \end{bmatrix}, \quad (4.5)$$

where:

$(x, y), (x', y')$  – positions of corresponding points in the original and rectified views,

$z_{x,y}, z_{x',y'}$  – distances between the point in 3D space and the planes of the original and the rectified view, respectively, calculated from depth map sample values using Formula (2.2),

$\mathbb{P}_{org}, \mathbb{P}_{circle}$  – projection matrices for the original and the rectified view, respectively,

$W, H$  – width and height of the original view,

$\mathbb{Z}$  – set of integer numbers.

For each position of a sample in the original image, the corresponding position in the rectified image is derived along with the distance to the rectified image plane, and the view sample is copied. It is possible that multiple positions from the original view are projected onto the same position in the rectified view – in such a case, the point closest to the image plane is picked as the rectified sample. If multiple samples are equally distant, they are averaged. If the rectified view contains empty samples after processing the whole original view, missing samples are interpolated from the surrounding content.

The projection matrix of the original view ( $\mathbb{P}_{org}$ ) is known and can be derived from the input camera parameters using Equation (4.2). The derivation of the projection matrix of the rectified view ( $\mathbb{P}_{circle}$ ) is presented in Sections 4.4.2 – 4.4.4.

#### 4.4.2. DERIVATION OF NEW CAMERA POSITIONS

This section presents the derivation of the parameters of the circle that best fits the original positions of the cameras, as well as the positions of the virtual cameras capturing the rectified views. The circle is represented by the position of its center  $(X_{cen}, 0, Z_{cen})$  and radius  $r$ . In order to find the aforementioned parameters, the author uses circle Equation (4.6) with positions  $(X_i, 0, Z_i)$  of each of the  $N$  cameras, and performs non-linear regression by minimizing the sum of squares  $S$  according to Equation (4.7).

$$(X_i - X_{cen})^2 + (Z_i - Z_{cen})^2 = r^2 \quad (4.6)$$

$$S = \sum_{i=1}^N (\sqrt{(X_i - X_{cen})^2 + (Z_i - Z_{cen})^2} - r)^2 \quad (4.7)$$

It should be noted that vertical positions are ignored ( $Y_{cen} = 0, Y_i = 0$ ) because the proposed rectification assumes that all cameras, as well as the center of the circle, are located at the same height.

After the derivation of circle parameters, i.e., the position of its center ( $X_{cen}, 0, Z_{cen}$ ) and radius  $r$ , the next step is to find for each camera its modified position ( $X'_i, 0, Z'_i$ ) on the circle, the closest to the original location. That position lies on a line appointed by the circle center and the original position of a camera and can be derived using Thales theorem:

$$\frac{r}{\sqrt{(X_i - X_{cen})^2 + (Z_i - Z_{cen})^2}} = \frac{X'_i - X_{cen}}{X_i - X_{cen}} . \quad (4.8)$$

Therefore:

$$X'_i = X_{cen} + \frac{X_i - X_{cen}}{\sqrt{(X_i - X_{cen})^2 + (Z_i - Z_{cen})^2}} \cdot r . \quad (4.9)$$

The rectified position along axis  $Z$  can then be derived from the circle equation (Equation (4.6)):

$$Z'_i = Z_{cen} + \sqrt{r^2 - (X'_i - X_{cen})^2} . \quad (4.10)$$

**EXAMPLE:**

Figure 4.6 presents an example of the correction of camera positions of one of the real 3D video test sequences - *Breakdancers*. It can be noticed that the differences are not significant; the cameras before rectification are located roughly on a circle. Table 4.7 presents a statistical analysis of the correction of camera positions. It can be seen that the positions of the *BBB\_Flowers* sequence are not corrected at all because that sequence is rendered, and therefore the original camera positions are already positioned ideally on a circle. For the remaining sequences, the difference is still not major and does not exceed 1.5% of the circle radius. Therefore, it is a sensible approach to rectify those viewpoints to a circle and adapt 3D-HEVC to circular camera arrangements.

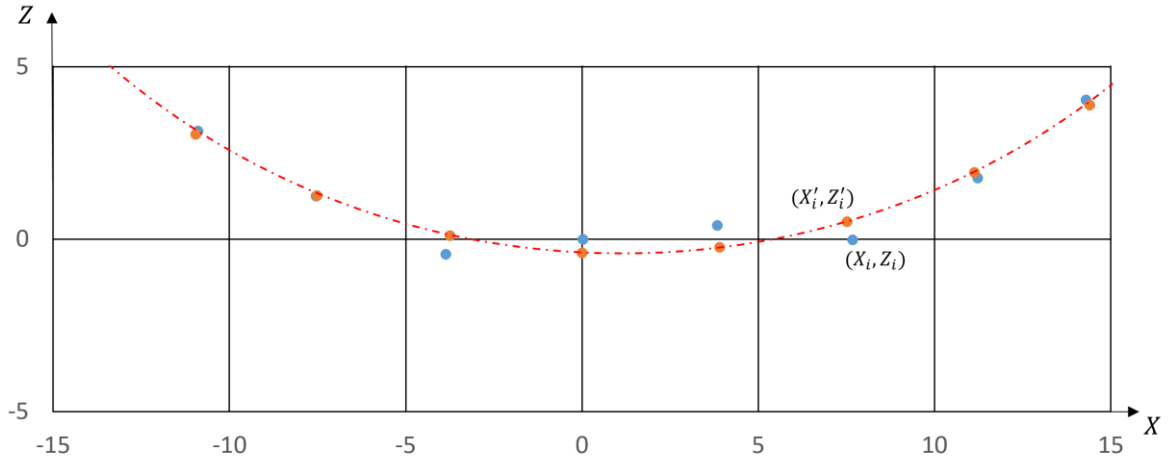


Figure 4.6. Top view of a multi-camera system with original camera positions (blue dots) and corrected to an ideal circle (orange dots). Breakdancers test sequence.

Table 4.7. The average difference between the camera positions before and after rectification, standard deviation, and the ratio of the average difference to the circle radius.

| Sequence      | average difference between original and rectified camera positions $\Delta(x,z)$ | standard deviation of $\Delta(x,z)$ | average difference to radius ratio $\Delta(x,z) / r$ |
|---------------|--|-------------------------------------|--|
| Ballet        | 0.2458   | 0.2142                              | 0.93%  |
| Breakdancers  | 0.3282   | 0.2209                              | 1.45%  |
| BBB_Flowers   | 0.0000   | 0.0000                              | 0.00%  |
| Poznan_Blocks | 0.1177   | 0.0992                              | 0.61%  |

#### 4.4.3. CAMERA ROTATION IN THE IDEALLY CIRCULAR ARRANGEMENT

In the proposed process of circular rectification, the goal is not only to correct the locations of the cameras but also to direct their optical axes precisely toward the center of a circle derived in the previous subsection. To achieve that, modification of rotation matrices is necessary.

The rotation matrix  $\mathbb{R}$  represents the combined rotation of a camera around three orthogonal axes. In the ideally circular arrangement, optical axes are assumed to be on a single plane. Such camera rotation can be represented by the following matrix (4.11):

$$\mathbb{R}'_i = \begin{bmatrix} \cos \alpha_i & 0 & -\sin \alpha_i \\ 0 & 1 & 0 \\ \sin \alpha_i & 0 & \cos \alpha_i \end{bmatrix}, \quad (4.11)$$

where  $\alpha_i$  is the angle between the direction of the  $i$ -th camera optical axis and circle radius along  $Z$  axis (Figure 4.5), therefore:

$$\cos \alpha_i = \frac{Z_{cen} - Z'_i}{r}, \quad \sin \alpha_i = \frac{X_{cen} - X'_i}{r}. \quad (4.12)$$

All the necessary parameters: circle center position  $(X_{cen}, Z_{cen})$  and its radius  $r$ , as well as the modified  $i$ -th camera position  $(X'_i, Z'_i)$  are already derived, thus there is no need to transmit more camera parameters in the bitstream to find the rotation matrix of rectified cameras.

#### 4.4.4. MODIFICATION OF THE INTRINSIC CAMERA PARAMETERS

Previous subsections 4.4.2 – 4.4.3 present the process of deriving extrinsic parameters of cameras located on an ideal circle. This subsection describes how the internal camera parameters are evaluated in the proposed circular rectification process.

First, the skew factor is set to  $\mathbf{c} = \mathbf{0}$ . As mentioned in Section 3.4, it is assumed that the cameras are calibrated, which includes correction of the skew factor. The same assumption is made in the state-of-the-art 3D-HEVC [Domański'13, Müller'13]. Next, the focal lengths  $f_x, f_y$  and the vertical component of the principal point  $\mathbf{o}_y$  are averaged and set equal for every camera, resulting in  $f'_x, f'_y$  and  $\mathbf{o}'_y$ . The same approximation is done in 3D-HEVC. However, since 3D-HEVC assumes that the views are coplanar and vertically aligned, the values of  $f_y$  and  $\mathbf{o}_y$  are not used at all (there is no vertical component in the inter-view prediction). A more sophisticated approach is required to derive the horizontal component of the principal point  $\mathbf{o}'_x$ . The cameras in a nearly-circular arrangement are usually directed toward the center of the recorded scene, which can be (and often is) much closer to the cameras than the center of a circle. Therefore, due to the modification of rotation matrices towards the center of a circle, the field of view of a camera can be significantly misaligned with the field of view of the original camera. This can result in only a small portion of the original field of view being covered by a given camera after circular rectification (Figure 4.7). In such a case, rectified views would contain only a small part of the original content, which is highly unwanted (Figure 4.8).



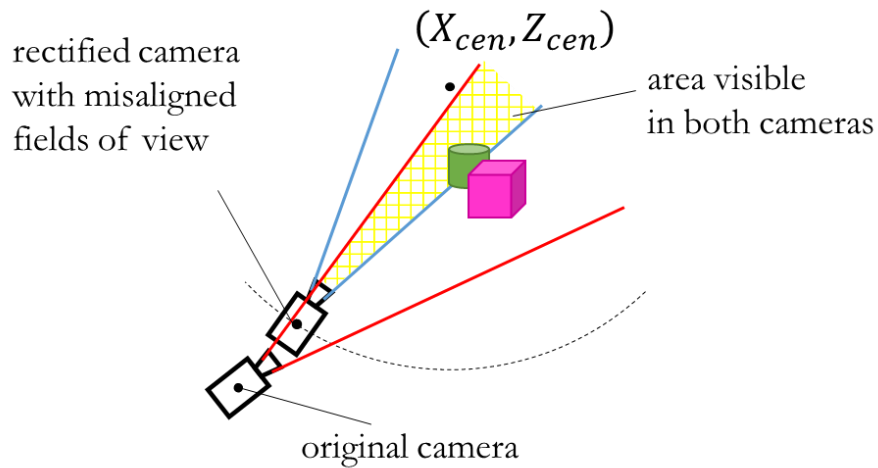


Figure 4.7. The problem with the misaligned fields of view after circular rectification.



Figure 4.8. A real example of the problem with the misaligned fields of view after circular rectification, Breakdancers test sequence. View number 4 (left) is slightly misaligned, and view number 6 (right) is significantly rotated towards the center of a circle but outside the center of the acquired scene.

Cancellation of the misalignment of the field of view can be achieved not only by rotating the camera itself but also by changing its principal point (Figure 4.9) [Hou'20, Hartley'03]. In the proposed circular rectification technique, the component  $o'_x$  of the rectified principal is calculated for each camera to assert roughly the coverage of the recorded scene before rectification. It is done by projecting a point equal to the original optical center  $(o_x, o_y)$  from the original view onto rectified camera plane. If the projected point is not located at the optical center, the difference between  $o_x$  and its projection is added to  $o'_x$  of rectified camera parameters. Therefore, the optical axes of original and projected cameras are directed at the same point in 3D space and rectification of the rotation matrix is compensated.

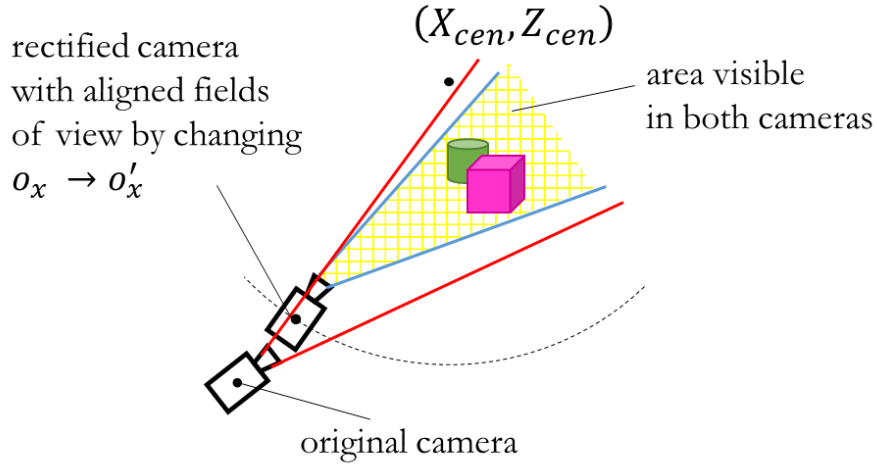


Figure 4.9. Rectified camera directed towards circle center and with the modified optical center  $o'_x$  to align its field of view with the original camera.

#### 4.4.5. RECTIFICATION OF VIDEO AND DEPTH

After deriving circular camera parameters, multiview video can be rectified by performing 3D point mapping for every view of a sequence using Equation (4.5). This requires the calculation of projection matrices  $\mathbb{P}_{org}$  (for original parameters) and  $\mathbb{P}_{circle}$  (for circular parameters). Projection matrix for the original camera ( $\mathbb{P}_{org}$ ) is calculated using all camera parameters according to Formula (4.2). Projection matrix for the rectified camera ( $\mathbb{P}_{circle}$ ) is calculated using rectified camera parameters derived in Sections 4.4.2 – 4.4.4 and, for each view, is represented by Formula (4.13):

$$\mathbb{P}_{circle} = \begin{bmatrix} f'_x & 0 & o'_x & 0 \\ 0 & f'_y & o'_y & 0 \\ 0 & 0 & 1 & 0 \\ 0 & 0 & 0 & 1 \end{bmatrix} \begin{bmatrix} \cos \alpha & 0 & -\sin \alpha & -X' \cos \alpha + Z' \sin \alpha \\ 0 & 1 & 0 & 0 \\ \sin \alpha & 0 & \cos \alpha & -X' \sin \alpha - Z' \cos \alpha \\ 0 & 0 & 0 & 1 \end{bmatrix}. \quad (4.13)$$

As mentioned before, a rectified view may contain some unfilled areas – these are interpolated from surrounding content. The author of the dissertation prepared **an original software for circular rectification**, which calculates rectified camera parameters from original parameters and transforms original MVD data into rectified multiview video with depth. Figure 4.10 presents an example of a frame of a test sequence *Poznan\_Blocks* rectified with the author's software, and the difference image between the original and rectified view. All the views and the corresponding depth maps were rectified and used as input data for the experiments described in Section 4.6.

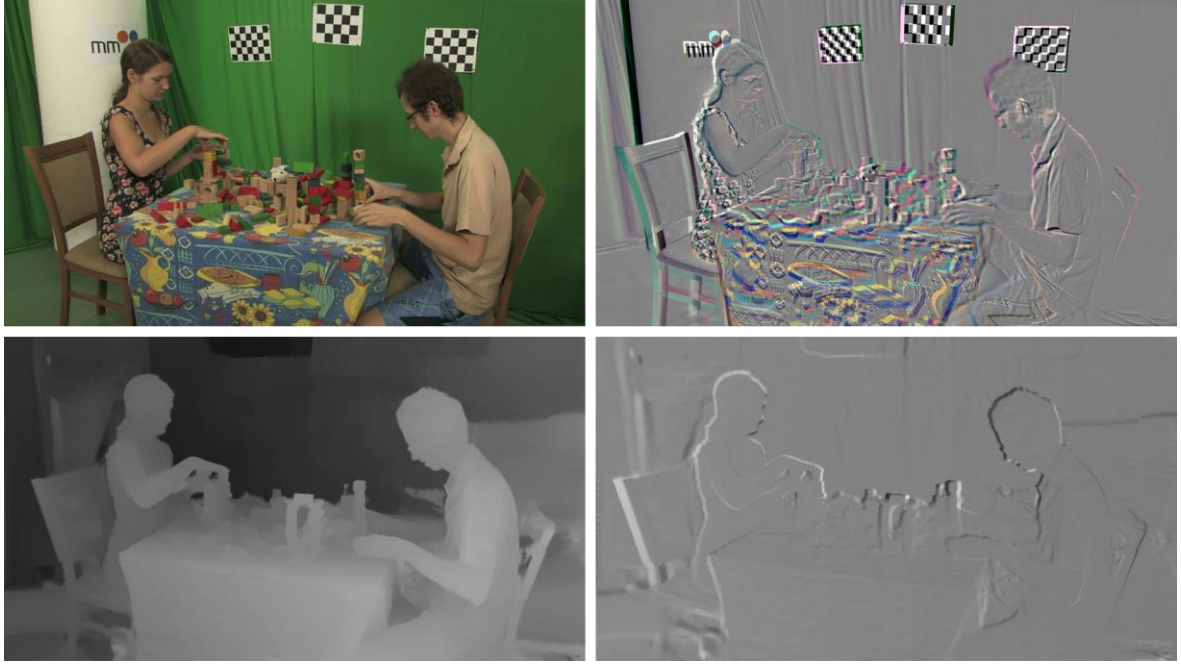


Figure 4.10. Rectified view (top-left), depth map (bottom-left), and the difference between the original and rectified view (top-right) and depth map (bottom-right), Poznan\_Blocks test sequence.

## 4.5. 3D-HEVC ADAPTED TO RECTIFIED CIRCULAR CAMERA ARRANGEMENT (ARC-HEVC)

### 4.5.1. INTER-VIEW PREDICTION FOR RECTIFIED CIRCULAR CAMERA ARRANGEMENT

In the previous section, 3D point mapping was used to project the views from the original camera planes onto planes of virtual cameras positioned ideally on a circle. Such an operation is referred to as circular rectification. In this section, the author proposes to utilize 3D point mapping for inter-view prediction, which is similar to the approach presented in ANY-HEVC. In this case, however, both reference and coded views are rectified, hence their projection matrices (Equation (4.13)) are less complex than the ones in ANY-HEVC (Equation (4.2)). In general, inter-view prediction for rectified circular camera arrangement is defined as follows:

$$\begin{bmatrix} z_2 \cdot x_2 \\ z_2 \cdot y_2 \\ z_2 \\ 1 \end{bmatrix} = \mathbb{P}_{circle\_2} \cdot \mathbb{P}_{circle\_1}^{-1} \begin{bmatrix} z_1 \cdot x_1 \\ z_1 \cdot y_1 \\ z_1 \\ 1 \end{bmatrix}, \quad (4.14)$$

where:

$$\mathbb{P}_{circle\_1} = \begin{bmatrix} f'_x & 0 & o'_{x1} & 0 \\ 0 & f'_y & o'_y & 0 \\ 0 & 0 & 1 & 0 \\ 0 & 0 & 0 & 1 \end{bmatrix} \begin{bmatrix} \cos \alpha_1 & 0 & -\sin \alpha_1 & -X'_1 \cos \alpha_1 + Z'_1 \sin \alpha_1 \\ 0 & 1 & 0 & 0 \\ \sin \alpha_1 & 0 & \cos \alpha_1 & -X'_1 \sin \alpha_1 - Z'_1 \cos \alpha_1 \\ 0 & 0 & 0 & 1 \end{bmatrix}, \quad (4.15)$$

$$\mathbb{P}_{circle\_2} = \begin{bmatrix} f'_x & 0 & o'_{x2} & 0 \\ 0 & f'_y & o'_y & 0 \\ 0 & 0 & 1 & 0 \\ 0 & 0 & 0 & 1 \end{bmatrix} \begin{bmatrix} \cos \alpha_2 & 0 & -\sin \alpha_2 & -X'_2 \cos \alpha_2 + Z'_2 \sin \alpha_2 \\ 0 & 1 & 0 & 0 \\ \sin \alpha_2 & 0 & \cos \alpha_2 & -X'_2 \sin \alpha_2 - Z'_2 \cos \alpha_2 \\ 0 & 0 & 0 & 1 \end{bmatrix}. \quad (4.16)$$

The multiplication of projection matrices  $\mathbb{P}_{circle\_2} \cdot \mathbb{P}_{circle\_1}^{-1}$  results in the following matrix:

$$\mathbb{P}_{circle\_2} \cdot \mathbb{P}_{circle\_1}^{-1} = \quad (4.17)$$

$$= \begin{bmatrix} \cos \Delta\alpha + \frac{o'_{x2}}{f'_x} \sin \Delta\alpha & 0 & (o'_{x2} - o'_{x1}) \cos \Delta\alpha - \left( f'_x + \frac{o'_{x1} o'_{x2}}{f'_x} \right) \sin \Delta\alpha & f'_x (\Delta X' \cos \alpha_2 - \Delta Z' \sin \alpha_2) + \\ & & & + o'_{x2} (\Delta X' \sin \alpha_2 + \Delta Z' \cos \alpha_2) \\ \frac{o'_y}{f'_x} \sin \Delta\alpha & 1 & o'_y \left( -\frac{o'_{x1}}{f'_x} \sin \Delta\alpha + \cos \Delta\alpha - 1 \right) & o'_y (\Delta X' \sin \alpha_2 + \Delta Z' \cos \alpha_2) \\ \frac{1}{f'_x} \sin \Delta\alpha & 0 & -\frac{o'_{x1}}{f'_x} \sin \Delta\alpha + \cos \Delta\alpha & \Delta X' \sin \alpha_2 + \Delta Z' \cos \alpha_2 \\ 0 & 0 & 0 & 1 \end{bmatrix},$$

where:

$\Delta\alpha = \alpha_2 - \alpha_1$  (difference between the angles of optical axes of source and target camera, see Figure 4.4),

$\Delta X' = X'_1 - X'_2$ , the difference between camera positions along axis X,

$\Delta Z' = Z'_1 - Z'_2$ , the difference between camera positions along axis Z.

From Formula (4.12), differences  $\Delta X'$  and  $\Delta Z'$  can be defined as follows:

$$\Delta X' = X'_1 - X'_2 = X_{cen} - r \sin \alpha_1 - X_{cen} + r \sin \alpha_2 = r(\sin \alpha_2 - \sin \alpha_1), \quad (4.18)$$

$$\Delta Z' = Z'_1 - Z'_2 = Z_{cen} - r \cos \alpha_1 - Z_{cen} + r \cos \alpha_2 = r(\cos \alpha_2 - \cos \alpha_1). \quad (4.19)$$

Therefore, Formula (4.17) can be further simplified:

$$\mathbb{P}_{circle_2} \cdot \mathbb{P}_{circle_1}^{-1} = \quad (4.20)$$

$$= \begin{bmatrix} \cos \Delta\alpha + \frac{o'_{x2}}{f'_x} \sin \Delta\alpha & 0 & (o'_{x2} - o'_{x1}) \cos \Delta\alpha - \left( f'_x + \frac{o'_{x1} o'_{x2}}{f'_x} \right) \sin \Delta\alpha & f'_x r \sin \Delta\alpha + o'_{x2} r (1 - \cos \Delta\alpha) \\ \frac{o'_y}{f'_x} \sin \Delta\alpha & 1 & o'_y \left( -\frac{o'_{x1}}{f'_x} \sin \Delta\alpha + \cos \Delta\alpha - 1 \right) & o'_y r (1 - \cos \Delta\alpha) \\ \frac{1}{f'_x} \sin \Delta\alpha & 0 & -\frac{o'_{x1}}{f'_x} \sin \Delta\alpha + \cos \Delta\alpha & r (1 - \cos \Delta\alpha) \\ 0 & 0 & 0 & 1 \end{bmatrix},$$

Equation (4.14) for point mapping between circularly rectified views (View 1 and View 2) may be represented as the following Equations (4.21 – 4.23):

$$z_2 = (x_1 - o'_{x1}) \frac{z_1}{f'_x} \sin \Delta\alpha + (z_1 - r) \cos \Delta\alpha + r, \quad (4.21)$$

$$y_2 = o'_y + \frac{z_1}{z_2} (y_1 - o'_y), \quad (4.22)$$

$$x_2 = o'_{x2} + \frac{1}{z_2} [(x_1 - o'_{x1}) z_1 \cos \Delta\alpha - (z_1 - r) f'_x \sin \Delta\alpha], \quad (4.23)$$

where:

$\Delta\alpha = \alpha_2 - \alpha_1$  (difference between the angles of optical axes of source and target camera, see Figure 4.4),

$(x_1, y_1, z_1)$  – point coordinates in rectified View 1 (reference view),

$(x_2, y_2, z_2)$  – point coordinates in rectified View 2 (target view),

$o'_{x1}, o'_{x2}$  – horizontal components of principal points of rectified Views 1 and 2,

$o'_y$  – averaged vertical component of principal points,

$f'_x$  – averaged horizontal focal length,

$r$  – circle radius.

The above formulas allow to predict the position of a point in View 2 from its position in View 1 and circular camera parameters, provided that both views are circularly rectified. The author of the dissertation modifies the inter-view prediction in 3D-HEVC by replacing standard disparity derivation with point projection that uses the above equations. The description of modifications is presented in the following sections.

#### 4.5.2. MODIFIED DISPARITY COMPENSATED PREDICTION

The disparity vector is calculated similarly as in ANY-HEVC (Section 4.2.2) as a difference between the position of the source sample and its projection in the reference view, according to Equation (4.4). This time, however, the projection is performed using the equations derived in Section 4.5.1. According to Formula (4.22), the vertical component of disparity vector (i.e.,  $d_y = y_2 - y_1$ ) is equal to zero only when the distance between the acquired point and the view plane is equal for both views, i.e.,  $z_2 = z_1$  (Figure 4.11). Otherwise, the DCP in ARC-HEVC works on two-dimensional disparity vectors, similarly to ANY-HEVC.

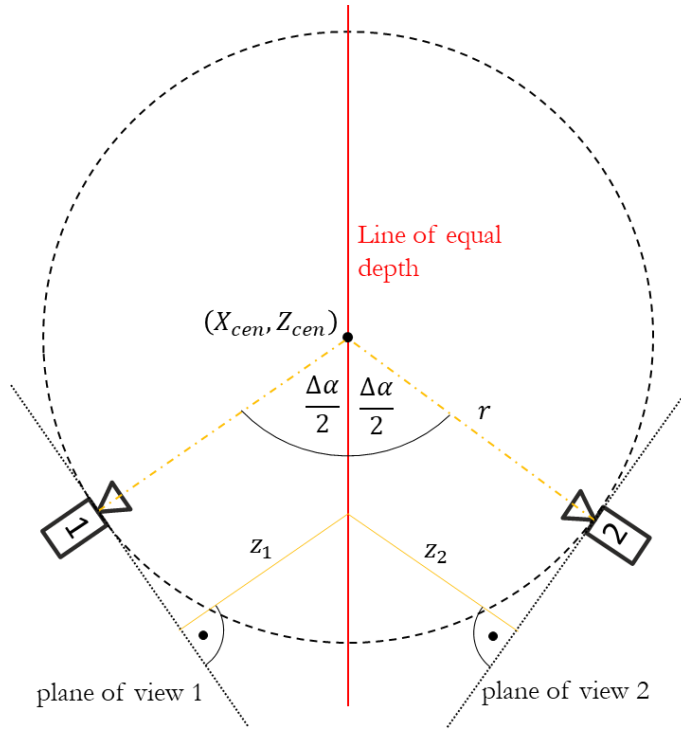


Figure 4.11. Visualization of the line of equal depth for a pair of cameras in a circular arrangement.

#### 4.5.3. MODIFIED INTER-VIEW PREDICTION TOOLS

Analogously to ANY-HEVC, the adaptation of 3D-HEVC to circular camera arrangements requires modification of inter-view coding tools that depend on disparity vectors or prediction of depth. The author of the dissertation applied the 2-dimensional disparity vector

and the proposed equations for inter-view prediction (Section 4.5.1) to the following coding tools:

- Inter-View Motion Prediction,
- View Synthesis Prediction,
- Neighboring Block Disparity Vector,
- Depth-oriented Neighboring Block Disparity Vector,
- Illumination Compensation.

In particular, the most significant change compared to ANY-HEVC is in the prediction of depth samples. In ANY-HEVC, the derivation of depth sample values in the coded view requires complex calculations, and it depends on the depth sample value ( $z_1$ ) in the reference depth map and sample position  $(x_1, y_1)$  in the reference view. In ARC-HEVC, the prediction formula is much simpler (Formula 4.21), and for a given pair of cameras (with constant parameters), it depends on the depth value from the reference view ( $z_1$ ) and only one, horizontal component of the sample position ( $x_1$ ). The author introduced a dedicated caching algorithm that stores in the encoder's memory the value of the predicted depth  $z_2$  for each processed pair of  $(x_1, z_1)$  for future use. It is a similar approach to the look-up tables from 3D-HEVC for mapping depth to disparity. The difference is that in 3D-HEVC, look-up tables are prepared before encoding a view, while in the proposal, they are continuously updated whenever a unique pair of values for  $(x_1, z_1)$  occurs. Nonetheless, such an approach reduces the number of 3D point mappings and therefore, the encoding time.

#### 4.5.4. MODIFIED BITSTREAM SYNTAX

As mentioned before, the proposed solution for efficient compression of circularly rectified video requires more information about the intrinsic and extrinsic camera parameters than 3D-HEVC. These parameters have to be transmitted in the bitstream because the derivation of disparity vectors has to be performed analogously by the decoder. The number of parameters and their representation in the bitstream varies depending on the compression technique.

Table 4.8 compares the parameters used by 3D-HEVC and modified encoders for compression of multiview video acquired with circular (ARC-HEVC) and arbitrary (ANY-HEVC) camera arrangements.

Table 4.8. Camera parameters required by different 3D video coding techniques.

| Parameter name            | 3D-HEVC<br>(linear camera setup) | ARC-HEVC<br>(circular camera setup) | ANY-HEVC<br>(arbitrary camera setup)  |
|---------------------------|----------------------------------|-------------------------------------|---|
| Horizontal focal length   | $f_x$ (1 for all views)          | $f_x$ (1 for all views)             | $f_x$   |
| Vertical focal length     | -                                | -                                   | $f_y$   |
| Horizontal optical center | $o_x$                            | $o_x$                               | $o_x$   |
| Vertical optical center   | -                                | $o_y$ (1 for all views)             | $o_y$   |
| Skew factor               | -                                | -                                   | $c$   |
| Translation               | $t_x$                            | $\alpha,$<br>$r$ (1 for all views)  | $\mathbb{T} = [t_x, t_y, t_z]$  |
| Rotation                  | -                                |                                     | $\mathbb{R} = \begin{bmatrix} r_{11} & r_{12} & r_{13} \\ r_{21} & r_{22} & r_{23} \\ r_{31} & r_{32} & r_{33} \end{bmatrix}$ |

It should be noted that rectified circular camera setup requires much fewer parameters than arbitrary and only two more values than unmodified 3D-HEVC. However, neither 3D-HEVC nor ANY-HEVC transmits the parameters directly. In 3D-HEVC, they are represented as “scale” and “offset” [ISO’21], while ANY-HEVC transmits calculated projection matrices (Section 4.2.4) [Samelak’16]. In the proposed ARC-HEVC, the parameters are included in the bitstream directly and transmitted in the dedicated 3D extension of the Video Parameter Set (Table 4.9) or in the Slice Header (Table 4.10), depending on whether the parameters are constant or change in time. The parameters for  $Z_{near}, Z_{far}$ , as well as metadata parameters (**cp\_precision, cp\_in\_slice\_segment\_header\_flag**) are transmitted in every technique.

Table 4.9. Proposed syntax of VPS extension for ARC-HEVC.

|   |       |
|---|-------|
| vps_3d_extension() {                      | Value |
| <b>cp_precision</b>                       | ue(v) |
| <b>vps_cp_focal_length_x</b>              | se(v) |
| <b>vps_cp_principal_point_y</b>           | se(v) |
| <b>vps_cp_radius</b>                      | se(v) |
| for (n = 0; n < NumViews; n++) {          |       |
| i = ViewOIdxList[n]                       |       |
| <b>cp_in_slice_segment_header_flag[i]</b> | u(1)  |
| if (cp_in_slice_segment_header_flag[i]) { |       |
| <b>vps_cp_znear[i]</b>                    | se(v) |
| <b>vps_cp_zfar[i]</b>                     | se(v) |
| <b>vps_cp_principal_point_x[i]</b>        | se(v) |
| <b>vps_cp_angle[i]</b>                    | se(v) |
| }   |       |
| }   |       |
| }   |       |



Table 4.10. Proposed syntax in Slice Header for ARC-HEVC.

|  |       |
|--|-------|
| if( cp_in_slice_segment_header_flag[ ViewIdx ] ) { | Value |
| cp_focal_length_x                                  | se(v) |
| cp_principal_point_y                               | se(v) |
| cp_radius  | se(v) |
| for ( i=0; i<num_cp[ ViewIdx ]; i++ ) {            |       |
| cp_znear[i]  | se(v) |
| cp_zfar[i]   | se(v) |
| cp_principal_point_x[i]                            | se(v) |
| cp_angle[i]  | se(v) |
| }  |       |
| }  |       |

It should be mentioned that if the camera parameters vary in time, the circular rectification has to be updated accordingly. However, such a case is out of the scope of the dissertation; the parameters of all test sequences used in the evaluation are constant.

The proposed changes in the bitstream result in ARC-HEVC not being compliant with the 3D-HEVC standard. This means that 3D-HEVC is not able to decode the bitstream produced by ARC-HEVC and vice versa. Nevertheless, the author of the dissertation proves that support for rectified circular 3D video compression could be added with only minor changes in the bitstream syntax.

## 4.6. EVALUATION OF THE PROPOSED ARC-HEVC

### 4.6.1. INTRODUCTION

In this section, ARC-HEVC, i.e., modified 3D-HEVC codec for efficient compression of circularly rectified video, is experimentally evaluated and compared to the state-of-the-art 3D-HEVC (designed for linear camera arrangement) and ANY-HEVC, which is the modified 3D-HEVC for arbitrary camera arrangement.

The goal of the experiments is to assess the rate-distortion compression efficiency and encoding time using the aforementioned codecs. Additionally, the author compares the encoding time of only intra-view prediction for both modified 3D-HEVC encoders (ARC-HEVC and ANY-HEVC). The RD compression efficiency is compared by measuring average bitrate reduction for the luma component of input views, using Bjøntegaard metric as described in Chapter 3. The experiments are conducted by encoding 7 rectified views of 4 commonly-used multiview test sequences, listed in Section 3.4. All the input views and the corresponding depth maps are rectified and used as the input for tested codecs (Figure 4.12). Rectified camera parameters and complete results of the conducted experiments can be found in the Appendix.

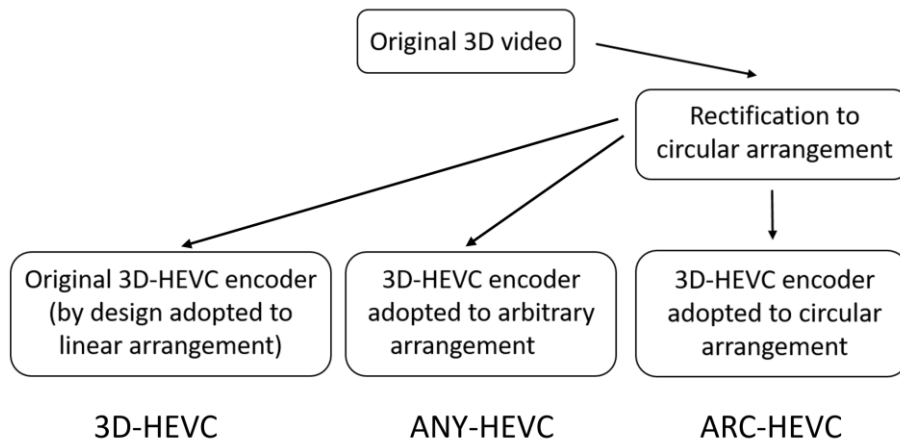


Figure 4.12. Block diagram of the evaluation of tested encoders in compression of circularly rectified video.

The configuration of all three encoders is the same as in the experiment presented in Section 4.3, except that this time the number of encoded frames is equal to 100. The remaining configuration follows Common Test Conditions for 3D video experiments [Müller’14] for Random Access coding scenario. The camera parameters are prepared according to the requirements of each of the encoders (Table 4.8). The rectification of test sequences is done in the pre-processing phase, so it does not affect encoding time results. Moreover, as described in Section 3.2, all three encoders are based on the same version of the 3D-HEVC publicly available test model [HTM].

#### 4.6.2. EXPERIMENTAL RESULTS

This section contains the results of conducted experiments. Table 4.11 shows the comparison of the three in terms of bitrate reduction. **For compression of 7 views, the proposed ARC-HEVC reduces bitrate on average by 6%** compared to the state-of-the-art technique. This is because 3D-HEVC does not perform accurate inter-view prediction if the video was acquired by camera arrangements other than linear. The more views are encoded, the bigger the difference is in favor of ARC-HEVC.

Compared to the encoder that supports arbitrary camera setup, i.e., ANY-HEVC, the solution adapted to circular arrangements provides very similar results. This is expected as both techniques perform an accurate inter-view prediction when the views are circularly rectified. It can be noticed that for a low number of views, ANY-HEVC is slightly better, but for more views, it is the opposite. The difference is caused by a lower number of camera parameters required by the proposed ARC-HEVC and simplified inter-view prediction, which results in a reduced number of rounding errors. Nevertheless, the difference is not significant, therefore **both encoders can be considered equally efficient in terms of compression rate.**

Table 4.11. Bitrate reduction comparison between tested encoders, only for views.  
 Negative values indicate lower bitrates at the same quality.  
 ANY=ANY-HEVC, ARC=ARC-HEVC, 3D=3D-HEVC

| Sequence       | 3 views       |               |              | 5 views       |               |              | 7 views       |               |               |
|----------------|---------------|---------------|--------------|---------------|---------------|--------------|---------------|---------------|---------------|
|                | ANY vs. 3D    | ARC vs. 3D    | ARC vs. ANY  | ANY vs. 3D    | ARC vs. 3D    | ARC vs. ANY  | ANY vs. 3D    | ARC vs. 3D    | ARC vs. ANY   |
| Poznan_Blocks  | -6.31%        | -6.15%        | 0.18%        | -7.76%        | -8.05%        | -0.31%       | -7.93%        | -8.14%        | -0.23%        |
| BBB_Flowers    | -6.87%        | -6.08%        | 0.86%        | -8.62%        | -7.86%        | 0.83%        | -8.96%        | -8.22%        | 0.82%         |
| Ballet         | -2.31%        | -2.30%        | 0.00%        | -2.67%        | -2.94%        | -0.27%       | -2.63%        | -3.15%        | -0.54%        |
| Breakdancers   | -3.70%        | -3.79%        | -0.09%       | -4.32%        | -4.52%        | -0.21%       | -4.39%        | -4.61%        | -0.23%        |
| <b>Average</b> | <b>-4.80%</b> | <b>-4.58%</b> | <b>0.24%</b> | <b>-5.84%</b> | <b>-5.84%</b> | <b>0.01%</b> | <b>-5.98%</b> | <b>-6.03%</b> | <b>-0.05%</b> |

Table 4.12 presents the results for the views and depth maps combined. The relation between the modified encoders, i.e., ARC-HEVC and ANY-HEVC, is not changed. However, when compared to 3D-HEVC, both encoders report slightly lower gains.

Table 4.12. Bitrate reduction comparison between tested encoders, views + depth maps.  
 Negative values indicate lower bitrates at the same quality.  
 ANY=ANY-HEVC, ARC=ARC-HEVC, 3D=3D-HEVC

| Sequence       | 3 views       |               |              | 5 views       |               |              | 7 views       |               |               |
|----------------|---------------|---------------|--------------|---------------|---------------|--------------|---------------|---------------|---------------|
|                | ANY vs. 3D    | ARC vs. 3D    | ARC vs. ANY  | ANY vs. 3D    | ARC vs. 3D    | ARC vs. ANY  | ANY vs. 3D    | ARC vs. 3D    | ARC vs. ANY   |
| Poznan_Blocks  | -5.50%        | -5.38%        | 0.17%        | -6.55%        | -6.76%        | -0.22%       | -6.62%        | -6.81%        | -0.17%        |
| BBB_Flowers    | -6.23%        | -5.57%        | 0.76%        | -7.70%        | -7.10%        | 0.74%        | -7.90%        | -7.32%        | 0.69%         |
| Ballet         | -1.99%        | -2.01%        | -0.04%       | -2.30%        | -2.57%        | -0.29%       | -2.28%        | -2.78%        | -0.51%        |
| Breakdancers   | -3.59%        | -3.68%        | -0.09%       | -4.18%        | -4.37%        | -0.21%       | -4.23%        | -4.44%        | -0.23%        |
| <b>Average</b> | <b>-4.33%</b> | <b>-4.16%</b> | <b>0.20%</b> | <b>-5.18%</b> | <b>-5.20%</b> | <b>0.01%</b> | <b>-5.26%</b> | <b>-5.34%</b> | <b>-0.06%</b> |

Table 4.13 presents the reduction of total encoding time, while Table 4.14 compares the inter-view prediction time between two modified encoders. It should be noted that **the proposed encoder is up to 10% faster than the encoder with full 3D point mapping (ARC-HEVC vs. ANY-HEVC)**. At the same time, its **inter-view prediction is, on average, 44 times faster**, due to much simpler equations for point mapping, optimized for circularly rectified 3D video. Surprisingly, **the proposed encoder is also faster than 3D-HEVC by more than 4%**, even though the inter-view prediction of the former is more complex than the

state-of-the-art technique. The reason for such a phenomenon is related to the results for compression efficiency (Table 4.11). As mentioned before, ARC-HEVC is more accurate in predicting the content of the circularly rectified video. Therefore, it is able to find the best match for the currently encoded unit faster, compensating for the overhead resulting from more complex calculations.

Table 4.13. Encoding time comparison between tested encoders for compression of 7 views. Negative values indicate faster encoding.

| <b>Sequence</b> | <b>ANY-HEVC<br/>vs.<br/>3D-HEVC</b> | <b>ARC-HEVC<br/>vs.<br/>3D-HEVC</b> | <b>ARC-HEVC<br/>vs.<br/>ANY-HEVC</b> |
|-----------------|-------------------------------------|-------------------------------------|--------------------------------------|
| Ballet          | 9.27%                               | -1.89%                              | -10.21%                              |
| Breakdancers    | -1.12%                              | -8.50%                              | -7.46%                               |
| BBB_Flowers     | 6.37%                               | -1.78%                              | -7.66%                               |
| Poznan_Blocks   | 5.98%                               | -4.50%                              | -9.89%                               |
| <b>Average</b>  | <b>5.09%</b>                        | <b>-4.17%</b>                       | <b>-8.81%</b>                        |

Table 4.14. Inter-view prediction time change between ARC-HEVC and ANY-HEVC. Negative values indicate faster inter-view prediction in ARC-HEVC.

| <b>Sequence</b> | <b>ARC-HEVC<br/>vs.<br/>ANY-HEVC</b> |
|-----------------|--------------------------------------|
| Ballet          | -97.96% / 49x                        |
| Breakdancers    | -97.79% / 45x                        |
| BBB_Flowers     | -97.77% / 44x                        |
| Poznan_Blocks   | -97.43% / 39x                        |
| <b>Average</b>  | <b>-97.74% / 44x</b>                 |

### 4.6.3. CONCLUSIONS

In this chapter, the author of the dissertation proposes a novel approach to the compression of multiview video with depth (3D video). Video acquired by cameras located roughly on a circle, as well as corresponding depth maps, is proposed to undergo circular rectification as presented and discussed in Section 4.4. The author of the dissertation develops a process for correcting camera parameters to an ideal circle together with circular video rectification. The state-of-the-art 3D-HEVC technique is proposed to be modified for efficient

compression of such video. Moreover, point mapping equations for simplified inter-view prediction of circularly rectified 3D video are derived and implemented on top of the 3D-HEVC reference test model. The proposed modifications are evaluated experimentally and compared to the unmodified 3D-HEVC and the 3D-HEVC codec adapted to the compression of video acquired by cameras at arbitrary locations (ANY-HEVC), as described in Section 4.2.

The results show that the proposed technique is better than the other 2 solutions, both in terms of compression efficiency and encoding time. The state-of-the-art 3D-HEVC is 6% less efficient due to its restriction to linear camera arrangement. On the other hand, ARC-HEVC is nearly as efficient as the proposal, however, its inter-view prediction is 44 times slower. The author states that circular rectification combined with an adapted encoder allows to exploit a more useful camera arrangement than a linear one without compromising encoder complexity or compression efficiency. Therefore, the technique seems to be an interesting proposal for modern multiview applications such as free-viewpoint television, virtual reality, or immersive video.



## 5. INTER-VIEW PREDICTION WITH SCREEN CONTENT CODING

### 5.1. INTRODUCTION

This chapter presents a novel approach to multiview video coding with the use of HEVC Screen Content Coding (SCC). In Sections 5.2 – 5.6, the author of the dissertation presents the original idea and methodology for adapting Screen Content Coding to compression of stereoscopic video, frame-compatible multiview video, and immersive video. Section 5.7 contains experimental results and the evaluation of the proposal.

It should be stressed that the application of SCC to compression of camera-captured multiview video is a novel approach. Given the initial purpose of the SCC, i.e., the compression of screen content, the proposed solution may seem counterintuitive. Nevertheless, the author of the dissertation provides a detailed explanation of this idea, supported by a series of experiments. In this chapter, the author focuses on adapting SCC to the new applications without making any modifications to the encoder other than changes in its configuration, to prove the usability of standard-compliant SCC. Modifications of the SCC encoder that further increase the compression efficiency at the cost of breaking its compatibility with the state-of-the-art standard are presented in Chapter 6.

### 5.2. SCREEN CONTENT CODING IN MULTIVIEW CODING

As described in Section 2.3, Screen Content Coding was designed for the efficient compression of screencasts, rendered graphics, and other computer-generated video content [Xu'16A]. One of the tools introduced in the SCC extension is Intra Block Copy (IBC), which performs an intra-frame prediction by searching for the most similar block of samples within the previously encoded area of the processed frame. The result of IBC prediction is a 2-dimensional vector that indicates the best matching block of samples, even if it is located in a distant part of the frame. This type of prediction is highly effective for frames containing fonts and other repeatable patterns.

The author of the dissertation observed that **the Intra Block Copy technique could be used for inter-view prediction if all the views from multiview video composed a single frame**. Figure 5.1 presents the block diagram of the **proposed multiview codec**.

Prediction techniques for compression of multiview video acquired using systems with various camera arrangements

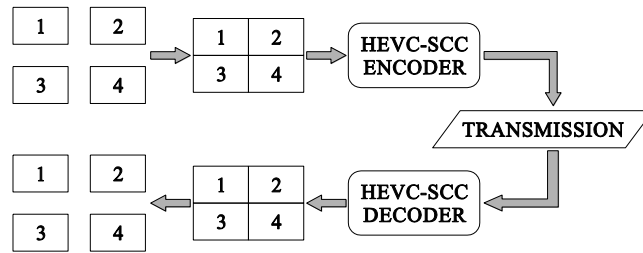


Figure 5.1. Block diagram of the proposed multiview video codec using HEVC Screen Content Coding. The numbers 1-4 denote subsequent views.

In the first step of the encoding process, all the views of a multiview sequence are joined into a single, frame-compatible video. Then, the resulting sequence is compressed with a video encoder that supports the Intra Block Copy technique. In the dissertation, the author uses the state-of-the-art HEVC Screen Content Coding. Obviously, depending on the resolution of the input sequences, the resolution of the frame-compatible video can be very high, and it has to be assured that the encoder is able to process this amount of data. Modern encoders support video compression at resolutions as high as “8K” (7680×4320), which accommodates a maximum of 16 views in the HD 1920×1080 format.

For the decoding, a state-of-the-art HEVC Screen Content Coding decoder is proposed to be used. The output is a reconstructed frame-compatible multiview video, which can then be split into separate views.

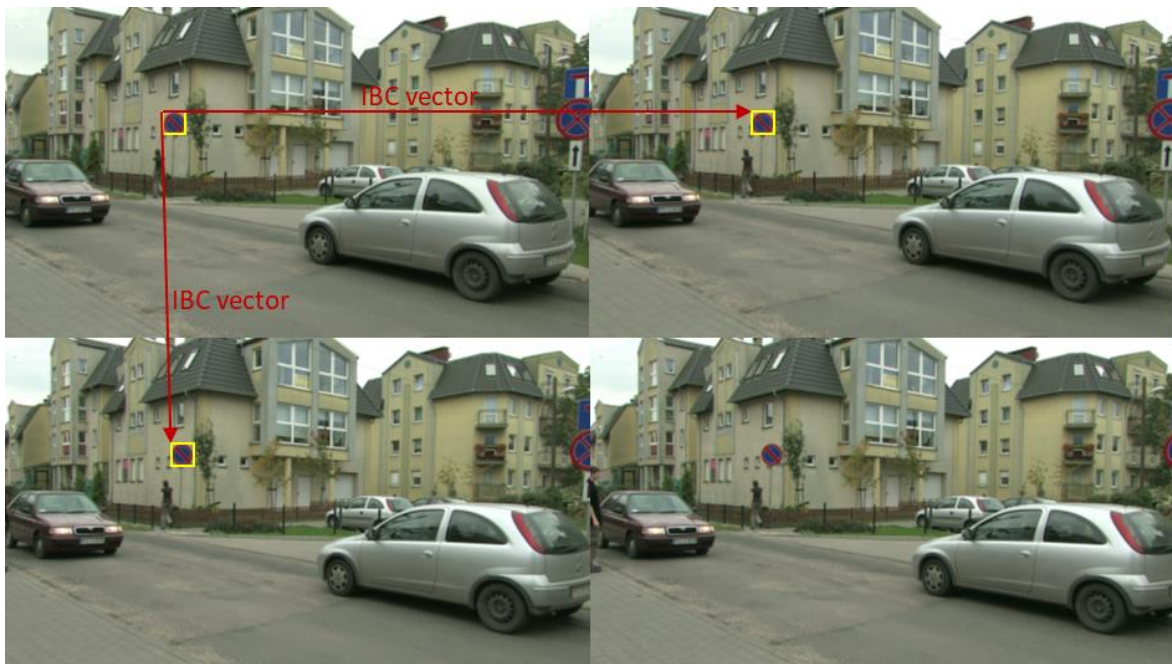


Figure 5.2. Intra Block Copy used on a frame composed of 4 views from a multiview sequence.



Figure 5.2 presents an example of a frame composed of 4 views from a multiview sequence. By the use of Intra Block Copy, the inter-view similarities can be predicted and compressed efficiently. It should be noted that the author of the dissertation proposes using IBC for the **compression of camera-captured content**, which is a **novel approach** and opposite to the original purpose of this technique – the compression of computer-generated video.

### 5.3. THE CHOICE OF VIEW ALIGNMENT FOR FRAME-COMPATIBLE MULTIVIEW VIDEO COMPRESSION

The first step of the proposed technique is to combine all the views of the input multiview video into one frame-compatible sequence. Figures 5.1 and 5.2 suggest joining the encoded views both horizontally and vertically. Such a solution seems natural because it preserves the original aspect ratio. On the other hand, it cannot be applied in some cases (e.g., 3 or 5 views) because the input sequence has to form a rectangular shape. For a four views coding scenario, the possible alignments are presented in Figure 5.3.

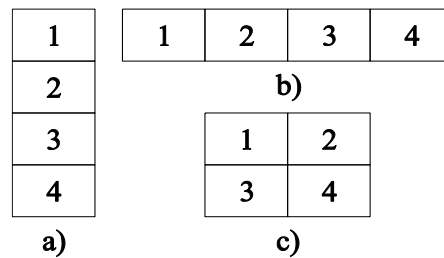


Figure 5.3. Different view alignments: a)  $1 \times 4$ , b)  $4 \times 1$ , c)  $2 \times 2$ .

In this section, the author of the dissertation compares experimentally the encoding time and the efficiency of the HEVC Screen Content Coding encoder in compression of the aforementioned three different view alignments. For the comparison, six commonly used multiview sequences are used. The  $2 \times 2$  view alignment (Figure 5.3c) is used as a reference. Table 5.1 presents the results of bitrate and time reduction.

Both compression efficiency and encoding time are the best for horizontal ( $4 \times 1$ ) alignment. In this case, the vector derived by the Intra Block Copy has only a horizontal component because the input views are vertically aligned. Thus, these vectors are encoded more efficiently compared to the remaining test cases. The  $4 \times 1$  view alignment is therefore used as the input for the remaining experiments presented in Chapter 5 and Chapter 6, as it is proven best for vertically aligned views.

Table 5.1. Bitrate and time reduction against 2×2 view alignment.  
Negative values indicate lower bitrates at the same quality or faster encoding.

| Sequence       | Bitrate reduction [%] |              | Encoding time reduction [%] |              |
|----------------|-----------------------|--------------|-----------------------------|--------------|
|                | 1×4                   | 4×1          | 1×4                         | 4×1          |
| Balloons       | 1.68                  | -5.57        | -0.22                       | -8.11        |
| BBB_Butterfly  | -0.62                 | -6.40        | 5.77                        | 1.44         |
| Kendo          | -1.75                 | -4.33        | 6.33                        | 2.80         |
| Newspaper      | -2.31                 | -4.13        | 0.60                        | -3.19        |
| Poznan_Hall2   | 3.89                  | -5.39        | 5.46                        | -4.04        |
| Poznan_Street  | -0.34                 | -4.02        | 9.38                        | 3.47         |
| <b>Average</b> | <b>-0.04</b>          | <b>-4.58</b> | <b>5.64</b>                 | <b>-0.69</b> |

## 5.4. THE CHOICE OF SCC CONFIGURATION FOR FRAME-COMPATIBLE MULTIVIEW VIDEO COMPRESSION

Apart from Intra Block Copy, the Screen Content Coding extension contains several other compression tools dedicated to computer-generated visual content. The author of the dissertation proposes applying SCC for camera-captured content, for which some of the SCC coding techniques may not be beneficial or even decrease the overall performance. This section contains the evaluation of selected SCC tools in terms of speed and efficiency in the compression of camera-captured content.

From the improvements introduced in Screen Content Coding, three techniques were selected for evaluation in the compression of camera-captured video:

- Intra Boundary Filter (disabled in Common Test Conditions) [Xu'16A]
- Hash-Based Intra Block Copy Search (enabled in CTC)
- Palette Mode (enabled in CTC)

Next, six commonly used multiview sequences are encoded using the HEVC SCC test model [HM+SCM] with a toggled configuration of the abovementioned tools, and compared to the results of compression with configuration compliant with Common Test Conditions for SCC [Yu'15]. Comparison results are presented in Table 5.2 and Table 5.3.

Table 5.2. Bitrate reduction against default Screen Content Coding configuration.  
Negative values indicate lower bitrates at the same quality.

| Sequence       | Intra Boundary Filter enabled | Hash-Based IBC Search disabled | Palette Mode disabled | all improvements |
|----------------|-------------------------------|--------------------------------|-----------------------|------------------|
| Balloons       | -0.30%                        | 0.00%                          | -0.07%                | -0.38%           |
| BBB_Butterfly  | -0.19%                        | 0.00%                          | 0.04%                 | -0.09%           |
| Kendo          | -0.17%                        | 0.00%                          | 0.00%                 | -0.23%           |
| Newspaper      | -0.44%                        | 0.00%                          | -0.05%                | -0.46%           |
| Poznan_Hall2   | -0.31%                        | 0.00%                          | -0.07%                | -0.30%           |
| Poznan_Street  | -0.31%                        | 0.00%                          | -0.01%                | -0.34%           |
| <b>Average</b> | <b>-0.30%</b>                 | <b>0.00%</b>                   | <b>-0.02%</b>         | <b>-0.32%</b>    |

Table 5.3. Encoding time reduction against default Screen Content Coding configuration.  
Negative values indicate faster encoding.

| Sequence       | Intra Boundary Filter enabled | Hash-Based IBC Search disabled | Palette Mode disabled | all improvements |
|----------------|-------------------------------|--------------------------------|-----------------------|------------------|
| Balloons       | 1.80%                         | -1.61%                         | -16.53%               | -20.28%          |
| BBB_Butterfly  | 0.84%                         | 0.13%                          | -19.58%               | -19.46%          |
| Kendo          | -2.95%                        | -3.06%                         | -21.55%               | -20.54%          |
| Newspaper      | 1.34%                         | -2.96%                         | -26.14%               | -25.33%          |
| Poznan_Hall2   | -1.59%                        | 3.21%                          | -18.15%               | -19.64%          |
| Poznan_Street  | 0.80%                         | -1.09%                         | -15.76%               | -17.73%          |
| <b>Average</b> | <b>0.12%</b>                  | <b>-0.58%</b>                  | <b>-18.55%</b>        | <b>-19.78%</b>   |

The results show that enabling Intra Boundary Filter slightly reduces the bitrate without a negative impact on the encoding time. The influence of Hash-Based IBC Search and Palette Mode on compression efficiency is negligible, which proves that those techniques are not beneficial for the camera-captured content. However, disabling them improves the encoding time significantly. In total, adapting Screen Content Coding configuration to camera-captured content provides roughly 0.3% of bitrate reduction and 20% faster encoding time. In the further evaluation of applying SCC to compression of camera-captured video, the author of the dissertation configures the HEVC SCC test model according to the modifications proposed in this section: enabled Intra Boundary Filter, disabled Hash-Based IBC Search and Palette Mode.

## 5.5. SCREEN CONTENT CODING IN STEREOSCOPIC VIDEO CODING

Stereoscopic video is a particular case of multiview video with a variety of applications, such as entertainment (3D television), surveillance, depth estimation, or navigation assistance for the visually impaired [Strumillo'18, Skulimowski'07, Müller'11, Ratajczak'12]. It comprises only two views, one for each of the spectator's eyes [Fujikawa'10]. The views are shifted horizontally by a distance that corresponds to the distance between humans' eyes. Therefore the majority of the content of the left view is also visible in the right view. A multiview encoder would exploit the inter-view similarities and provide the highest compression efficiency. In practice, however, the use of a dedicated multiview codec for stereoscopic video coding is very limited. Usually, in order to use the existing broadcasting infrastructure and receivers, both views of a stereoscopic video are accommodated into a single frame and compressed using a single-layer encoder with additional signalization information provided in SEI (Supplemental Enhancement Information) [ISO'21]. In such a case, the benefit of the inter-view prediction is sacrificed at the cost of simpler implementation.

In this section, the author of the dissertation proposes to apply HEVC Screen Content Coding to the compression of frame-compatible stereoscopic video as an alternative to the commonly used HEVC Main profile encoder. There are two main ways of packing left and right view into a single frame: Side-by-Side and Top-and-Bottom [Vetro'10]. Given the results presented in Section 5.3, the Side-by-Side solution is considered. Contrary to the approach for multiview video (Section 5.2), both views of the stereoscopic video are decimated in the horizontal direction by a factor of 2, as it is done in practice. The proposed block diagram is presented in Figure 5.4.

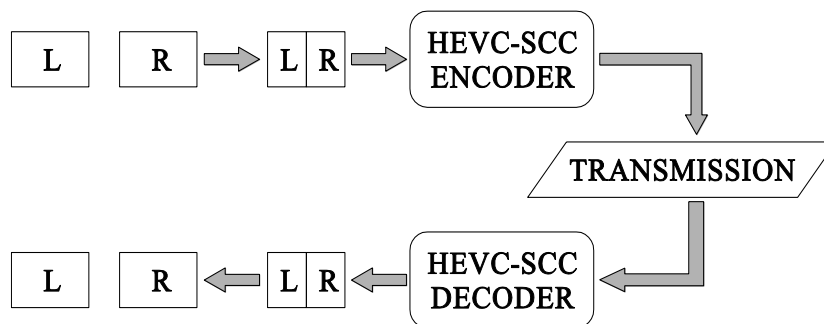


Figure 5.4. The proposed solution for stereoscopic video coding with Screen Content Coding.

## 5.6. SCREEN CONTENT CODING IN IMMERSIVE VIDEO COMPRESSION

The state-of-the-art in immersive video coding, as described in Section 2.4, is MPEG Immersive Video (MIV). The encoding process in MIV can be divided into three parts:

1. Preparation of atlases. This part includes dividing input views into base views and additional views, removing inter-view redundancies in the process of pruning, and creating atlases with patches and stacked base views during packing.
2. Compression of atlases. The output sequences from the previous step are fed into a general video encoder, such as HEVC or VVC. Each of the atlases is encoded individually with a separate instance of video encoder.
3. Preparation of MIV bitstream. The bitstreams produced by general video encoders in step 2 are combined into a single bitstream, with additional MIV metadata included.

In this section, the author proposes to use Screen Content Coding as the video encoder in step 2 **instead of the general video encoder**. In the dissertation, replacing HEVC with HEVC SCC is considered. The block diagram of the proposed solution is presented in Figure 5.5.

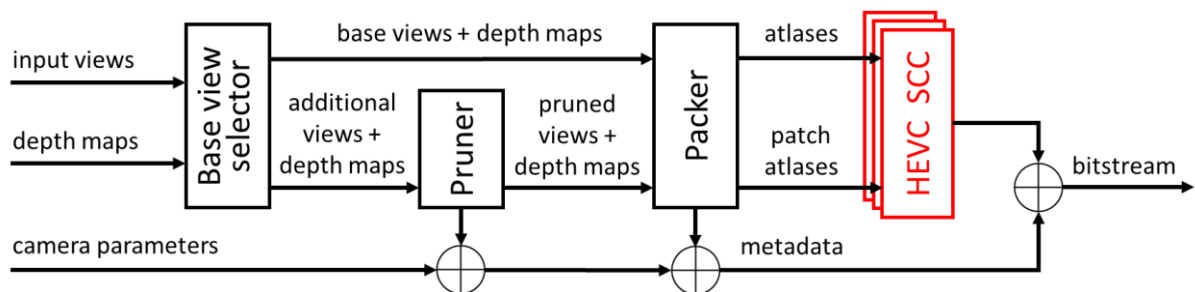


Figure 5.5. MPEG Immersive Video codec with HEVC Screen Content Coding as the internal video encoder.

The rationale for the above change is as follows:

- **Intra Block Copy can be beneficial for the compression of atlases containing base views.** Packing base views into atlases by MIV encoder is principally the same as creating frame-compatible multiview video, proposed in Section 5.2. It is expected that the Intra Block Copy technique would make use of the inter-view similarities between the views that compose an atlas. The difference is that the MIV encoder joins the base views vertically (Figure 2.6), while it was experimentally checked in Section 5.3 that Intra Block Copy is more efficient for horizontally aligned views. However,

modifications of the MIV codec are out of the scope of this dissertation, therefore in this case, the vertical accommodation of base views is preserved.

- **Intra Block Copy can be beneficial for the compression of atlases containing patches from additional views.** Such atlases can contain similar patches located far from each other. Obviously, their number depends on the effectiveness of MIV in reducing the inter-view redundancy. Such repeated patches would be efficiently predicted with IBC, similarly to fonts in screen content.
- **Palette Mode can be beneficial for the compression of depth atlases.** As mentioned in Section 2.3, Palette Mode increases the overall compression efficiency if the encoded content has locally only a few colors separated by sharp edges [Pu'16]. It is often true for depth maps, where, e.g., the depth of an object is constant, and there is a sharp edge between an object and the background. In the case of atlases with camera-captured content, using Palette Mode would not provide such gain – it was experimentally checked in Section 5.4.

To summarize, using Screen Content Coding as the internal encoder can be beneficial due to the characteristics of atlases prepared in the initial phase of MIV encoding. The following section contains the results of the experiments conducted to verify the above thesis.

## 5.7. EVALUATION OF THE PROPOSAL

### 5.7.1. GOALS OF THE EXPERIMENTS

The goal of the experiments presented in this chapter is to evaluate the use of Screen Content Coding in compression of stereoscopic (side-by-side), frame-compatible multiview, and immersive video. The solutions proposed by the author of the dissertation are compared with the state-of-the-art techniques in terms of compression efficiency and encoding time (in the case of multiview and stereoscopic video) or the quality of synthesized views (in the case of immersive video). The author also performs experiments to determine if using SCC has to be combined with frame-compatibility to provide bitrate reduction.

The general information about the methodology of the experiments (e.g., versions of encoders used or definitions of metrics) is provided in Chapter 3. Sections 5.7.2 - 5.7.4 contain details specific to each experiment and the evaluation results. The complete results of the conducted experiments can be found in the Appendix.

### 5.7.2. EVALUATION OF SCC IN STEREOSCOPIC VIDEO CODING

In the first experiment, the application of HEVC SCC to stereoscopic video compression is compared with the common approach, which is using the HEVC Main profile. The encoders are obtained from publicly available test models as described in Chapter 3. The comparison is made by coding 100 frames of 2 arbitrarily chosen views obtained from 6 test sequences. The views are chosen according to Table 5.4. The experiments are conducted in All Intra and Random Access configurations according to appropriate Common Test Conditions [Bossen'13, Yu'15]. The configuration of tools specific to Screen Content Coding is prepared as proposed in Section 5.4.

Table 5.4. Chosen views of sequences used in the experiment.

| Sequence      | Views (left, right) |
|---------------|---------------------|
| Balloons      | 3, 4                |
| BBB_Butterfly | 45, 50              |
| Kendo         | 3, 4                |
| Newspaper     | 4, 6                |
| Poznan_Hall2  | 6, 5                |
| Poznan_Street | 4, 3                |

In order to fully evaluate the proposed solution, the following coding scenarios are applied:

- HEVC Main simulcast – the views are not joined into a frame-compatible sequence, only decimated horizontally and encoded independently with the HEVC Main profile. This approach is used as a reference as it is the most straightforward solution.
- HEVC Main side-by-side – both views decimated and packed next to each other and encoded with HEVC Main profile. This approach is commonly used in systems broadcasting stereoscopic video [Vetro'10]. Comparing it to simulcast would show if the HEVC encoder would benefit from frame-compatibility itself.
- HEVC SCC simulcast – both views are decimated and encoded individually with HEVC SCC to check if Screen Content Coding provides compression gain if the views are not accommodated into a single frame.
- HEVC SCC side-by-side – **the proposed solution**. Combines frame-compatibility and using Screen Content Coding.

All four encoders are compared in terms of encoding time and compression efficiency, represented as bitrate reduction at a constant quality of the reconstructed video (Chapter 3). The results are presented in Table 5.5 and Table 5.6.

Table 5.5. Bitrate reduction compared to HEVC Main simulcast for All Intra (AI) and Random Access (RA) coding scenarios. Negative values indicate lower bitrates at the same quality.

| Sequence       | Main side-by-side |              | SCC simulcast |               | SCC side-by-side |                |
|----------------|-------------------|--------------|---------------|---------------|------------------|----------------|
|                | AI                | RA           | AI            | RA            | AI               | RA             |
| Balloons       | 0.03%             | 0.32%        | 0.27%         | 0.45%         | -21.95%          | -13.65%        |
| BBB_Butterfly  | -0.05%            | -0.62%       | 0.28%         | -0.13%        | -25.70%          | -19.92%        |
| Kendo          | 0.07%             | 0.37%        | 0.23%         | -0.35%        | -23.36%          | -16.05%        |
| Newspaper      | 0.04%             | -0.30%       | 0.13%         | 0.20%         | -17.75%          | -13.97%        |
| Poznan_Hall2   | 0.04%             | 0.70%        | -0.60%        | -0.45%        | -14.01%          | -8.65%         |
| Poznan_Street  | 0.06%             | -0.11%       | -0.89%        | -0.59%        | -20.49%          | -16.23%        |
| <b>Average</b> | <b>0.09%</b>      | <b>0.12%</b> | <b>-0.33%</b> | <b>-0.15%</b> | <b>-20.07%</b>   | <b>-14.70%</b> |

Table 5.6. Encoding time reduction compared to HEVC Main simulcast for All Intra (AI) and Random Access (RA) coding scenarios. Negative values indicate faster encoding.

| Sequence       | Main side-by-side |               | SCC simulcast |               | SCC side-by-side |                |
|----------------|-------------------|---------------|---------------|---------------|------------------|----------------|
|                | AI                | RA            | AI            | RA            | AI               | RA             |
| Balloons       | 2.82%             | -4.94%        | 84.65%        | 1.74%         | 84.32%           | -1.45%         |
| BBB_Butterfly  | -0.41%            | 6.20%         | 42.61%        | -1.10%        | 15.20%           | -6.53%         |
| Kendo          | 6.12%             | 6.91%         | 68.17%        | 17.70%        | 55.26%           | 11.51%         |
| Newspaper      | 3.93%             | 7.88%         | 125.22%       | -3.66%        | 113.25%          | -3.80%         |
| Poznan_Hall2   | 2.07%             | -5.90%        | 39.07%        | -26.34%       | 30.37%           | -30.11%        |
| Poznan_Street  | -1.27%            | -3.68%        | 113.24%       | -17.07%       | 103.75%          | -20.92%        |
| <b>Average</b> | <b>1.41%</b>      | <b>-0.68%</b> | <b>78.48%</b> | <b>-9.60%</b> | <b>67.51%</b>    | <b>-13.45%</b> |

The conclusions from the results presented in Tables 5.5 and 5.6 are as follows:

- **The influence of frame-compatibility is negligible when using the HEVC Main encoder**, both in terms of bitrate and encoding time. This confirms that the inter-view similarities between the left and right views are not exploited by the standard HEVC encoder.
- **Using HEVC SCC for simulcast compression of camera-captured content does not affect the efficiency** and has a negative impact on encoding time. Such a result is expected because Screen Content Coding tools were designed for the compression of computer-generated content.



- **Application of HEVC SCC for compression of frame-compatible stereoscopic video provides a significant gain** of roughly 20% bitrate reduction for All Intra and 15% for Random Access, compared to other compression scenarios. This result indicates that Intra Block Copy can be successfully used to predict the inter-view similarities. In the case of All Intra, bitrate reduction is achieved at the cost of considerably longer encoding time, which is expected since the IBC and other SCC tools are additionally applied to every frame. On the other hand, for Random Access, the encoding time is reduced on average by 14%. In this case, intra frames are encoded longer due to the Intra Block Copy, but thanks to the higher quality of the reconstructed I-frame, the remaining B-frames are encoded much faster, compensating for the time increase of the I-frame.

### 5.7.3. EVALUATION OF SCC IN MULTIVIEW VIDEO CODING

The experiment presented in this section aims to measure the impact of Screen Content Coding in the compression of multiview video and compare it to the state-of-the-art Multiview HEVC. The methodology of this experiment is similar to the previous one (Section 5.7.2). This time, however, 4 views of each sequence are chosen according to Table 5.7, and they are not decimated. The frame-compatible sequences are prepared by joining all 4 views horizontally, as described in Section 5.3. In addition, encoding with Multiview HEVC is performed.

Table 5.7. Chosen views of sequences used in the experiment.

| Sequence      | Views (from left to right) |
|---------------|----------------------------|
| Balloons      | 2, 3, 4, 5                 |
| BBB_Butterfly | 40, 45, 50, 55             |
| Kendo         | 2, 3, 4, 5                 |
| Newspaper     | 2, 4, 6, 8                 |
| Poznan_Hall2  | 7, 6, 5, 4                 |
| Poznan_Street | 5, 4, 3, 2                 |

Table 5.8 presents the results of bitrate reduction, compared to simulcast compression of all views using the HEVC Main profile, both for the All Intra (AI) and Random Access (RA) configuration. The results of encoding time reduction are gathered in Table 5.9.

Table 5.8. Bitrate reduction compared to HEVC Main simulcast for All Intra (AI) and Random Access (RA) coding scenarios. Negative values indicate lower bitrates at the same quality.

| Sequence       | Main side-by-side |              | SCC simulcast |               | SCC side-by-side |                | Multiview      |                |
|----------------|-------------------|--------------|---------------|---------------|------------------|----------------|----------------|----------------|
|                | AI                | RA           | AI            | RA            | AI               | RA             | AI             | RA             |
| Balloons       | 0.02%             | 0.29%        | 0.27%         | 0.27%         | -32.35%          | -20.88%        | -42.59%        | -36.66%        |
| BBB_Butterfly  | -0.09%            | -0.84%       | 0.10%         | -0.25%        | -38.93%          | -29.21%        | -45.17%        | -41.02%        |
| Kendo          | 0.04%             | 0.16%        | 0.19%         | -0.19%        | -33.19%          | -22.71%        | -44.97%        | -41.07%        |
| Newspaper      | 0.35%             | 0.17%        | 0.06%         | 0.29%         | -23.98%          | -18.06%        | -31.13%        | -30.79%        |
| Poznan_Hall2   | 0.00%             | 0.75%        | -0.66%        | -0.60%        | -15.16%          | -9.98%         | -26.70%        | -22.18%        |
| Poznan_Street  | 0.06%             | -0.06%       | -0.73%        | -0.55%        | -23.49%          | -19.27%        | -34.70%        | -40.19%        |
| <b>Average</b> | <b>0.06%</b>      | <b>0.08%</b> | <b>-0.13%</b> | <b>-0.17%</b> | <b>-27.85%</b>   | <b>-20.02%</b> | <b>-37.54%</b> | <b>-35.32%</b> |

Table 5.9. Encoding time reduction compared to HEVC Main simulcast for All Intra (AI) and Random Access (RA) coding scenarios. Negative values indicate faster encoding.

| Sequence       | Main side-by-side |              | SCC simulcast |                | SCC side-by-side |               | Multiview      |              |
|----------------|-------------------|--------------|---------------|----------------|------------------|---------------|----------------|--------------|
|                | AI                | RA           | AI            | RA             | AI               | RA            | AI             | RA           |
| Balloons       | 0.00%             | -8.43%       | 42.75%        | -9.48%         | 54.93%           | -9.72%        | 120.80%        | -2.76%       |
| BBB_Butterfly  | -4.77%            | -2.44%       | 40.77%        | -7.72%         | 11.85%           | -5.08%        | 51.80%         | 10.99%       |
| Kendo          | 3.68%             | 0.33%        | 58.40%        | 0.47%          | 74.57%           | 4.04%         | 152.19%        | 9.59%        |
| Newspaper      | -10.30%           | 0.61%        | 88.88%        | -13.04%        | 93.24%           | -9.03%        | 157.34%        | 13.56%       |
| Poznan_Hall2   | -3.24%            | 5.60%        | 34.42%        | -24.10%        | 38.58%           | -24.39%       | 119.57%        | 8.52%        |
| Poznan_Street  | -9.94%            | 5.81%        | 79.67%        | -14.60%        | 110.56%          | -14.40%       | 104.26%        | 5.18%        |
| <b>Average</b> | <b>-4.09%</b>     | <b>0.25%</b> | <b>57.48%</b> | <b>-11.41%</b> | <b>63.96%</b>    | <b>-9.76%</b> | <b>117.66%</b> | <b>7.51%</b> |

The conclusions for using frame-compatible HEVC Main and simulcast HEVC SCC are the same as for stereoscopic video compression: these encoders provide roughly the same efficiency as simulcast HEVC Main. Regarding frame-compatible compression with HEVC SCC, the bitrate reduction is even bigger than for stereoscopic video - on average, 28% for All Intra and 20% for Random Access. This is caused by the bigger impact of inter-view prediction due to more views being compressed. Nevertheless, the best results in terms of compression efficiency are achieved by Multiview HEVC. Bitrate reduction for this encoder is as high as 37% for All Intra and 35% for Random Access. On the other hand, the encoding time is much longer compared to frame-compatible HEVC SCC, which means that the proposed solution is less efficient in terms of compression efficiency, but much faster than the state-of-the-art Multiview HEVC.

#### 5.7.4. EVALUATION OF SCC IN IMMERSIVE VIDEO CODING

This section evaluates the efficiency of Screen Content Coding applied to the compression of immersive video. The experiments are conducted using the publicly available MPEG Immersive Video test model [TMIV]. In the assessment, 97 frames of 7 immersive video test sequences are used. The atlases generated by the TMIV encoder are first compressed with the HEVC Main profile, which is the state-of-the-art approach in MIV coding. Then, the compression of atlases is repeated using HEVC SCC as proposed by the author of the dissertation in Section 5.6. The configuration of coding parameters is in line with MPEG Common Test Conditions for Immersive Video [CTC MIV], and it is the same for both encoders. Obviously, in the case of HEVC SCC, the Screen Content Coding tools are additionally configured according to MPEG Common Test Conditions for Screen Content Coding [Yu'15]. It should be stressed that Palette Mode is enabled, contrary to the experiments for stereoscopic and multiview video. As explained in Section 5.6, Palette Mode should be beneficial for the compression of depth maps; therefore, it is not disabled this time.

The results of the experiments are divided into two subsections. In the first subsection, the proposal is evaluated by comparing it to HEVC Main in terms of bitrate reduction and quality of reconstructed atlases after the coding cycle. Moreover, the results of the compression of views and depth atlases are presented and discussed separately. The second subsection focuses on the quality of virtual view synthesis performed using the reconstructed data. In this comparison, five commonly used objective quality metrics were calculated: Weighted-to-Spherically-Uniform PSNR (WS-PSNR) [Sun'17], Multi-Scale SSIM (MS-SSIM) [Wang'04], Visual Information Fidelity (VIF) [Sheikh'06], Video Multimethod Assessment Fusion (VMAF) [Li'16] and ISO/IEC MPEG's metric for immersive video: IV-PSNR [Dziembowski'22]. The results of such a comparison are more consistent with the subjective quality assessment of an end user of an immersive video system.

##### A. COMPRESSION EFFICIENCY OF ATLASES

Experimental results in this subsection are presented separately for views and depth data. First, the outcome of the comparison between HEVC Main and HEVC SCC in compression of views data is presented in Table 5.10. The results are divided based on the input data type (base views or patch atlases) and the content: computer-generated (CG) or natural content (NC). Figures 5.6 and 5.7 present rate-distortion curves of compression of views data for computer-generated and natural content, respectively.

Table 5.10. Bitrate reduction and quality improvement of HEVC SCC for views data, compared to HEVC Main. A positive number indicates a lower bitrate or better quality.

| Sequence           | Bitrate reduction [%] |               | Quality improvement [dB] |               |
|--------------------|-----------------------|---------------|--------------------------|---------------|
|                    | Base views            | Patch atlases | Base views               | Patch atlases |
| ClassroomVideo     | 0.78                  | 1.74          | 0.02                     | 0.04          |
| TechnicolorMuseum  | 1.16                  | 4.00          | 0.01                     | -0.01         |
| TechnicolorHijack  | 0.00                  | 6.55          | 0.03                     | 0.22          |
| OrangeKitchen      | 0.49                  | 7.44          | 0.05                     | 0.11          |
| <b>CG average</b>  | <b>0.61</b>           | <b>4.93</b>   | <b>0.03</b>              | <b>0.09</b>   |
| TechnicolorPainter | -0.09                 | 1.53          | -0.01                    | 22.86         |
| IntelFrog          | 0.44                  | 1.39          | 0.00                     | 33.00         |
| Poznan_Fencing2    | 0.30                  | 0.69          | 0.00                     | 0.02          |
| <b>NC average</b>  | <b>0.22</b>           | <b>1.20</b>   | <b>0.00</b>              | <b>18.63</b>  |
| <b>Average</b>     | <b>0.44</b>           | <b>3.33</b>   | <b>0.01</b>              | <b>8.03</b>   |

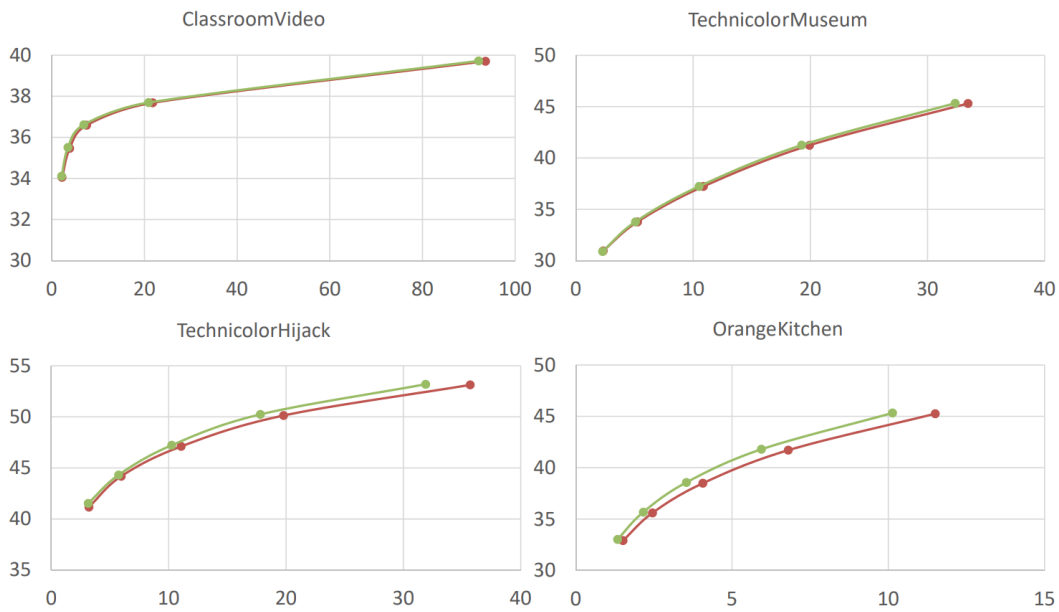


Figure 5.6. RD curves for compression of computer-generated sequences with HEVC (red) and HEVC SCC (green), views data. Horizontal axis – bitrate [Mbps], vertical axis – PSNR [dB].

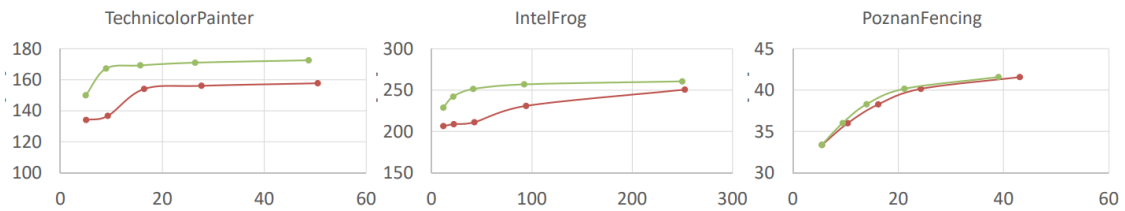


Figure 5.7. RD curves for compression of natural sequences with HEVC (red) and HEVC SCC (green), views data. Horizontal axis – bitrate [Mbps], vertical axis – PSNR [dB].

The results show that using HEVC SCC for compression of views data is more efficient than the state-of-the-art solution with HEVC Main profile. The difference in bitrate is more significant for patch atlases. In the case of quality, the difference is usually negligible, however, for patch atlases of two sequences, *TechnicolorPainter* and *IntelFrog*, the difference in quality is surprisingly high. Detailed investigation shows that such difference is caused by frames with no patches within sequences produced by the TMIV encoder. When using HEVC SCC, reconstruction images of such empty frames are ideal, which results in a very high PSNR value (99.99 dB) and strongly affects mean PSNR.

An analogous comparison of results is made for depth data. Table 5.11 presents bitrate reduction and quality improvement of base views and atlases encoded with HEVC SCC, compared to using HEVC Main. Rate-distortion curves for compression of depth data per sequence are presented in Figure 5.8 (computer-generated content) and Figure 5.9 (natural content). The numbers and plots clearly show that the proposed solution outperforms the state-of-the-art, both in terms of bitrate and quality of encoded video data. The gain is much higher than for views, which is expected due to the characteristics of depth maps. First of all, depth maps often contain large and smooth areas, as well as repeatable patterns, which can be efficiently predicted by the Intra Block Copy technique. Secondly, the values in fragments of depth maps (especially computer-generated) often belong to a very limited set, which can be utilized by Palette Mode.

Table 5.11. Bitrate reduction and quality improvement of HEVC SCC for depth data, compared to HEVC Main. A positive number indicates a lower bitrate or better quality.

| Sequence           | Bitrate reduction [%] |               | Quality improvement [dB] |               |
|--------------------|-----------------------|---------------|--------------------------|---------------|
|                    | Base views            | Patch atlases | Base views               | Patch atlases |
| ClassroomVideo     | 11.76                 | 18.38         | 1.85                     | 3.14          |
| TechnicolorMuseum  | 8.52                  | 13.12         | 0.56                     | 0.62          |
| TechnicolorHijack  | 7.89                  | 9.25          | 1.09                     | 1.43          |
| OrangeKitchen      | 15.34                 | 25.10         | 1.28                     | 1.80          |
| <b>CG average</b>  | <b>10.88</b>          | <b>16.47</b>  | <b>1.20</b>              | <b>1.75</b>   |
| TechnicolorPainter | 4.60                  | 4.27          | 0.27                     | 8.77          |
| IntelFrog          | 2.01                  | 3.16          | 0.12                     | 32.32         |
| Poznan_Fencing2    | 14.23                 | 12.22         | 0.90                     | 0.87          |
| <b>NC average</b>  | <b>6.95</b>           | <b>6.55</b>   | <b>0.43</b>              | <b>13.99</b>  |
| <b>Average</b>     | <b>9.19</b>           | <b>12.22</b>  | <b>0.87</b>              | <b>6.99</b>   |

Prediction techniques for compression of multiview video acquired using systems with various camera arrangements

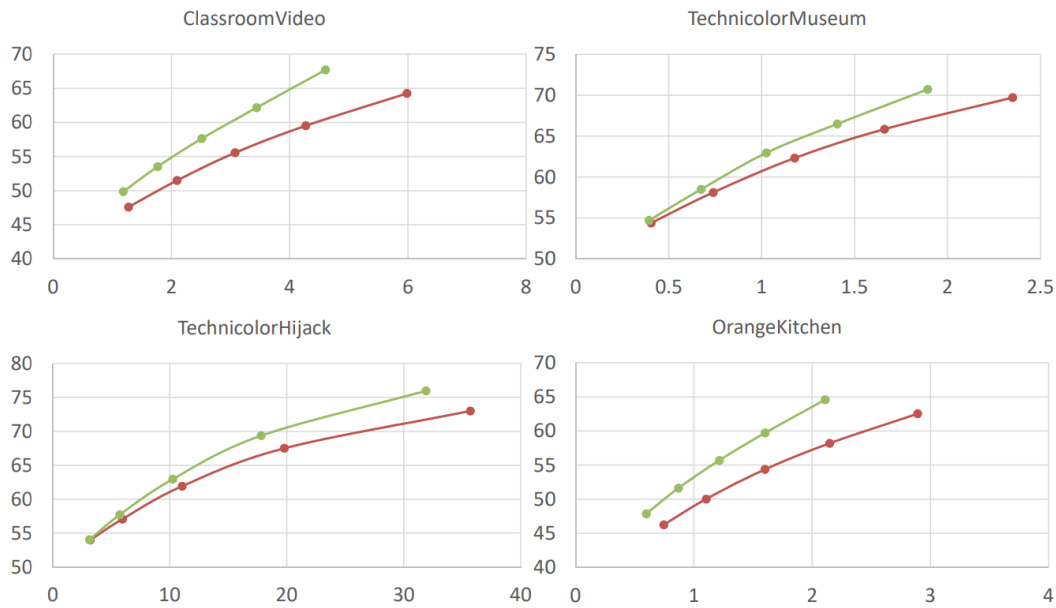


Figure 5.8. RD curves for compression of computer-generated sequences with HEVC (red) and HEVC SCC (green), depth data. Horizontal axis – bitrate [Mbps], vertical axis – PSNR [dB].

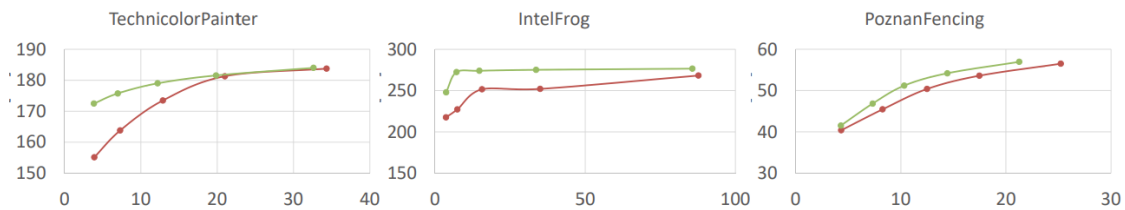


Figure 5.9. RD curves for compression of natural sequences with HEVC (red) and HEVC SCC (green), depth data. Horizontal axis – bitrate [Mbps], vertical axis – PSNR [dB].

Regarding differences between results for base views and patch atlases, it is observed that for computer-generated video, bitrate reduction is noticeably higher for patch atlases than for base views. In the case of natural content, however, the gain is comparable or even worse for patch atlases. Such an effect is a result of differences in creating depth maps. For computer-generated video, depth maps are usually rendered, and therefore they are smooth across whole objects and have sharp edges between objects and the background. On the contrary, depth maps for camera-captured video are usually estimated algorithmically from the input views, which causes some artifacts, e.g., grained objects or the background, blurred edges. These issues negatively affect the efficiency of both Intra Block Copy and Palette Mode. Nonetheless, the overall performance of standard-compliant HEVC Screen Content Coding in compression of atlases with depth maps and patches is much better than the commonly used HEVC Main profile.

## B. VIEW SYNTHESIS QUALITY COMPARISON

In the previous subsection, it was proven that HEVC SCC improves the compression efficiency and the quality of immersive video patch atlases, especially those containing depth data. However, the quality of depth does not concern end users of immersive video systems, but they care about the quality of synthesized video data that is generated from base views and depth maps and presented to end users. This subsection evaluates the quality of synthesized virtual views when using the proposed compression technique – HEVC SCC. It is compared to the synthesis quality achieved with video data compressed using the HEVC Main profile.

Figures 5.10 and 5.11 present rate-distortion plots for computer-generated and natural sequences, respectively. Bitrates (horizontal axis) are calculated as the sum of all atlases, while the quality (vertical axis) is represented by averaged WS-PSNR metric for the luma component of synthesized views. The results show that when using HEVC SCC, as proposed by the author of the dissertation, the quality of virtual views is higher at a given bitrate than when using standard HEVC.

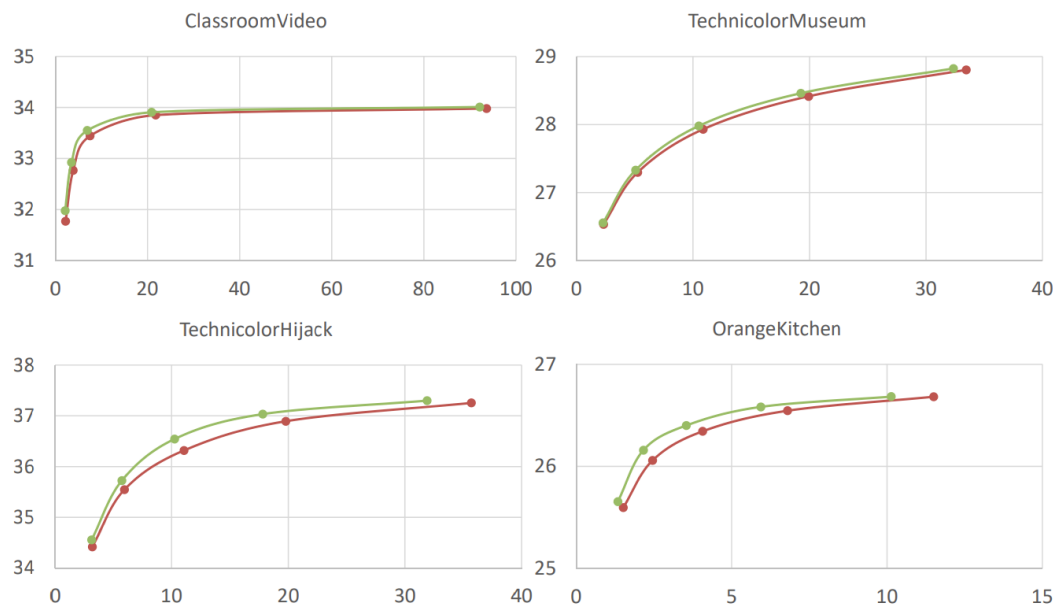


Figure 5.10. RD curves for view synthesis of computer-generated sequences with HEVC (red) and HEVC SCC (green). Horizontal axis – bitrate [Mbps], vertical axis – WS-PSNR [dB].

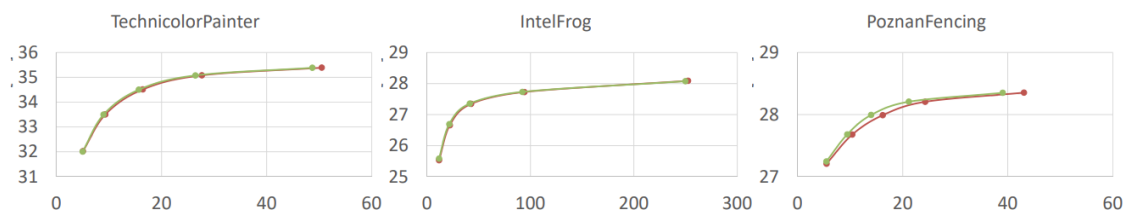


Figure 5.11. RD curves for view synthesis of natural sequences with HEVC (red) and HEVC SCC (green). Horizontal axis – bitrate [Mbps], vertical axis – WS-PSNR [dB].

Table 5.12 presents the average bitrate reduction calculated as Bjøntegaard Delta for WS-PSNR and four other commonly used objective quality metrics: VIF, VMAF, SSIM, and IV-PSNR. It can be noticed that the proposal is better than HEVC Main in all cases, and the gain can be as high as 30% (VMAF, sequence *OrangeKitchen*). Another observation is that the performance is better for computer-generated sequences than for natural content. This is in line with the compression efficiency results, where computer-generated depth maps were encoded more efficiently. As mentioned before, depth maps of higher quality allow to synthesize virtual views with fewer artifacts, thus higher quality.

Table 5.12. Bitrate reduction for different quality metrics.  
Positive values indicate bitrate reduction for a given quality metric.

| Sequence           | WSPSNR       | VIF          | VMAF         | SSIM         | IVPSNR      |
|--------------------|--------------|--------------|--------------|--------------|-------------|
| ClassroomVideo     | 22.36        | 10.87        | 16.42        | 10.28        | 10.24       |
| TechnicolorMuseum  | 7.82         | 4.07         | 8.77         | 4.48         | 4.78        |
| TechnicolorHijack  | 19.83        | 14.91        | 20.06        | 15.88        | 9.20        |
| OrangeKitchen      | 22.64        | 16.35        | 30.19        | 16.30        | 5.65        |
| <b>CG average</b>  | <b>18.16</b> | <b>11.55</b> | <b>18.86</b> | <b>11.74</b> | <b>7.47</b> |
| TechnicolorPainter | 3.37         | 3.75         | 2.92         | 3.37         | 3.33        |
| IntelFrog          | 3.85         | 2.70         | 5.04         | 4.14         | 1.48        |
| Poznan_Fencing2    | 11.41        | 11.18        | 10.23        | 10.31        | 9.46        |
| <b>NC average</b>  | <b>6.21</b>  | <b>5.88</b>  | <b>6.06</b>  | <b>5.94</b>  | <b>4.76</b> |
| <b>Average</b>     | <b>13.04</b> | <b>9.12</b>  | <b>13.38</b> | <b>9.25</b>  | <b>6.31</b> |

Figure 5.12 presents the comparison of fragments of virtual views synthesized with original data (left), reconstructed data after compression with HEVC Main (middle), and reconstructed data after compression with HEVC SCC (right). It can be observed that the proposed solution results in fewer artifacts in view synthesis, especially at the edges between objects, which has a positive influence on the subjective quality when viewed by the end user of an immersive video system.



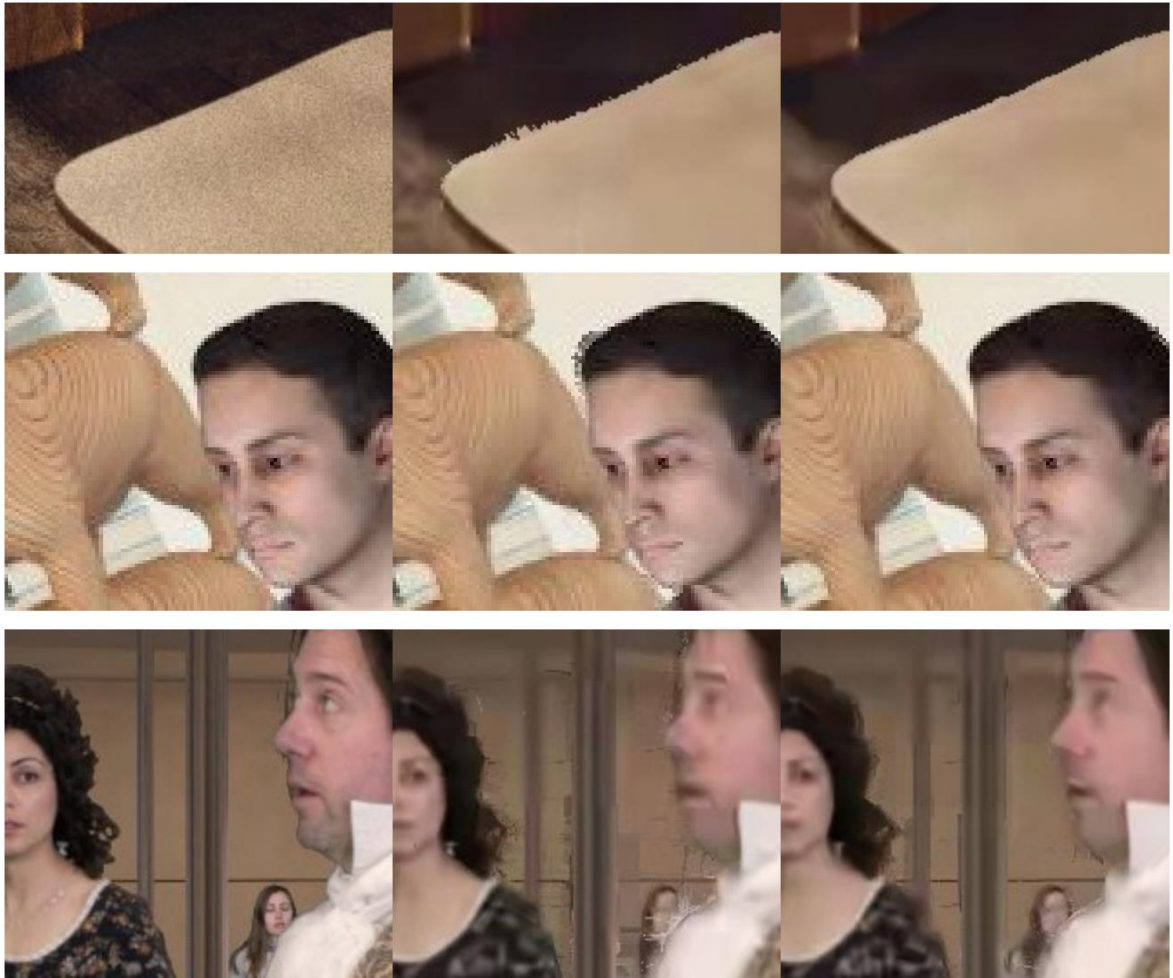


Figure 5.12. Fragments of: input views (left), views synthesized using data encoded with HEVC Main (middle), and views synthesized using data encoded with HEVC SCC (right).

## 5.8. CONCLUSIONS

In this chapter, the author of the dissertation considers using Screen Content Coding as an inter-view compression technique and proposes methods for using it in several new applications: stereoscopic, multiview, and immersive video coding. The proposal is a novel approach, and using it to compress camera-captured content may appear unintuitive because Screen Content Coding was developed to compress computer-generated content. Although SCC does not improve the compression efficiency of a single view containing camera-captured content, combining Intra Block Copy technique with frame-compatibility turns out to be an efficient way to exploit the inter-view similarities. Moreover, the author evaluates the influence of view alignment in frame-compatible sequence, as well as the impact of SCC coding tools other than IBC, on the overall performance of Screen Content Coding in the compression of natural content. The results help in preparing optimal configurations of the proposal and applying it in experiments presented in Section 5.7.

A complete proposal assessment is performed by conducting several experiments, comparing HEVC Screen Content Coding with state-of-the-art solutions for stereoscopic, multiview, and immersive video compression.

In the case of stereoscopic video coding, the proposed solution is compared to the HEVC Main profile in compression of decimated views joined side-by-side, which is a common approach in broadcasting so-called “3D video” content. The results show that **HEVC SCC provides, on average, 15% lower bitrate than HEVC Main profile**. Taking into account that HEVC SCC can be efficiently applied to screen content, and by design is less complex than Multiview HEVC (which is a multi-layer codec), using SCC for stereoscopic video compression in practical systems is possible. Moreover, support for Screen Content Coding was already provided in the recently developed video coding standard, Versatile Video Coding, therefore the proposed approach could be easily applied in the new generation of codecs.

Regarding multiview video, **using HEVC SCC in compression of 4 views provides roughly 20% bitrate reduction compared to simulcast encoding**. However, the gain is significantly lower than when using the state-of-the-art Multiview HEVC encoder. It should be noted that this chapter only describes encoding with standard-compliant HEVC SCC, which is not optimized for efficient compression of camera-captured multiview video content. In the next chapter (Chapter 6), the author of the dissertation proposes several modifications of standard HEVC SCC to adapt it to the new applications and achieve as high bitrate savings as the dedicated Multiview HEVC extension.

Finally, the proposed HEVC SCC method is applied to immersive video coding. MPEG Immersive Video (MIV) standard uses a general video encoder internally to compress atlases. MIV is, however, codec-agnostic, so replacing HEVC with HEVC SCC could be done effortlessly and without violating the standard. The evaluation of such change also proves the superiority of the proposal over the HEVC Main profile, especially in the compression of computer-generated content and depth maps. Further assessment shows that the improved quality of depth maps results in **a significantly better quality of synthesized virtual views** – the proposal is compared to HEVC Main with 5 different quality metrics, and it turns out to be **noticeably more efficient in all cases**.

The idea of using SCC as an internal video encoder in MIV was proposed by the author during one of MPEG meetings [Samelak’20A-B]. As a result, MPEG group investigated such a possibility by evaluating using VVC with Screen Content Coding as an internal MIV encoder, compared to plain VVC. Experimental results confirmed that the application of Screen Content

Coding is beneficial in the compression of immersive video data [Vadakital'20]. Therefore, **the novel approach proposed by the author of the dissertation remains valid for the forthcoming generation of video coding standards.**



## 6. ADVANCED SCREEN CONTENT CODING

### 6.1. INTRODUCTION

In the previous chapter (Chapter 5), the author of the dissertation proposes using Screen Content Coding for efficient compression of frame-compatible multiview and immersive video. The main idea for such change is to exploit similarities between the views with Intra Block Copy. The experiments presented in Section 5.7 prove that the proposed approach significantly improves the compression efficiency of frame-compatible video compared to the HEVC Main encoder. Nevertheless, the proposal is less efficient than the state-of-the-art dedicated solution for multiview compression – Multiview HEVC (Section 5.7.3). Despite that, HEVC SCC has a few important advantages over Multiview HEVC, such as shorter encoding time, less complex implementation, and broader versatility (one encoder for multiple applications).

In this chapter, the author of the dissertation focuses on **improving the efficiency of Screen Content Coding in the compression of multiview and immersive video**. The author proposes a novel approach to multiview video compression, including **adapting the configuration of HEVC SCC** to the new application and **a set of improvements** aimed at increasing the compression efficiency of frame-compatible multiview video and immersive video. The goal of the work is to prepare a **competitive alternative for the state-of-the-art Multiview HEVC** with comparable compression efficiency and better usability. In the dissertation, the encoder with the author's improvements is called **Advanced Screen Content Coding (ASCC)**. The ASCC encoder is also applied to immersive video coding, and the author proposes a MIV metadata parser for controlling tools, depending on the type of input video, to achieve the highest compression efficiency.

### 6.2. IMPROVEMENTS OF SCC FOR MULTIVIEW VIDEO COMPRESSION

#### 6.2.1. FRAME-COMPATIBILITY WITH SPECIFIC ORDERING

As explained in Section 5.2, the views of a multiview video have to compose a single frame to allow the Intra Block Copy technique to take advantage of the similarities between them. In Section 5.3, different view alignments are compared, which results in choosing horizontal view alignment as the most efficient. In this section, the author of the dissertation proposes to change the order of the views that compose a frame-compatible sequence. The preferred order for compression of 3 views is middle-leftmost-rightmost, as presented in

Figure 6.1. Such an ordering reflects the most common approach in Multiview HEVC, where the middle view is encoded as the first and then becomes a reference for inter-view prediction of the remaining views [Müller’14]. Obviously, the information about the order of encoded views has to be included in the bitstream to allow the decoder to properly organize the output after decoding and splitting the frame-compatible video into separate views. The author includes such information in the bitstream as an extension of the Video Parameter Set (VPS) [ISO’21].

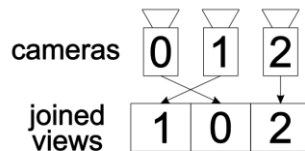


Figure 6.1. Order of positioning 3 cameras in a scene and joining acquired views.

### 6.2.2. TILE ENCODING

When processing a video using the default configuration, the HEVC encoder divides each frame into so-called Coding Tree Units (CTUs) and then compresses them in rows from left to right, starting from the top left CTU. Considering a frame-compatible format, the top rows of each view are encoded first, then the second rows, etc. As explained in Section 2.3, the reference area for Intra Block Copy has to be restricted to the part of the frame that was already compressed, otherwise, it would not be possible to reproduce the prediction at the decoder side. Therefore, in the unmodified SCC compression of frame-compatible multiview video, Intra Block Copy cannot perform inter-view prediction by matching the area of another view below the vertical position of the compressed unit. Due to such limitations, the efficiency of IBC as an inter-view prediction technique may be deteriorated.

As a solution for this issue, the author of the dissertation proposes to apply compression in tiles, as presented in Figure 6.2. In the proposal, the division of a frame into tiles is analogous to the accommodation of views within a frame-compatible video, which means that every view corresponds to a single tile. In such a configuration, the leftmost tile (which corresponds to the middle view according to the proposed accommodation of views presented in Section 6.2.1) is compressed in whole before the compression of the remaining views begins. Therefore, the restriction for IBC on vertical position does not apply if the block matching is performed within the area of the previously encoded tile. This way, Intra Block Copy can search for the best matching block of samples within a bigger area, even below the vertical position of the currently processed unit. However, it should be mentioned that the application of the proposed solution

introduces a dependency between tiles, which disables the capability of parallel processing of tiles.



Figure 6.2. HEVC coding order without (above) and with (below) tile encoding.

### 6.2.3. INTRA BLOCK COPY VECTORS PRECISION

As described in Section 2.3, Intra Block Copy produces a block vector that points to the best matching block of samples within the reconstructed part of the current picture. The resulting vector's precision is full-pel because, in the case of computer-generated images, the benefit from using sub-pel precision is usually negligible or even negative, while the processing time is noticeably longer. The author of the dissertation proposes to apply Intra Block Copy as an inter-view prediction technique for multiview camera-captured content, for which performing a sub-pel block matching could be beneficial. The state-of-the-art dedicated multiview video coding technique, Multiview HEVC, supports inter-view prediction at a quarter-pel level. Therefore, for a fair comparison, the author of the dissertation improves the Intra Block Copy by implementing a quarter-pel block matching. Obviously, such a change can affect the efficiency of Advanced SCC in the compression of screen content. The impact of the proposed modification on screen content compression is evaluated in Section 6.4.3.

### 6.2.4. STARTING POINT FOR BLOCK MATCHING IN INTRA BLOCK COPY

Application of Screen Content Coding for compression of frame-compatible multiview video aims at utilizing Intra Block Copy as an inter-view prediction technique, and tile encoding allows the IBC to use the whole previously encoded tile as a reference. The expected result of Intra Block Copy search is a prediction vector that points to the best matching block of samples in a different tile (Figure 6.3). Such a vector is relatively long, which is not desired due to the relatively high cost of representing it in the bitstream. Moreover, Intra Block Copy has to search

distant areas to find the best matching block of samples, which can deteriorate the processing time.



Figure 6.3. Long inter-view prediction vector derived by Intra Block Copy.

In the ASCC, the author of the dissertation proposes to change the starting point for the Intra Block Copy search to the position of the collocated unit in the leftmost tile. This way, the probability of finding the expected best-matching block of samples in the reference view is higher, and the IBC processing time is shorter. Additionally, the distance between the processed unit and the collocated one in the reference tile is subtracted from the horizontal component of the block vector returned by Intra Block Copy. This means that the block vector  $(0, 0)$  indicates the collocated position in the reference view instead of the current position. Such an approach reduces the average length of vectors found by the Intra Block Copy algorithm, which is beneficial for the overall compression efficiency.

### 6.2.5. IN-LOOP FILTERING PER TILE

As mentioned, Intra Block Copy searches for the best matching block of samples in the previously encoded area of the same picture. Therefore, the prediction is made on a reconstructed part of a frame before the in-loop filtering. Loop filters are executed at the end of the compression of each slice to reduce the encoding artifacts and thus improve the quality of the reconstructed picture, which can then be used as a reference for the compression of the following frames [Sullivan'12].

In the proposed Advanced SCC, the author of the dissertation applies the in-loop filtering after the compression of each tile. This improves the quality of the reference view (which is represented by a single tile) and allows Intra Block Copy to predict the content of the side views more accurately. Moreover, HEVC allows choosing whether the in-loop filters should be applied at the boundaries between tiles [ISO'21]. In the frame-compatible multiview video, the sharp edges between the views are intended, therefore the filtering at the boundaries of tiles is disabled to preserve them.



### 6.2.6. DIFFERENT QUANTIZATION PARAMETER FOR SIDE VIEWS

The compression level in HEVC is mainly controlled by Quantization Parameter (QP). The higher the QP, the lower the bitrate, but at the same time, the quality of decoded video becomes worse. In Multiview HEVC, the QP can be set individually for each view, which is the case in the default configuration in Common Test Conditions for Multiview HEVC [Müller'14]. In order to prepare a fair comparison, the author of the dissertation adds to the ASCC a possibility to specify Quantization Parameter per tile. It is a non-standard information that must be provided in the bitstream to allow the decoder to decompress it correctly. In the proposal, the difference between the QP of the leftmost tile and another one is included in the Video Parameter Set extension.

### 6.2.7. REFERENCE TILE BORDER EXTENSION

When a Prediction Unit (PU) is close to the right border of a tile, the search area of Intra Block Copy can cover the border between tiles, as well as a part of a tile next to the reference one (Figure 6.4). Therefore, the prediction error of matching a PU with a block of samples that contains parts of two tiles is very high.

In the Advanced SCC, the author of the dissertation implements an algorithm that extracts the reconstructed reference tile and extends its borders by interpolating the values from the edge of a tile. Such a solution results in better prediction than matching the boundaries of two tiles and is in line with inter-frame prediction, where the borders of reference views are also extended in a similar manner.

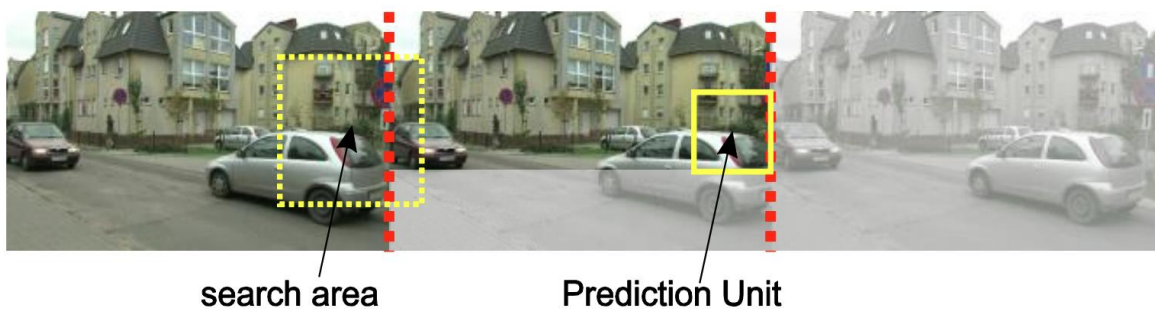


Figure 6.4. Intra Block Copy search at the border of two tiles.

## 6.3. IMPROVEMENTS OF SCC FOR IMMERSIVE VIDEO COMPRESSION

### 6.3.1. ADAPTATION OF ADVANCED SCC TO IMMERSIVE VIDEO

The improvements of Screen Content Coding (collectively called Advanced SCC) for compression of frame-compatible multiview video, presented in Section 6.2, are also applied to immersive video coding. However, some of the proposed improvements cannot be applied in the same manner as for multiview video, while others cannot be applied at all. The list of changes compared to ASCC for multiview video is as follows:

- Ordering of view accommodation in frame-compatible input video (Section 6.2.1) is not changed. In the case of immersive video, the views are stacked into atlases directly by the TMIV encoder. Modifications of TMIV are out of the scope of the dissertation. The video data produced by TMIV is encoded with ASCC “as is”, therefore no manipulation with the ordering of views is done.
- Starting point for IBC block matching (Section 6.2.4) is shifted vertically instead of horizontally. Since the views in atlases are stacked vertically, the Intra Block Copy search should start from the position of a collocated block in the topmost tile instead of the leftmost. Also, in this case, the vertical distance between the current and collocated position is subtracted from the vertical component of the Intra Block Copy vector.
- Different Quantization Parameters for side views (QPs) are not applied. All tiles composing a frame are compressed with the same QP. This is to assert that the view synthesis is performed using base views of similar quality.
- Enabled Palette Mode. As presented in Chapter 5, Palette Mode can be beneficial for the compression of depth maps, therefore it was enabled for immersive video coding using Advanced Screen Content Coding.

The remaining improvements prepared for the frame-compatible multiview video are applied to the compression of immersive video with no changes.

### 6.3.2. USING MIV METADATA TO CONTROL THE MODIFICATIONS

As described in Section 2.4, MPEG Immersive Video encoder reduces the inter-view similarities and forms the remaining video data into so-called patch atlases, which are then compressed individually with general video encoders such as HEVC or, as proposed in Chapter 5, HEVC SCC. The atlases, however, have different characteristics, and therefore the efficiency

of the encoder may differ depending on the type of atlas provided at the input. This observation was experimentally proven in Section 5.7.4, where the benefit from using HEVC SCC was, e.g., greater for atlases with depth patches than views patches.

In this section, on top of the ASCC modifications, the author proposes to incorporate a dedicated metadata parser into the MIV coding scheme for controlling the configuration of video encoders, depending on the type of input atlas. Figure 6.5 presents a block diagram of the proposed modified MIV encoder. In the state-of-the-art MIV encoder, metadata is directly included in the resulting bitstream. At the same time, in the proposal, it is additionally parsed and can be used to configure such options as the precision of Intra Block Copy vectors (full-pel or quarter-pel), configuration for tile encoding, enabling Palette Mode for depth atlases, etc. Another advantage of such a solution is that it doesn't require any additional signaling because metadata is already present in the MIV bitstream.

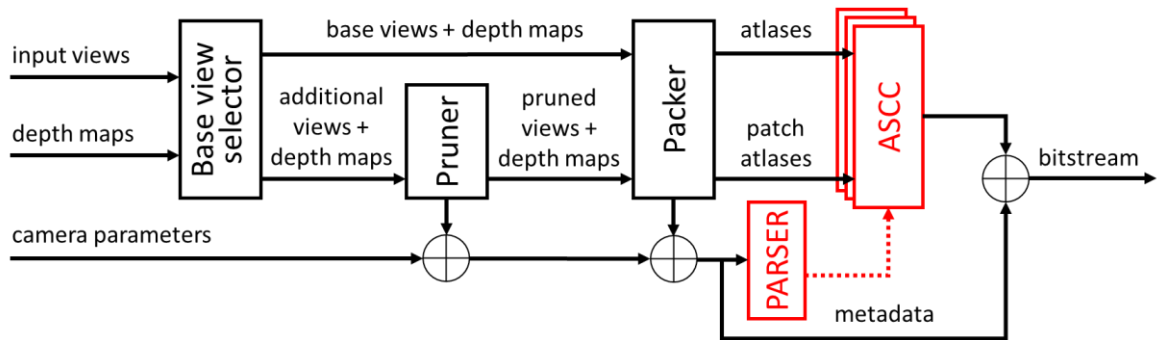


Figure 6.5. MPEG Immersive Video coding scheme with ASCC encoder controlled by MIV metadata.

The evaluation of Advanced SCC modifications in the compression of different types of atlases is presented in Section 6.4, along with comments on how the encoders should be set up for each atlas to achieve the highest compression efficiency.

## 6.4. EVALUATION OF THE PROPOSAL

### 6.4.1. GOALS OF THE EXPERIMENTS

In this chapter, the author's several modifications of Screen Content Coding are described. The goal of these changes is to better adapt SCC to new applications, namely multiview and immersive video compression. The proposed improvements are implemented in a publicly available test model for the HEVC SCC codec (details in Chapter 3). In the case of multiview video coding, the goal of the author's proposal is to achieve compression efficiency comparable to Multiview HEVC, which is the dedicated coding technique for multiview video

content. A comparison of the proposal with the state-of-the-art is presented in Section 6.4.2. Additionally, the author of the dissertation conducts an experiment that evaluates the influence of the proposed modifications in the compression of screen content (Section 6.4.3).

Regarding the application of ASCC to immersive video coding, the main goal of the experiments (presented in Section 6.4.4) is to assess the compression efficiency of different types of video data generated by the MIV encoder. Based on the results, the author proposes a novel approach to immersive video coding that would adjust the coding tools to the input video data to increase the compression efficiency and the quality of synthesized video presented to end users.

The complete results of the conducted experiments can be found in the Appendix.

#### **6.4.2. EVALUATION OF ADVANCED SCC IN MULTIVIEW VIDEO CODING**

In this section, the proposed ASCC is compared to Multiview HEVC in terms of encoding time and compression efficiency. The base configuration of both encoders is set up according to the appropriate Common Test Conditions as described in Chapter 3, with some additional changes. Regarding the configuration of ASCC, tools specific to Screen Content Coding are configured as proposed in Section 5.4. Moreover, the configuration is adapted to tile encoding and modified in-loop filtering as proposed in Sections 6.2.2 and 6.2.5. Regarding Multiview HEVC configuration, the vertical range limit for disparity search is set to 64 (from default 128), and Early Skip Detection is enabled to make the configuration fair and consistent with HEVC SCC. The experiments are conducted using 3 views of 8 multiview sequences, chosen and ordered according to Common Test Conditions for multiview video coding. The evaluation is performed in All Intra and Random Access coding scenarios.

Experimental results of the comparison are presented in Tables 6.1 – 6.4. Negative numbers indicate better compression efficiency (lower bitrate at constant quality) or shorter encoding time.

Table 6.1. Bitrate reduction [%] against HEVC simulcast and MV-HEVC; All Intra.  
Negative values indicate lower bitrates.

| Sequence       | HEVC simulcast |               |               |               | MV-HEVC      |             |              |              |
|----------------|----------------|---------------|---------------|---------------|--------------|-------------|--------------|--------------|
|                | 2 views        |               | 3 views       |               | 2 views      |             | 3 views      |              |
|                | SCC            | ASCC          | SCC           | ASCC          | SCC          | ASCC        | SCC          | ASCC         |
| Poznan_Hall2   | -16.79         | -28.01        | -21.08        | -40.57        | 17.24        | 2.93        | 27.36        | -1.67        |
| Poznan_Street  | -20.66         | -31.57        | -27.53        | -47.35        | 15.30        | 2.69        | 29.05        | -0.55        |
| Kendo          | -20.25         | -29.19        | -26.33        | -40.76        | 14.10        | 2.19        | 22.34        | 0.06         |
| Balloons       | -21.49         | -29.29        | -30.08        | -41.90        | 12.01        | 1.80        | 18.27        | 0.00         |
| Newspaper      | -18.32         | -25.37        | -25.51        | -39.06        | 9.75         | 1.87        | 18.56        | -0.35        |
| Dancer         | -35.14         | -39.98        | -47.16        | -55.71        | 8.86         | 1.25        | 17.12        | -0.79        |
| GT_Fly         | -38.56         | -42.27        | -50.71        | -58.22        | 6.85         | 0.62        | 15.36        | -1.54        |
| Shark          | -35.39         | -40.50        | -49.78        | -57.29        | 8.89         | 0.64        | 15.68        | -0.97        |
| <b>Average</b> | <b>-26.28</b>  | <b>-34.21</b> | <b>-34.56</b> | <b>-48.52</b> | <b>12.47</b> | <b>1.94</b> | <b>22.25</b> | <b>-0.90</b> |

Table 6.2. Encoding time reduction [%] against HEVC simulcast and MV-HEVC; All Intra.  
Negative values indicate faster encoding.

| Sequence       | HEVC simulcast |            |             |            | MV-HEVC    |           |            |           |
|----------------|----------------|------------|-------------|------------|------------|-----------|------------|-----------|
|                | 2 views        |            | 3 views     |            | 2 views    |           | 3 views    |           |
|                | SCC            | ASCC       | SCC         | ASCC       | SCC        | ASCC      | SCC        | ASCC      |
| Poznan_Hall2   | +56            | +8         | +63         | +22        | +43        | -1        | +32        | -5        |
| Poznan_Street  | +170           | +38        | +183        | +48        | +79        | -9        | +67        | -12       |
| Kendo          | +169           | +117       | +183        | +147       | +25        | +1        | +11        | -4        |
| Balloons       | +195           | +121       | +212        | +148       | +35        | +1        | +24        | -1        |
| Newspaper      | +242           | +131       | +259        | +151       | +51        | +2        | +37        | -3        |
| Dancer         | +330           | +30        | +319        | +31        | +224       | -2        | +204       | -5        |
| GT_Fly         | +150           | +11        | +126        | +4         | +124       | +0        | +111       | -3        |
| Shark          | +180           | +35        | +142        | +27        | +111       | +2        | +87        | -2        |
| <b>Average</b> | <b>+175</b>    | <b>+41</b> | <b>+175</b> | <b>+50</b> | <b>+99</b> | <b>-2</b> | <b>+85</b> | <b>-5</b> |

Table 6.3. Bitrate reduction [%] against HEVC simulcast and MV-HEVC; Random Access.  
Negative values indicate lower bitrates.

| Sequence       | HEVC simulcast |               |               |               | MV-HEVC      |              |              |             |
|----------------|----------------|---------------|---------------|---------------|--------------|--------------|--------------|-------------|
|                | 2 views        |               | 3 views       |               | 2 views      |              | 3 views      |             |
|                | SCC            | ASCC          | SCC           | ASCC          | SCC          | ASCC         | SCC          | ASCC        |
| Poznan_Hall2   | -11.30         | -23.55        | -13.82        | -32.09        | 13.47        | -1.92        | 25.43        | -0.63       |
| Poznan_Street  | -13.88         | -25.78        | -19.29        | -38.91        | 16.73        | 1.43         | 30.82        | 0.51        |
| Kendo          | -10.30         | -19.45        | -13.80        | -27.52        | 12.37        | 1.45         | 18.39        | 0.37        |
| Balloons       | -13.26         | -21.38        | -18.44        | -30.11        | 11.28        | 1.34         | 16.19        | 0.33        |
| Newspaper      | -16.00         | -23.55        | -20.46        | -33.04        | 8.93         | -0.03        | 17.74        | 0.46        |
| Dancer         | -25.82         | -35.02        | -34.32        | -47.59        | 11.89        | -1.69        | 24.67        | 0.05        |
| GT_Fly         | -21.74         | -31.09        | -31.67        | -46.23        | 13.87        | 0.21         | 27.18        | 0.05        |
| Shark          | -29.50         | -37.76        | -40.39        | -52.22        | 12.82        | -0.10        | 23.93        | -0.18       |
| <b>Average</b> | <b>-16.61</b>  | <b>-26.98</b> | <b>-22.58</b> | <b>-38.47</b> | <b>13.67</b> | <b>-0.11</b> | <b>25.30</b> | <b>0.07</b> |

Table 6.4. Encoding time reduction [%] against HEVC simulcast and MV-HEVC; Random Access.  
Negative values indicate faster encoding.

| Sequence       | HEVC simulcast |            |             |            | MV-HEVC     |           |            |           |
|----------------|----------------|------------|-------------|------------|-------------|-----------|------------|-----------|
|                | 2 views        |            | 3 views     |            | 2 views     |           | 3 views    |           |
|                | SCC            | ASCC       | SCC         | ASCC       | SCC         | ASCC      | SCC        | ASCC      |
| Poznan_Hall2   | +80            | -5         | +77         | -2         | +88         | -1        | +80        | +0        |
| Poznan_Street  | +141           | +22        | +140        | +23        | +102        | +2        | +99        | +2        |
| Kendo          | +169           | +45        | +127        | +47        | +88         | +1        | +56        | +1        |
| Balloons       | +190           | +45        | +183        | +45        | +100        | +0        | +92        | -1        |
| Newspaper      | +184           | +47        | +189        | +50        | +97         | +2        | +94        | +0        |
| Dancer         | +175           | +17        | +176        | +17        | +137        | +1        | +138       | +1        |
| GT_Fly         | +162           | +10        | +142        | +7         | +134        | -2        | +123       | -1        |
| Shark          | +164           | +30        | +123        | +28        | +104        | +0        | +74        | +0        |
| <b>Average</b> | <b>+145</b>    | <b>+18</b> | <b>+132</b> | <b>+18</b> | <b>+110</b> | <b>+0</b> | <b>+99</b> | <b>+0</b> |

Experimental results confirm that the proposed modifications significantly improve both compression efficiency and encoding time compared to the unmodified HEVC SCC. For Random Access, **encoding 3 views with ASCC results in a nearly 40% smaller bitrate** compared to simulcast, at the cost of around 20% longer encoding time. Compared to Multiview HEVC, the proposed solution is **as efficient as a dedicated technique with no significant difference in encoding time**. The above results prove that such a novel approach to multiview compression could substitute the state-of-the-art complex codec.

### 6.4.3. EVALUATION OF ADVANCED SCC IN SCREEN CONTENT CODING

As mentioned earlier in this chapter, the author's modifications to SCC are supposed to improve the compression efficiency of camera-captured multiview video. Therefore, some of the proposed changes may negatively impact the compression of screen content. In this section, this influence is evaluated. Advanced SCC is used for the compression of 13 test sequences commonly used in the evaluation of HEVC SCC. Since only one view is encoded, some of the ASCC modifications (e.g., frame-compatibility, tile encoding) do not apply.

As in previous experiments, tests are performed in All Intra and Random Access coding scenarios. The configuration is in line with Common Test Conditions for screen content coding, including enabled Palette Mode. The results of the comparison between ASCC and unmodified SCC are presented in Table 6.5.

Table 6.5. Experimental results for ASCC against HEVC-SCC in compression of single view screen content.

| Sequence            | All Intra   |                   | Random Access |                   |
|---------------------|-------------|-------------------|---------------|-------------------|
|                     | Bitrate [%] | Encoding time [%] | Bitrate [%]   | Encoding time [%] |
| Basketball_Screen   | 3.90        | +22               | 2.60          | +10               |
| ChinaSpeed          | 0.58        | +14               | 0.32          | +23               |
| ChineseEditing      | 3.95        | +13               | 3.50          | +12               |
| MissionControlClip2 | 0.56        | +19               | 0.42          | +10               |
| MissionControlClip3 | 3.05        | +20               | 2.38          | +10               |
| sc_console          | 15.07       | +30               | 8.34          | +15               |
| sc_desktop          | 13.40       | +23               | 8.82          | +13               |
| sc_flyingGraphics   | 9.07        | +20               | 5.38          | +31               |
| sc_map              | 2.35        | +16               | 1.42          | +10               |
| sc_programming      | 4.61        | +18               | 1.89          | +13               |
| sc_robot            | 0.28        | +13               | 0.10          | +20               |
| sc_web_browsing     | 15.24       | +26               | 11.27         | +18               |
| SlideShow           | -0.98       | +23               | -0.77         | +33               |
| <b>Average</b>      | <b>5.47</b> | <b>+20</b>        | <b>3.51</b>   | <b>+17</b>        |

The results indicate that ASCC is slower by roughly 20% than the unmodified SCC. That is because ASCC performs Intra Block Copy search at quarter-pel precision, while originally it is limited to full-pel. Obviously, this introduces overhead in encoding time. Regarding compression efficiency, the sub-pel accuracy of IBC is not beneficial for computer-generated content. However, the results strongly depend on the content of the video. As observed, the compression efficiency of ASCC is close to the unmodified SCC for sequences that contain a lot of fluent motion, gradients, parts with camera-captured content, or computer-generated images that are supposed to imitate natural images. On the other hand, the bitrate is significantly increased for the compression of mostly computer-generated content with simple graphics and motion. In this case, full-pel precision from the original SCC seems enough, and further improving it to quarter-pel does not improve the IBC prediction but generates a significant amount of redundant bits. Therefore, if the ASCC would be applied both to compression of multiview video and screen content, the accuracy of Intra Block Copy search would need to be dynamically adjusted by the encoder to optimize the efficiency for various types of input data.

#### **6.4.4. EVALUATION OF ADVANCED SCC IN IMMERSIVE VIDEO CODING**

This section presents the evaluation of ASCC adapted to immersive video coding as described in Section 6.3. The tests are performed according to Common Test Conditions for immersive video [CTC MIV] on 17 frames of 6 camera-captured and 9 computer-generated sequences. The state-of-the-art Test Model for MIV [TMIV] was used in the experiments. It should be noted that the process of preparing atlases is not changed; only the internal video encoder is replaced with ASCC and compared to HEVC Main in terms of encoding time and quality of video synthesized from reconstructed data after the encoding and decoding cycle. The assessment of quality is performed using two full-reference metrics: WS-PSNR and IV-PSNR, described in Chapter 3. Then, bitrate reduction represented as Bjøntegaard delta is calculated for both metrics.

The experiments are divided into two sections. Section A presents experimental results of using only quarter-pel IBC precision in compression of all types of atlases, while Section B additionally evaluates the efficiency of tile encoding.



### A. QUARTER-PEL IBC ACCURACY

In order to fully evaluate the influence of IBC accuracy on immersive video coding, three experiments are performed. In the first experiment, quarter-pel accuracy is compared to full-pel used by unmodified Screen Content Coding. The results of such a comparison are presented in Tables 6.6 – 6.7. Table 6.8 gathers encoding results of the remaining experiments: in one of them, quarter-pel accuracy is applied only to depth data, while in the other, only to atlases of views.

Table 6.6. Results for compression of SCC with quarter-pel IBC accuracy compared to basic SCC. Negative values indicate lower bitrates at the same quality or faster encoding.

| Sequence           | BD-rate<br>WS-<br>PSNR <sub>Y</sub> | BD-rate<br>IV-PSNR | $\Delta$<br>Encoding<br>time |
|--------------------|-------------------------------------|--------------------|------------------------------|
| ClassroomVideo     | − 0.3%                              | +0.7%              | +7.2%                        |
| TechnicolorMuseum  | +0.6%                               | +0.9%              | +8.7%                        |
| Fan                | +0.3%                               | +0.5%              | +3.7%                        |
| OrangeKitchen      | +0.1%                               | − 0.2%             | +6.3%                        |
| Chess              | − 0.5%                              | − 1.3%             | +4.3%                        |
| Group              | +0.6%                               | +0.5%              | +8.0%                        |
| ChessPieces        | − 1.0%                              | − 3.0%             | +8.3%                        |
| TechnicolorHijack  | − 0.1%                              | − 0.5%             | +13.2%                       |
| Mirror             | +0.5%                               | +0.0%              | +1.5%                        |
| <b>CG average</b>  | <b>+0.0%</b>                        | <b>− 0.3%</b>      | <b>+6.8%</b>                 |
| TechnicolorPainter | − 1.6%                              | − 1.9%             | +10.4%                       |
| IntelFrog          | +0.1%                               | − 0.0%             | +7.5%                        |
| Poznan_Carpark     | − 1.3%                              | − 1.4%             | +8.7%                        |
| Poznan_Fencing2    | − 2.0%                              | − 2.4%             | +7.2%                        |
| Poznan_Hall2       | − 6.0%                              | − 7.3%             | +6.2%                        |
| Poznan_Street      | − 2.9%                              | − 3.1%             | +8.6%                        |
| <b>NC average</b>  | <b>− 2.3%</b>                       | <b>− 2.7%</b>      | <b>+8.1%</b>                 |
| <b>Average</b>     | <b>− 0.9%</b>                       | <b>− 1.2%</b>      | <b>+7.3%</b>                 |

The results presented in Table 6.6 show that using quarter-pel IBC search accuracy instead of full-pel is more efficient when encoding camera-captured content. In the case of computer-generated content, the influence on the efficiency is much smaller for IV-PSNR and negligible for WS-PSNR. In terms of encoding time, more accurate IBC block matching results in longer processing, with an average increase of 7% compared to unmodified Screen Content Coding.

Table 6.7 presents the results separately for views and depth data and shows an average bitrate reduction at each of the four rate points. Additionally, the values of IV-PSNR quality for synthesized views are compared. As observed, a more accurate IBC vector search does not impact the quality of synthesized views nor the bitrates of compressed computer-generated content. However, a significant gain was observed for the compression of depth data estimated for camera-captured sequences.

Table 6.7. Results for compression of SCC with quarter-pel IBC accuracy compared to basic SCC, bitrate, and quality change for different rate points. Rate points are defined in CTC separately for each sequence, therefore they are denoted as R1-R4.

| Content type | Rate | Views bitrate [Mbps] |       |          | Depth bitrate [Mbps] |       |          | IV-PSNR [dB] |       |
|--------------|------|----------------------|-------|----------|----------------------|-------|----------|--------------|-------|
|              |      | FPel                 | QPel  | $\Delta$ | FPel                 | QPel  | $\Delta$ | FPel         | QPel  |
| CG           | R1   | 58.95                | 58.38 | - 1%     | 7.38                 | 7.35  | 0%       | 44.31        | 44.31 |
|              | R2   | 15.81                | 15.72 | - 1%     | 5.39                 | 5.37  | 0%       | 43.04        | 43.05 |
|              | R3   | 5.01                 | 5.07  | 1%       | 3.72                 | 3.71  | 0%       | 40.89        | 40.90 |
|              | R4   | 1.65                 | 1.66  | 1%       | 2.78                 | 2.78  | 0%       | 38.14        | 38.14 |
| NC           | R1   | 79.46                | 79.02 | - 1%     | 31.07                | 28.95 | - 7%     | 45.41        | 45.42 |
|              | R2   | 16.59                | 16.53 | 0%       | 13.81                | 12.74 | - 8%     | 43.92        | 43.93 |
|              | R3   | 5.42                 | 5.51  | 2%       | 6.19                 | 5.90  | - 5%     | 41.76        | 41.75 |
|              | R4   | 2.02                 | 2.04  | 1%       | 3.76                 | 3.69  | - 2%     | 38.46        | 38.47 |

Since the results in Table 6.7 indicate a significant difference in bitrate reduction between depth and views atlases, another experiment is conducted to assess the performance of mixed full-pel and quarter-pel solutions. Table 6.8 gathers the results of two tests: in the first one, the quarter-pel accuracy is applied only to the compression of depth atlases, while in the second one, it is applied only to views atlases.

According to the results, the optimal configuration of IBC search precision is quarter-pel for depth atlases and full-pel for views atlases. Although the achieved gain is small for computer-generated content, bitrate reduction can be as high as 7% for natural content. Moreover, using the proposed mixed precision does not negatively impact encoding time – the results indicate roughly the same encoding time compared to the full-pel only scenario.

Table 6.8. Results for compression of SCC with mixed full-pel and quarter-pel IBC accuracy, compared to SCC. Negative values indicate lower bitrates at the same quality or faster encoding.

| Sequence           | QPel accuracy for depth,<br>FPel for views |                    |                           | FPel accuracy for depth,<br>QPel for views |                    |                           |
|--------------------|--|--------------------|---------------------------|--|--------------------|---------------------------|
|                    | BD-rate<br>WS-PSNR <sub>y</sub>            | BD-rate<br>IV-PSNR | $\Delta$ Encoding<br>time | BD-rate<br>WS-PSNR <sub>y</sub>            | BD-rate<br>IV-PSNR | $\Delta$ Encoding<br>time |
| ClassroomVideo     | - 0.2%                                     | - 0.2%             | + 0.8%                    | - 0.1%                                     | + 0.9%             | + 7.0%                    |
| TechnicolorMuseum  | - 0.0%                                     | - 0.1%             | + 0.3%                    | + 0.6%                                     | + 1.0%             | + 8.3%                    |
| Fan                | + 0.3%                                     | + 0.2%             | - 0.9%                    | - 0.0%                                     | + 0.3%             | + 2.7%                    |
| OrangeKitchen      | - 0.1%                                     | - 0.3%             | - 2.8%                    | + 0.2%                                     | + 0.0%             | + 5.9%                    |
| Chess              | - 0.1%                                     | - 0.1%             | - 2.4%                    | - 0.4%                                     | - 1.1%             | + 3.7%                    |
| Group              | + 0.4%                                     | + 0.2%             | + 1.9%                    | + 0.3%                                     | + 0.3%             | + 7.4%                    |
| ChessPieces        | - 1.0%                                     | - 1.5%             | - 0.2%                    | - 0.0%                                     | - 1.5%             | + 7.8%                    |
| TechnicolorHijack  | + 0.1%                                     | - 0.2%             | + 0.9%                    | - 0.2%                                     | - 0.4%             | +12.0%                    |
| Mirror             | - 0.2%                                     | - 0.2%             | - 0.6%                    | + 0.7%                                     | + 0.3%             | + 1.1%                    |
| <b>CG average</b>  | <b>- 0.1%</b>                              | <b>- 0.2%</b>      | <b>- 0.3%</b>             | <b>+ 0.1%</b>                              | <b>- 0.0%</b>      | <b>+ 6.2%</b>             |
| TechnicolorPainter | - 1.3%                                     | - 1.3%             | + 0.4%                    | - 0.3%                                     | - 0.6%             | + 8.9%                    |
| IntelFrog          | - 0.5%                                     | - 1.0%             | + 1.1%                    | + 0.6%                                     | + 1.0%             | + 6.9%                    |
| Poznan_Carpark     | - 1.5%                                     | - 1.7%             | + 3.2%                    | + 0.2%                                     | + 0.3%             | + 7.8%                    |
| Poznan_Fencing2    | - 1.9%                                     | - 2.5%             | + 0.8%                    | - 0.0%                                     | + 0.0%             | + 6.3%                    |
| Poznan_Hall2       | - 6.3%                                     | - 7.1%             | + 1.3%                    | + 0.4%                                     | - 0.2%             | + 5.9%                    |
| Poznan_Street      | - 4.5%                                     | - 4.6%             | + 0.6%                    | + 1.5%                                     | + 1.5%             | + 8.2%                    |
| <b>NC average</b>  | <b>- 2.7%</b>                              | <b>- 3.0%</b>      | <b>+ 1.2%</b>             | <b>+ 0.4%</b>                              | <b>+ 0.3%</b>      | <b>+ 7.3%</b>             |
| <b>Average</b>     | <b>- 1.1%</b>                              | <b>- 1.4%</b>      | <b>+ 0.3%</b>             | <b>+ 0.2%</b>                              | <b>+ 0.1%</b>      | <b>+ 6.6%</b>             |

## B. QPEL + TILE-BASED IBC ANALYSIS

In this section, the performance of tile-based IBC analysis is evaluated. The reference for the experiments is HEVC SCC with quarter-pel accuracy of IBC vector search. In the first experiment, tile-based encoding is enabled only for atlas with base views. The reason for that is because such type of an atlas is somewhat a frame-compatible multiview video, where the views are stacked vertically. Therefore, tile encoding is set up in such a way that each tile contains exactly one of the views. The results of the abovementioned experiments are presented in Table 6.9.

Table 6.9. Results for compression of SCC with quarter-pel IBC accuracy and tile-based IBC analysis for the first atlas of views, compared to basic SCC. Negative values indicate lower bitrates at the same quality or faster encoding.

| Sequence           | BD-rate<br>WS-PSNR <sub>Y</sub> | BD-rate<br>IV-PSNR | Δ Encoding<br>time |
|--------------------|---------------------------------|--------------------|--------------------|
| ClassroomVideo     | + 2.6%                          | - 5.2%             | - 45.6%            |
| TechnicolorMuseum  | + 1.3%                          | + 2.1%             | - 21.5%            |
| Fan                | + 0.7%                          | + 1.4%             | - 19.3%            |
| OrangeKitchen      | + 1.6%                          | + 2.8%             | - 9.6%             |
| Chess              | + 0.3%                          | - 0.5%             | - 9.4%             |
| Group              | + 0.8%                          | + 0.3%             | - 22.9%            |
| ChessPieces        | - 0.6%                          | - 2.4%             | - 6.5%             |
| TechnicolorHijack  | + 0.6%                          | + 1.4%             | +13.0%             |
| Mirror             | + 2.4%                          | + 2.8%             | - 8.6%             |
| <b>CG average</b>  | <b>+ 1.1%</b>                   | <b>+ 0.3%</b>      | <b>- 15.5%</b>     |
| TechnicolorPainter | - 2.3%                          | - 4.2%             | - 4.3%             |
| IntelFrog          | - 0.7%                          | - 5.6%             | - 24.2%            |
| Poznan_Carpark     | - 6.1%                          | - 8.2%             | - 24.0%            |
| Poznan_Fencing2    | - 1.5%                          | - 3.5%             | - 17.5%            |
| Poznan_Hall2       | - 6.7%                          | - 7.7%             | - 9.3%             |
| Poznan_Street      | - 10.5%                         | - 12.3%            | - 23.2%            |
| <b>NC average</b>  | <b>- 4.6%</b>                   | <b>- 6.9%</b>      | <b>- 17.1%</b>     |
| <b>Average</b>     | <b>- 1.2%</b>                   | <b>- 2.6%</b>      | <b>- 15.5%</b>     |

In the remaining experiments, the tile-based IBC is enabled either for both views atlases or for all atlases. The gathered results are collectively presented in Table 6.10.

The results of the first experiment (Table 6.9) show that enabling tile-encoding for atlases containing base views with natural content significantly improves compression efficiency. At constant IV-PSNR, the **bitrate is reduced by nearly 7%**. Moreover, the **encoding time is noticeably shorter (15.5% on average)**. That is due to tile-based encoding, in which the IBC search is performed only on the referenced tile, much faster than analyzing the whole previously encoded area.

Regarding computer-generated content, enabling tile-based encoding slightly decreases the overall compression efficiency, nevertheless, the encoding time is reduced at a similar level as for natural content. Therefore, the results clearly indicate that tile encoding should be enabled for the first views atlas with natural content. It is possible to automate the configuration setup based on the atlas type by adding a MIV metadata parser, as described in Section 6.3.2.

Table 6.10 presents the influence of tile-based IBC enabled for different sets of atlases. The left part of the table contains experimental results of immersive video compression with tile-based encoding enabled for atlases with views data. The right part presents the results achieved when all atlases (views + depth) are compressed with tile-based encoding.

Table 6.10. Results for compression of SCC with Quarter-Pel IBC Accuracy and Tile-Based IBC Analysis for different sets of Atlases, compared to basic SCC. Negative values indicate lower bitrates at the same quality or faster encoding.

| Sequence           | Tile-based IBC analysis<br>for views atlases |                    |                           | Tile-based IBC analysis<br>for all atlases (views + depth) |                    |                           |
|--------------------|--|--------------------|---------------------------|--|--------------------|---------------------------|
|                    | BD-rate<br>WS-PSNR <sub>y</sub>              | BD-rate<br>IV-PSNR | $\Delta$ Encoding<br>time | BD-rate<br>WS-PSNR <sub>y</sub>                            | BD-rate<br>IV-PSNR | $\Delta$ Encoding<br>time |
| ClassroomVideo     | 3.7%   | - 4.5%             | - 60.3%                   | 9.0%   | - 1.8%             | - 58.4%                   |
| TechnicolorMuseum  | 2.2%   | 2.9%               | - 52.7%                   | 4.4%   | 4.7%               | - 49.1%                   |
| Fan                | 1.6%   | 2.5%               | - 48.2%                   | 6.4%   | 6.8%               | - 56.4%                   |
| OrangeKitchen      | 3.8%   | 4.9%               | - 42.4%                   | 8.4%   | 8.7%               | - 36.6%                   |
| Chess              | 2.1%   | 0.9%               | - 43.4%                   | 7.4%   | 5.3%               | - 39.6%                   |
| Group              | 1.7%   | 1.1%               | - 54.0%                   | 6.9%   | 4.5%               | - 54.8%                   |
| ChessPieces        | 1.4%   | 0.4%               | - 43.9%                   | 7.7%   | 4.9%               | - 40.3%                   |
| TechnicolorHijack  | 1.8%   | 2.8%               | - 42.0%                   | 8.5%   | 8.9%               | - 46.3%                   |
| Mirror             | 4.3%   | 4.6%               | - 44.2%                   | 7.0%   | 7.1%               | - 46.0%                   |
| <b>CG average</b>  | <b>2.5%</b>                                  | <b>1.7%</b>        | - 47.9%                   | <b>7.3%</b>  | <b>5.5%</b>        | - 47.5%                   |
| TechnicolorPainter | - 1.9%                                       | - 4.0%             | - 47.3%                   | 2.0%   | - 0.2%             | - 61.0%                   |
| IntelFrog          | - 0.1%                                       | - 5.6%             | - 55.6%                   | 3.3%   | - 2.6%             | - 66.3%                   |
| Poznan_Carpark     | - 5.6%                                       | - 7.9%             | - 36.2%                   | - 2.6%   | - 5.1%             | - 44.3%                   |
| Poznan_Fencing2    | - 0.7%                                       | - 3.0%             | - 46.0%                   | 4.6%   | 1.9%               | - 55.2%                   |
| Poznan_Hall2       | - 6.3%                                       | - 7.2%             | - 28.2%                   | 3.5%   | 2.5%               | - 46.0%                   |
| Poznan_Street      | - 10 %                                       | - 12 %             | - 33.7%                   | - 6.2%   | - 8.0%             | - 41.6%                   |
| <b>NC average</b>  | <b>- 4.1%</b>                                | <b>- 6.6%</b>      | - 41.2%                   | <b>0.8%</b>  | <b>- 1.9%</b>      | - 52.4%                   |
| <b>Average</b>     | <b>- 0.1%</b>                                | <b>- 1.6%</b>      | - 45.2%                   | <b>4.7%</b>  | <b>2.5%</b>        | - 49.5%                   |

When comparing Tables 6.10 and 6.9, it can be observed that performing tile-based encoding on patch atlases for views decreases the overall compression efficiency. Such a result is expected because patches in atlases are packed pseudo-randomly, therefore, it is not guaranteed that similar patches will be placed in different tiles.

Enabling tile-based encoding in compression of depth atlases significantly deteriorates the BD-rates for both quality metrics. Such results can be explained by different characteristics

of views and depth maps. The latter often contain sharp edges between objects or between objects and the background, as well as large, smooth, self-similar areas. Such characteristics make standard IBC more efficient as it takes advantage of self-similarities, opposite to the proposed tile-encoding. On the other hand, tile-based encoding has a positive impact on encoding time, which is almost halved compared to HEVC SCC encoding with only quarter-pel IBC search enabled.

## 6.5. CONCLUSIONS

In this chapter, the author of the dissertation proposes several modifications of Screen Content Coding aimed at improving the compression efficiency of multiview and immersive video. The proposal includes changes that are compatible with HEVC SCC, as well as modifications that require modifying the standard. The improvements are implemented on top of the test model for HEVC Screen Content Coding and adapted to the new applications – multiview and immersive video compression.

The evaluation of the author’s novel compression technique, Advanced SCC, includes a series of experiments and a comparison of the results with the state-of-the-art multiview and immersive video compression techniques. The results show that **ASCC is significantly more efficient than standard-compliant SCC**. In the case of multiview encoding, **the proposal is as efficient as the dedicated solution – Multiview HEVC**, without a negative impact on encoding time. When applied to camera-captured immersive video, the author’s improvements **significantly decrease the output bitrate and the encoding time**, compared to using state-of-the-art SCC as a video encoder in TMIV. Due to the different characteristics of atlases generated by MIV and differences between computer-generated and camera-captured content, the author also proposes including a MIV metadata parser as a controller of internal video encoder to adjust the configuration of ASCC to the input data and thus optimizing the overall performance.

The influence of the proposed modifications is also evaluated for the compression of screen content (Section 6.4.3). The results highly depend on the content of the test sequence, but usually, the proposal is less efficient than the original SCC. Therefore, modifications of Screen Content Coding should be adaptively toggled based on the input video data, similarly to the depth flag in 3D-HEVC that enables additional coding techniques dedicated to depth maps [ISO’21].

To sum up, the Advanced SCC technique proposed by the author of the dissertation appears to be an efficient, versatile solution that can provide high performance in multiple applications. The need for such versatile video codecs can be observed during the development of modern standards such as MPEG Immersive Video, which aims at efficient compression of both natural and computer-generated content acquired with different camera setups (omnidirectional, multi-camera systems, etc.) and is codec-agnostic to assure that the internal video codec can be easily changed when more efficient solutions appear. Moreover, the practical use of video extensions dedicated to one type of application is very limited, while the development of such extensions requires a lot of effort.





## 7. SUMMARY OF THE DISSERTATION

### 7.1. RECAPITULATION

This dissertation focuses on inter-view prediction techniques for the compression of multiview video acquired using systems with various camera arrangements. In Chapter 2, the author describes the state-of-the-art of multiview video coding and explains the motivation for the research. As stated, the dedicated codec for compression of such video, 3D-HEVC, is not efficient in the compression of video acquired using multi-camera systems with camera arrangements other than linear. Moreover, dedicated multiview profiles built on top of single-layer codecs, significantly increase the complexity of the codec, are not reusable in other applications, and require a lot of additional research to be developed. In order to address those issues, the author of the dissertation formulated two theses in Section 1.2:

- 1. It is possible to reduce both bitrate and encoding time of 3D-HEVC encoder in compression of rectified multiview video acquired with cameras located on a circle, compared to the state-of-the-art 3D-HEVC encoder, through adaptation of inter-view prediction to circular camera arrangements.**
- 2. It is possible to use standard-compliant HEVC Screen Content Coding for compression of stereoscopic video, frame-compatible multiview video, and immersive video. With additional improvements, the rate-distortion compression efficiency of such an approach can be comparable or even higher than the state-of-the-art dedicated techniques.**

Chapter 4 presents the verification of the first thesis. The author of the dissertation proposes a process for rectification of multiview video acquired roughly on a circle, using full 3D point mapping. Then, the author introduces a novel method for efficient inter-view prediction in compression of circularly rectified video. The proposal is implemented on top of 3D-HEVC through modification of Disparity Compensated Prediction, Inter-View Motion Prediction, View Synthesis Prediction, and other inter-view prediction tools. The new approach entails changes in the representation of camera parameters in 3D-HEVC bitstream syntax. In Section 4.6, the author presents experimental results of comparison between state-of-the-art and ARC-HEVC, in compression of circularly rectified video. The results are additionally compared to 3D-HEVC adapted to arbitrary camera arrangement (ANY-HEVC), which is also a non-standard codec co-authored by the author of this dissertation.

The verification of the second thesis is presented in Chapter 5 and Chapter 6. First, the author of the dissertation presents the idea of adapting standard-compliant Screen Content Coding for the compression of frame-compatible multiview video. In that idea, Intra Block Copy works as an inter-view prediction, even though its original purpose was different. The author describes the process of choosing the optimal view alignment, as well as the best configuration of other SCC tools. Then, the novel approach is used in 3 applications: stereoscopic, multiview, and immersive video compression. Section 5.7 presents the experimental evaluation of the proposal. In Chapter 6, the author's idea is further developed by several improvements. The goal of the modifications is to improve the inter-view prediction accuracy of SCC for multiview and immersive video coding. The proposal is experimentally evaluated, and the results are compared to the state-of-the-art dedicated solutions.

## 7.2. RESEARCH WORK DONE

During the research, the author created an original implementation of the following software:

- ANY-HEVC – part of modifications added on top of 3D-HEVC; ~2000 lines of code in C++,
- ARC-HEVC – all modifications added on top of 3D-HEVC; ~3500 lines of code in C++,
- Circular rectifier – software for deriving rectified camera parameters and performing video rectification; ~1000 lines of code in C++ and Python,
- Advanced SCC – modifications of HEVC SCC; ~2500 lines of code in C++.

Additionally, the author created software for preparing and running the experiments, and for processing their results. In total, the author prepared roughly 10000 lines of code. It should also be noted that the author's improvements were added on top of test models for 3D-HEVC and HEVC SCC, which are very complex software implementations of state-of-the-art video codecs. For example, as mentioned in Chapter 3, the test model for 3D-HEVC contains roughly 120 thousand lines of code. Introducing modifications to the core algorithms of such advanced software requires many hours of code analysis and debugging.

To assess the solutions presented in the dissertation, the author conducted multiple time-consuming experiments. If they were performed on a single core of a CPU, the processing would take roughly 180 days. The amount of video data used in the experiments was close to

300 GB. The aforementioned numbers show that the research on multiview video compression is a challenging task that requires a lot of effort and computational power.

### 7.3. ORIGINAL ACHIEVEMENTS OF THE AUTHOR AND CONCLUSIONS

In the dissertation, several original achievements of the author can be found. The most important ones are summarized below.

- **Development of the concept and the procedure for circular rectification.** The author proposes the process of derivation of circle parameters and virtual camera positions that best fit the real positions of the cameras. Both intrinsic and extrinsic camera parameters are rectified to an ideal circle with optical axes collocated on a single plane and intersecting in the center of the circle. The author also proposes a solution for the problem of misalignment of the field of view if the optical axis of a camera before rectification is far from the center of the circle.
- **Efficient modification of 3D-HEVC codec for processing of the circularly rectified 3D video (ARC-HEVC).** The author proposes formulas for mapping points between circularly rectified views. They are used in the author's modification of 3D-HEVC that includes adapting Disparity Compensated Prediction and other inter-view prediction tools to circular camera arrangements. The author also proposes modifications of 3D-HEVC syntax. Experimental results show that the proposed codec **reduces bitrate on average by 6% when compared to standard 3D-HEVC**. At the same time, the average encoding time is **reduced by more than 4%**. Therefore, for compression of multiview video with depth acquired with cameras sparsely distributed around the scene, **the proposed codec is objectively better than the dedicated state-of-the-art solution**, both in terms of compression efficiency and encoding time.
- **Adaptation of standard-compliant HEVC Screen Content Coding to efficient stereoscopic, multiview, and immersive video compression.** The author presents a novel and unexpected use of Intra Block Copy as an inter-view prediction tool. Even though SCC is designed to compress computer-generated video, the author proves that it can be successfully reused as a multiview codec for camera-captured content. This idea requires the preparation of a multiview video in a frame-compatible structure. The author experimentally found the best view alignment within a frame and the optimal configuration of SCC tools. The evaluation of the proposal proves that for stereoscopic

video compression, **SCC reduces the bitrate roughly by 20% for All-Intra and 15% for Random Access** when compared to the HEVC Main profile. In the case of multiview video coding (4 views), the bitrate reduction is even higher – **roughly 28% for All-Intra and 20% for Random Access**. Nevertheless, without further modifications, the proposed method is not as efficient as the dedicated MV-HEVC profile. When HEVC SCC is used as an internal MIV codec instead of HEVC Main, **the bitrate is also reduced, especially in the compression of computer-generated content (up to more than 7%) and depth maps (up to more than 15% for base views and 25% for patch atlases)**, however, the results depend on the content. Increased quality of depth maps results in a significantly better quality of synthesized virtual views, which is a crucial factor for immersive video applications. The idea of using **SCC as an internal MIV codec has been independently evaluated by the MPEG** group responsible for the development of MIV, and **it has been confirmed to be beneficial**.

- **Efficient modifications of HEVC SCC for compression of camera-captured multiview and immersive video.** The author proposes a set of modifications to SCC, aimed at increasing its compression efficiency. Experimental results show that **with the proposed modifications, SCC can be as efficient as MV-HEVC**, and slightly faster (on average 5% for 3 views) at the same time. Therefore, modified SCC could successfully replace MV-HEVC as a more versatile solution. Regarding immersive video coding, the efficiency of the proposed modifications strongly depends on the content, however, for camera-captured video they usually provide a significant gain both in terms of bitrate and encoding time reduction.

To sum up, in the dissertation, the author proves both theses to be valid. For compression of circularly rectified multiview video, the proposed modifications of inter-view prediction in 3D-HEVC reduce both bitrate and encoding time, compared to the state-of-the-art 3D-HEVC, even though ARC-HEVC is more complex and introduces additional parameters.

Regarding the second thesis, the author proposes a novel approach that reuses existing Screen Content Coding technique and improves it to provide equally efficient inter-view prediction as in the dedicated Multiview HEVC. This achievement shows that the development of future video coding should be directed toward the unification of coding techniques rather than creating dedicated extensions. Research presented in the dissertation can be the starting point for adapting the emerging Versatile Video Coding to frame-compatible multiview video coding and immersive video coding.

## REFERENCES

- [Bjøntegaard'01] G. Bjøntegaard, *Calculation of Average PSNR Differences between RD-curves*, ITU-T SG16, Doc. VCEG-M33, Austin, USA, April 2001.
- [Boissonade'18] P. Boissonade and J. Jung, *[MPEG-I Visual] Proposition of new sequences for Windowed6DoF experiments on compression, synthesis, and depth estimation*, ISO/IEC JTC1/SC29/WG11 MPEG/M43318, Ljubljana, Slovenia, 2018.
- [Bonatto'21] D. Bonatto, S. Fachada, S. Rogge, A. Munteanu and G. Lafruit, *Real-Time Depth Video-Based Rendering for 6-DoF HMD Navigation and Light Field Displays*, in *IEEE Access*, vol. 9, pp. 146868-146887, 2021, doi: 10.1109/ACCESS.2021.3123529.
- [Bossen'13] F. Bossen, *Common Test Conditions and software reference configurations*, JCT-VC of ITU-T SG16 WP3 and ISO/IEC JTC1/SC29/WG11 12th Meeting: Doc: JCTVC-L1100, Geneva, CH, January 2013.
- [Boyce'21] J. Boyce, R. Doré, A. Dziembowski, J. Fleureau, J. Jung, B. Kroon, B. Salahieh, V. K. Vadakital, Lu Yu, *MPEG Immersive Video Coding Standard*, *Proceedings of the IEEE*, vol. 109, no. 9, pp. 1521-1536, 2021.
- [Bross'21] B. Bross et al., *Overview of the Versatile Video Coding (VVC) Standard and its Applications*, *IEEE Transactions on Circuits and Systems for Video Technology*, vol. 31, no. 10, pp. 3736-3764, October 2021, doi: 10.1109/TCSVT.2021.3101953.
- [Ceulemans'18] B. Ceulemans et al., *Robust Multiview Synthesis for Wide-Baseline Camera Arrays*, *IEEE Tr. on Multimedia*, 2018.
- [Chen'97] X. Chen and A. Luthra, *MPEG-2 multi-view profile and its application in 3DTV*, *Proc. SPIE IS&T Multimedia Hardware Architectures*, San Diego, USA, Vol. 3021, pp. 212-223, February 1997.
- [Choi'12] M. Choi, J. Kim, W. -K. Cho and Y. Chung, *Low complexity image rectification for multi-view video coding*, *2012 IEEE International Symposium on Circuits and Systems (ISCAS)*, 2012, pp. 381-384.
- [Cisco'18] *VNI Complete Forecast Highlights*  
[https://www.cisco.com/c/dam/m/en\\_us/solutions/service-provider/vni-forecast-highlights/pdf/Global\\_Device\\_Growth\\_Traffic\\_Profiles.pdf](https://www.cisco.com/c/dam/m/en_us/solutions/service-provider/vni-forecast-highlights/pdf/Global_Device_Growth_Traffic_Profiles.pdf),  
 Accessed 8 May 2023
- [Cisco'20] *Cisco Annual Internet Report (2018-2023)*  
<https://www.cisco.com/c/en/us/solutions/collateral/executive-perspectives/annual-internet-report/white-paper-c11-741490.pdf>,  
 Accessed 8 May 2023

- [Collins'99] R. T. Collins and Y. Tsin, *Calibration of an Outdoor Active Camera System*, Proc. of the IEEE Conf. on Computer Vision and Pattern Recognition 1999, vol. 1, pp. 528-534.
- [Cserkaszkzy'18] A. Cserkaszkzy, P. A. Kara, A. Barsi, M. G. Martini and T. Balogh, *Light - fields of Circular Camera Arrays*, 2018 26th European Signal Processing Conference (EUSIPCO), Rome, Italy, 2018, pp. 241-245, doi: 10.23919/EUSIPCO.2018.8552998.
- [CTC MIV] *Common Test Conditions for MPEG Immersive Video. Standardization document*, ISO/IEC JTC1/SC29/WG04 MPEG VC N0051, Online, January 2021.
- [Cui'19] L. Cui et al., *Point-Cloud Compression: Moving Picture Experts Group's New Standard in 2020*, IEEE Consumer Electronics Magazine, 2019
- [Cyganek'09] B. Cyganek, J. Siebert, *An Introduction to 3D Computer Vision Techniques and Algorithms*, Wiley, 2009.
- [Domański'09] M. Domański, T. Grajek, K. Klimaszewski, M. Kurc, O. Stankiewicz, J. Stankowski, K. Wegner, *Poznań multiview video test sequences and camera parameters*, ISO/IEC JTC1/SC29/WG11 MPEG Doc. M17050, Xian, China, October 2009.
- [Domański'13] M. Domański, O. Stankiewicz, K. Wegner, M. Kurc, J. Konieczny, J. Siast, J. Stankowski, R. Ratajczak, *High efficiency 3D video coding using new tools based on view synthesis*, in IEEE Transactions on Image Processing, vol. 22, no. 9, pp. 3517-3527, September 2013
- [Domański'15A] M. Domański, A. Dziembowski, T. Grajek, A. Grzelka, Ł. Kowalski, M. Kurc, A. Łuczak, D. Mieloch, R. Ratajczak, J. Samelak, O. Stankiewicz, J. Stankowski, K. Wegner, *Methods of high efficiency compression for transmission of spatial representation of motion scenes*, IEEE International Conference on Multimedia and Expo, ICME 2015, Turyn, Włochy, 29.06-3.07, 2015
- [Domański'15B] M. Domański, A. Dziembowski, M. Kurc, A. Łuczak, D. Mieloch, J. Siast, O. Stankiewicz, K. Wegner, *Poznan University of Technology test multiview video sequences acquired with circular camera arrangement – "Poznan Team" and "Poznan Blocks" sequences*, ISO/IEC JTC1/SC29/WG11 MPEG Doc. M35846, Geneva, Switzerland, February 2015.
- [Domański'15C] M. Domański, A. Dziembowski, D. Mieloch, A. Łuczak, O. Stankiewicz, K. Wegner, *A Practical Approach to Acquisition and Processing of Free Viewpoint Video*, 31st Picture Coding Symposium PCS 2015, Cairns, Australia, 31 May - 3 June 2015, pp. 10-14,
- [Domański'16A] M. Domański, M. Bartkowiak, A. Dziembowski, T. Grajek, A. Grzelka, A. Łuczak, D. Mieloch, J. Samelak, O. Stankiewicz, J. Stankowski, K. Wegner, *New results in free-viewpoint television systems for horizontal virtual navigation*, IEEE International Conference on Multimedia and Expo, ICME 2016, Seattle, Stany Zjednoczone, 11-15.07.2016

- [Domański'16B] M. Domanski et al., *Multiview test video sequences for free navigation exploration obtained using pairs of cameras*, ISO/IEC JTC1/SC29/WG11 MPEG/M38247, Geneva, Switzerland, 2016.
- [Domański'17] M. Domański, O. Stankiewicz, K. Wegner and T. Grajek, *Immersive visual media — MPEG-I: 360 video, virtual navigation and beyond*, 2017 International Conference on Systems, Signals and Image Processing (IWSSIP), Poznan, Poland, 2017, pp. 1-9, doi: 10.1109/IWSSIP.2017.7965623.
- [Domański'19] M. Domański, T. Grajek, C. Conti, C. Debono, S. de Faria, P. Kovacs, L. Lucas, P. Nunes, C. Perra, N. Rodrigues, M. Sjöström, L. Soares, O. Stankiewicz, *Emerging Imaging Technologies: Trends and Challenges*, 3D Visual Content Creation, Coding and Delivery, Signals and Communication Technology: Springer International, 2019, pp. 5-39, ISBN: 978-3-319-77841-9, ISSN: 1860-4862.
- [Doré'18] R. Doré, *Technicolor 3DoF+ test materials*, ISO/IEC JTC1/SC29/WG11 MPEG/M42349, San Diego, USA, 2018.
- [Doré'20A] R. Doré, G. Briand, F. Thudor, *[MPEG-I Visual] InterdigitalFan0 content proposal for MIV*, ISO/IEC JTC1/SC29/WG11 MPEG/M54732, online, July 2020.
- [Doré'20B] R. Doré, G. Briand, F. Thudor, *[MPEG-I Visual] InterdigitalGroup content proposal*, ISO/IEC JTC1/SC29/WG11 MPEG/M54731, online, July 2020.
- [Doré'21] R. Doré, G. Briand, *[MPEG-I] Interdigital Mirror Content Proposal for advanced MIV investigations on reflection*, ISO/IEC JTC1/SC29/WG11 MPEG/M55710, online, January 2021.
- [Doyen'17] D. Doyen et al., *Light field content from 16- camera rig*, ISO/IEC JTC1/SC29/WG11 MPEG, M40010, Geneva, Switzerland, 2017.
- [Dziembowski'17A] A. Dziembowski, A. Grzelka, D. Mieloch, O. Stankiewicz, M. Domański, *Enhancing view synthesis with image and depth map upsampling*, International Conference on Systems, Signals and Image Processing, IWSSIP 2017, Poznań, Polska, 22-24.05.2017
- [Dziembowski'17B] A. Dziembowski, A. Grzelka, D. Mieloch, *Zwiększanie rozdzielczości obrazu i mapy głębi w celu poprawy jakości syntezy widoków wirtualnych*, Przegląd Telekomunikacyjny, tom 86, nr 6, s. 405-408, 2017
- [Dziembowski'22] A. Dziembowski, D. Mieloch, J. Stankowski, A. Grzelka, *IV-PSNR – the objective quality metric for immersive video applications*, IEEE Transactions on Circuits and Systems for Video Technology, Vol. 32, 1 June 2022, pp. 7575 - 7591, ISSN: 1558-2205
- [Fachada'18] S. Fachada, D. Bonatto, A. Schenkel and G. Lafruit, *Depth image based view synthesis with multiple reference views for virtual reality*, 2018 - 3DTV-Conference: The True Vision - Capture, Transmission and Display of 3D Video (3DTV-CON), Helsinki, Finland, 2018, pp. 1-4, doi: 10.1109/3DTV.2018.8478484.

- [Fujikawa'10] S. Fujikawa, *Three-dimensional imaging technology: A revolution in the world of imaging*, 2010 Symposium on VLSI Circuits, Honolulu, HI, USA, 2010, pp. 9-12, doi: 10.1109/VLSIC.2010.5560254.
- [Guillo'18] L. Guillo, X. Jiang, G. Lafruit, C. Guillemot, *[MPEG-I Visual] Light field video dataset captured by a R8 Raytrix camera (with disparity maps)*, ISO/IEC JTC1/SC29/WG11 MPEG Doc. M42468, San Diego, USA, April 2018.
- [Hannuksela'15] M. M. Hannuksela, Y. Yan, X. Huang and H. Li, *Overview of the multiview high efficiency video coding (MV-HEVC) standard*, 2015 IEEE International Conference on Image Processing (ICIP), Quebec City, QC, Canada, 2015, pp. 2154-2158, doi: 10.1109/ICIP.2015.7351182.
- [Hartley'03] R. Hartley, A. Zisserman, *Multiple View Geometry in Computer Vision*, Cambridge: Cambridge Univ. Press, 2nd ed., 2003.
- [Hartley'99] Hartley, R.I., *Theory and Practice of Projective Rectification*, International Journal of Computer Vision 35, 115–127 (1999).  
<https://doi.org/10.1023/A:1008115206617>
- [HM] JCT-VC, *HEVC reference software repository*,  
[https://hevc.hhi.fraunhofer.de/svn/svn\\_HEVCSoftware/tags/HM-16.9](https://hevc.hhi.fraunhofer.de/svn/svn_HEVCSoftware/tags/HM-16.9). Accessed 8 May 2023
- [HM+SCM] JCT-VC, *HEVC Screen Content Coding reference software repository*,  
[https://hevc.hhi.fraunhofer.de/svn/svn\\_HEVCSoftware/tags/HM-16.9+SCM-8.0](https://hevc.hhi.fraunhofer.de/svn/svn_HEVCSoftware/tags/HM-16.9+SCM-8.0). Accessed 8 May 2023
- [Ho'07] Ho, Yo-Sung & Oh, Kwan-Jung, *Overview of Multi-view Video Coding*, 5 - 12. 10.1109/IWSSIP.2007.4381085, 2007
- [Ho'08] Y.S. Ho, E.K. Lee, C. Lee, *Multiview video test sequence and camera parameters*, ISO/IEC JTC1/SC29/WG11 MPEG Doc. M15419, Archamps, France, April 2008.
- [Ho'12] Y. Ho, *Video processing techniques for 3D television*, 2012 *Visual Communications and Image Processing*, 2012, pp. 1-13.
- [Hou'20] Y. Hou, X. Su, W. Chen, *Alignment Method of an Axis Based on Camera Calibration in a Rotating Optical Measurement System*, Applied Sciences. 2020; 10(19):6962. <https://doi.org/10.3390/app10196962>
- [HTM] JCT-3V, *Multiview HEVC reference software repository*,  
[https://hevc.hhi.fraunhofer.de/svn/svn\\_3DVCSsoftware/tags/HTM-16.2](https://hevc.hhi.fraunhofer.de/svn/svn_3DVCSsoftware/tags/HTM-16.2). Accessed 8 May 2023
- [Hu'23] P. Hu, E. S. L. Ho and A. Munteanu, *AlignBodyNet: Deep Learning-Based Alignment of Non-Overlapping Partial Body Point Clouds From a Single Depth Camera*, in IEEE Transactions on Instrumentation and Measurement, vol. 72, pp. 1-9, 2023, Art no. 2502609, doi: 10.1109/TIM.2022.3222501.
- [Ilola'19] L. Ilola, V.K.M. Vadakital, K. Roimela, J. Keränen, *New test content for Immersive Video – Nokia Chess*, ISO/IEC JTC1/SC29/WG11 MPEG/M50787, Geneva, Switzerland, 2019.



- [ISO'12] ISO/IEC IS 13818-2: 2013 and ITU-T Rec. H.262 (V3.1) (2012), *Generic coding of moving pictures and associated audio information – Part 2: Video*,
- [ISO'14] ISO/IEC IS 14496-10: 2014, *Coding of audio-visual objects - Part 10: Advanced Video Coding*, and ITU-T Rec. H.264 (V9) (2014), *Advanced video coding for generic audiovisual services*
- [ISO'19] ISO/IEC MPEG. *Software manual of IV-PSNR for Immersive Video*. ISO/IEC JTC1/SC29/WG11 MPEG/N18709, Goeteborg, Sweden, 2019
- [ISO'21] ISO/IEC Int. Standard 23008-2: 2020, *High efficiency coding and media delivery in heterogeneous environment – Part 2: High efficiency video coding*, and ITU-T Rec. H.265 (V8) (2021), *High efficiency video coding*.
- [ISO'22] ISO/IEC Int. Standard 23090-3: 2022, *Information technology — Coded representation of immersive media — Part 3: Versatile video coding*, and ITU-T Rec. H.266 (V2) (2022), *Versatile video coding*.
- [Jhu'20] H. -J. Jhu, X. Xiu, Y. -W. Chen, T. -C. Ma and X. Wang, *Adaptive Color Transform in VVC Standard*, 2020 IEEE International Conference on Visual Communications and Image Processing (VCIP), Macau, China, 2020, pp. 314-317, doi: 10.1109/VCIP49819.2020.9301798.
- [Kang'08] Y. -S. Kang, C. Lee and Y. -S. Ho, *An Efficient Rectification Algorithm for Multi-View Images in Parallel Camera Array*, 2008 3DTV Conference: The True Vision - Capture, Transmission and Display of 3D Video, Istanbul, Turkey, 2008, pp. 61-64, doi: 10.1109/3DTV.2008.4547808.
- [Kovacs'15] P. T. Kovacs, *[FTV AHG] Big Buck Bunny light-field test sequences*, MPEG M35721, Geneva, February 2015.
- [Kroon'18] B. Kroon, *3DoF+ test sequence ClassroomVideo*, ISO/IEC JTC1/SC29/WG11 MPEG/M42415, San Diego, USA, 2018.
- [LaValle'20] S. LaValle, *Virtual Reality*, Cambridge Univ. Press, 2020.
- [Li'16] Z. Li et al., *Toward a practical perceptual video quality metric*, Netflix Technology Blog, 2016.
- [Li'20] L. Li et al., *Advanced 3D Motion Prediction for Video-Based Dynamic Point Cloud Compression*, IEEE Tr. on Image Processing, 2020.
- [Lucchese'03] L. Lucchese and S. K. Mitra, *Correction of geometric lens distortion through image warping*, 3rd International Symposium on Image and Signal Processing and Analysis, 2003. ISPA 2003. Proceedings of the, Rome, Italy, 2003, pp. 516-521 Vol.1, doi: 10.1109/ISPA.2003.1296951.
- [Ma'05] S. Ma, W. Gao and Yan Lu, *Rate-distortion analysis for H.264/AVC video coding and its application to rate control*, in IEEE Transactions on Circuits and Systems for Video Technology, vol. 15, no. 12, pp. 1533-1544, December 2005, doi: 10.1109/TCSVT.2005.857300.

- [Mieloch'17A] D. Mieloch, A. Dziembowski, A. Grzelka, O. Stankiewicz, M. Domański, *Graph-based multiview depth estimation using segmentation*, IEEE International Conference on Multimedia and Expo, ICME 2017, Hongkong, Chiny, 10-14.07.2017
- [Mieloch'17B] D. Mieloch, A. Dziembowski, A. Grzelka, O. Stankiewicz, M. Domański, *Temporal enhancement of graph-based depth estimation method*, International Conference on Systems, Signals and Image Processing, IWSSIP 2017, Poznań, Polska, 22-24.05.2017
- [Mieloch'17C] D. Mieloch, A. Dziembowski, A. Grzelka, *Estymacja głębi dla systemów wielowidokowych*, Przegląd Telekomunikacyjny, tom 86, nr 6, s. 479-482, 2017
- [Mieloch'21] D. Mieloch, A. Dziembowski and M. Domański, *Depth Map Refinement for Immersive Video*, in IEEE Access, vol. 9, pp. 10778-10788, 2021, doi: 10.1109/ACCESS.2021.3050554.
- [Müller'11] K. Müller, P. Merkle, T. Wiegand, *3D video representation using depth maps*, Proceedings of the IEEE, tom 99, nr 4, s. 643-656, 04.2011
- [Müller'13] K. Müller, H. Schwarz, D. Marpe, Ch. Bartnik, S. Bosse, H. Brust, T. Hinz, H. Lakshman, Ph. Merkle, F. Hunn Rhee, G. Tech, M. Winken, Th. Wiegand, *3D High Efficiency Video Coding for multi-view video and depth data*, IEEE Trans. Image Processing, IEEE Trans. Image Processing, vol. 22, pp. 3366-3378, 2013.
- [Müller'14] K. Müller, A. Vetro, *Common Test Conditions of 3DV Core Experiments*, JCT-3V of ITU-T SG16 WP3 and ISO/IEC JTC1/SC29/WG11 7th Meeting: Doc. JCT3V-G1100, San José, US, January 2014.
- [Ohm'99] J.-R. Ohm, *Stereo/Multiview Video Encoding Using the MPEG Family of Standards*, Proc. SPIE Conf. Stereoscopic Displays and Virtual Reality Systems VI, San Jose, CA, January 1999.
- [Pu'16] W. Pu et al., *Palette Mode Coding in HEVC Screen Content Coding Extension*, in IEEE Journal on Emerging and Selected Topics in Circuits and Systems, vol. 6, no. 4, pp. 420-432, December 2016, doi: 10.1109/JETCAS.2016.2605661.
- [Rahaman'18] D. Rahaman and M. Paul, *Virtual view synthesis for free viewpoint video and multiview video compression using Gaussian mixture modelling*, IEEE Tr. on Image Processing, 2018.
- [Ratajczak'12] R. Ratajczak, M. Domański and K. Wegner, *Vehicle size estimation from stereoscopic video*, 2012 19th International Conference on Systems, Signals and Image Processing (IWSSIP), Vienna, Austria, 2012, pp. 405-408.
- [Rogge'19] S. Rogge, D. Bonatto, J. Sancho, R. Salvador, E. Juarez, A. Munteanu, G. Lafruit, *MPEG-I Depth Estimation Reference Software*, 2019 International Conference on 3D Immersion (IC3D), Brussels, Belgium, 2019, pp. 1-6, doi: 10.1109/IC3D48390.2019.8975995.

- [Rusanovskyy'11] D. Rusanovskyy, P. Aflaki, and M. M. Hannuksela, *Undo dancer 3DV sequence for purposes of 3DV standardization*, ISO/IEC JTC1/SC29/WG11, Geneva, Switzerland, Tech. Rec. M20028, March 2011.
- [Salahieh'19] B. Salahieh et al., *Kermit test sequence for Windowed 6DoF Activities*, ISO/IEC JTC1/SC29/WG11/M43748, Ljubljana, 2019.
- [Samelak'16] J. Samelak, J. Stankowski, M. Domański, *Adaptation of the 3D-HEVC coding tools to arbitrary locations of cameras*, International Conference on Signals and Electronic Systems, ICSES 2016, Kraków, Poland, September 5-7 2016.
- [Samelak'17A] J. Samelak, J. Stankowski, M. Domański, *Efficient frame-compatible stereoscopic video coding using HEVC Screen Content Coding*, IEEE International Conference on Systems, Signals and Image Processing IWSSIP 2017, Poznań, Poland, 22-24 May 2017.
- [Samelak'17B] J. Samelak, O. Stankiewicz, M. Domański, *Do we need multiview profiles for future video coding generations?*, ISO/IEC JTC1/SC29/WG11 MPEG2017, M41699, Macao, China, October 2017
- [Samelak'17C] J. Samelak, O. Stankiewicz, M. Domański, *Do we need multiview profiles for future video coding generations?*, ISO/IEC JTC1/SC29/WG11 Joint Video Exploration Team (JVET), JVET\_H0044, Macao, China, October 2017
- [Samelak'17D] J. Samelak, J. Stankowski, M. Domański, *Experimental results for frame – compatible multiview video coding using HEVC SCC*, ISO/IEC JTC1/SC29/WG11 Joint Collaborative Team on Video Coding (JCT-VC), JCTVC-Z0041, Geneva, Switzerland, January 2017
- [Samelak'20A] J. Samelak, A. Dziembowski, D. Mieloch, M. Domański, *[MPEG-I Visual] Impact of HEVC profile on TMIV performance*, MPEG130/m53910, Alpbah, Austria, April 2020
- [Samelak'20B] J. Samelak, A. Dziembowski, D. Mieloch, M. Domański, *[MPEG-I Visual] HEVC-SCC in TMIV*, MPEG130/m53427, Alpbah, Austria, April 2020
- [Samelak'21A] J. Samelak, A. Dziembowski, D. Mieloch, M. Domański, M. Wawrzyniak, *Efficient Immersive Video Compression using Screen Content Coding*, 29th International Conference in Central Europe on Computer Graphics, Visualization and Computer Vision : WSCG 2021, WSCG 2021, Prague, Czech Republic, 17-20 May 2021
- [Samelak'21B] J. Samelak, M. Domański, *Multiview Video Compression Using Advanced HEVC Screen Content Coding*, <https://arxiv.org/abs/2106.13574>
- [Samelak'22] J. Samelak, A. Dziembowski, D. Mieloch, *Advanced HEVC Screen Content Coding for MPEG Immersive Video*, Electronics, Vol. 11, No. 23, December 2022, ISSN: 2079-9292
- [Schwarz'19] S. Schwarz et al., *Emerging MPEG Standards for Point Cloud Compression*. IEEE J. on Emerging and Sel. Topics in Circuits and Systems, 2019.

- [Senoh'14] T. Senoh, A. Ishikawa, M. Okui, K. Yamamoto, N. Inoue, *FTV AHG: Super-Multiview Sequences of NICT*, ISO/IEC JTC1/SC29/WG11 MPEG Doc. M32201, San Jose, USA, January 2014.
- [Sheikh'06] H. Sheikh and A. Bovik, *Image information and visual quality*, IEEE *Tr. on Image Proc.*, 2006.
- [Skulimowski'07] P. Skulimowski, P. Strumillo, *Obstacle localization in 3D scenes from stereoscopic sequences*, 2007 15th European Signal Processing Conference, Poznan, Poland, 2007, pp. 2095-2099.
- [Stankiewicz'18] O. Stankiewicz, M. Domański, A. Dziembowski, A. Grzelka, D. Mieloch, J. Samelak, *A free-viewpoint television system for horizontal virtual navigation*, IEEE *Transactions on Multimedia*, tom PP, nr 99, s. 1-1, 2018
- [Stankowski'10] J. Stankowski, K. Klimaszewski, *Application of epipolar rectification algorithm in 3D Television*, *Image Processing and Communications Challenges 2, Advances in Intelligent and Soft Computing: Vol. 84*, Springer-Verlag, Berlin, 2010, pp. 345-352, ISBN: 978-3-642-16294-7, ISSN: 1867-5662
- [Stankowski'15] J. Stankowski, Ł. Kowalski, J. Samelak, M. Domański, T. Grajek, K. Wegner, *3D-HEVC extension for circular camera arrangements*, 3DTV-Conference: The True Vision - Capture, Transmission and Display of 3D Video (3DTV-CON), Lizbona, Portugalia, 8-10.07.2015
- [Strumillo'18] Strumillo, P. et al. (2018). *Different Approaches to Aiding Blind Persons in Mobility and Navigation in the "Naviton" and "Sound of Vision" Projects*. In: Pissaloux, E., Velazquez, R. (eds) *Mobility of Visually Impaired People*. Springer, Cham.
- [Sullivan'09] G. J. Sullivan, *Standards-based approaches to 3D and multiview video coding*, Proc. SPIE Conf. Applications of Digital Image Processing XXXII, San Diego, CA, August 2009.
- [Sullivan'12] G. J. Sullivan, J. Ohm, W. J. Han, and T. Wiegand, *Overview of the High Efficiency Video Coding (HEVC) Standard*, in *IEEE Transactions on Circuits Systems for Video Technology*, vol. 22, no. 12, pp. 1649-1668, December 2012.
- [Sullivan'13] G.J. Sullivan, J.M. Boyce, Y. Chen, J.R. Ohm, C.A. Segall, A. Vetro, *Standardized extensions of High Efficiency Video Coding (HEVC)*, IEEE *Journal of Selected Topics in Signal Processing*, tom 7, nr 6, s. 1001-1016, 12.2013
- [Sun'17] Y. Sun et al., *Weighted-to-Spherically-Uniform Quality Evaluation for Omnidirectional Video*, *IEEE Sig. Proc. Lett.*, vol. 24, no. 9, September 2017.

- [Sun'19] Y. -C. Sun, J. Lou, Y. -H. Chao, H. Wang, V. Seregin and M. Karczewicz, *Analysis of Palette Mode on Versatile Video Coding*, 2019 IEEE Conference on Multimedia Information Processing and Retrieval (MIPR), San Jose, CA, USA, 2019, pp. 455-458, doi: 10.1109/MIPR.2019.00091.
- [Suzuki'09] K. Suzuki, M. Tanimoto, *Multiview Video Test Sequence in Circular Camera Arrangement for 3DV/FTV*, ISO/IEC JTC1/SC29/WG11, MPEG Doc. M24846, Geneva, Switzerland, May 2012.
- [Suzuki'14] T. Suzuki, R. Choen, T. K. Tan, S. Wenger, *JCT-VC AHG report: Test sequence material (AHG16)*, ISO/IEC JTC1/SC29/WG11 MPEG Doc. M33409, Valencia, Spain, March 2014.
- [Tanimoto'09] M. Tanimoto, T. Fujii, M.P. Tehrani, M. Wildeboer, N. Fukushima, H. Furihata, *Moving Multiview Camera Test Sequences for MPEG-FTV*, ISO/IEC JTC1/SC29/WG11, MPEG Doc. M16922, Xian, China, October 2009.
- [Tanimoto'12] M. Tanimoto, M. Panahpour Tehrani, T. Fujii and T. Yendo, *FTV for 3-D Spatial Communication*, in Proceedings of the IEEE, vol. 100, no. 4, pp. 905-917, April 2012, doi: 10.1109/JPROC.2011.2182101.
- [Tech'16] G. Tech, Y. Chen, K. Müller, J. R. Ohm, A. Vetro and Y. K. Wang, *Overview of the Multiview and 3D Extensions of High Efficiency Video Coding*, in IEEE Transactions on Circuits and Systems for Video Technology, vol. 26, no. 1, pp. 35-49, September 2015.
- [TMIV] *Test Model 8 for MPEG Immersive Video*, Standardization document: ISO/IEC JTC1/SC29/WG04 MPEG VC N0050, Online, January 2021
- [Vadakital'20] V. K. M. Vadakital, A. Dziembowski, D. Mieloch, *[MPEG-I Video][MIV] Using VVC Class-F configuration improves the performance of MIV*, MPEG131/m54390, online, June 2020
- [Vetro'10] A. Vetro, *Frame compatible formats for 3D video distribution*, 2010 IEEE International Conference on Image Processing, 2010, pp. 2405-2408, doi: 10.1109/ICIP.2010.5651071.
- [Vetro'11A] A. Vetro, T. Wiegand and G. J. Sullivan, *Overview of the Stereo and Multiview Video Coding Extensions of the H.264/MPEG-4 AVC Standard*, Proceedings of the IEEE, vol. 99, no. 4, pp. 626-642, April 2011, doi: 10.1109/JPROC.2010.2098830.
- [Vetro'11B] A. Vetro, A. M. Tourapis, K. Muller and T. Chen, *3D-TV Content Storage and Transmission*, in IEEE Transactions on Broadcasting, vol. 57, no. 2, pp. 384-394, June 2011, doi: 10.1109/TBC.2010.2102950.
- [Wang'04] Z. Wang, A.C. Bovik, H.R. Sheikh, E.P. Simoncelli, *Image quality assessment: from error visibility to structural similarity*, IEEE Transactions on Image Processing, tom 13, nr 4, s. 600-612, 04.2004

- [Wegner'14] K. Wegner, O. Stankiewicz, K. Klimaszewski, M. Domański, *Poznan Blocks – a multiview video test sequence and camera parameters for FTV*, ISO/IEC JTC1/SC29/WG11, Doc. MPEG M32243, San Jose, January 2014.
- [Xu'16A] J. Xu, R. Joshi, and R. A. Cohen, *Overview of the Emerging HEVC Screen Content Coding Extension*, in IEEE Transactions on Circuits and Systems for Video Technology, vol. 26, no. 1, pp. 50-62, January 2016.
- [Xu'16B] X. Xu et al., *Intra Block Copy in HEVC Screen Content Coding Extensions*, in IEEE Journal on Emerging and Selected Topics in Circuits and Systems, vol. 6, no. 4, pp. 409-419, December 2016.
- [Xu'19] X. Xu, X. Li and S. Liu, *Current Picture Referencing in Versatile Video Coding*, 2019 IEEE Conference on Multimedia Information Processing and Retrieval (MIPR), San Jose, CA, USA, 2019, pp. 26-31, doi: 10.1109/MIPR.2019.00013.
- [Xu'22] X. Xu and S. Liu, *Overview of Screen Content Coding in Recently Developed Video Coding Standards*, in IEEE Transactions on Circuits and Systems for Video Technology, vol. 32, no. 2, pp. 839-852, February 2022, doi: 10.1109/TCSVT.2021.3064210.
- [Yu'15] H. Yu, R. Cohen, K. Rapaka, J. Xu, *Common Test Conditions for Screen Content Coding*, JCT-VC of ITU-T SG16 WP3 and ISO/IEC JTC1/SC29/WG11 21st Meeting: Doc. JCTVC-U1015r2, Warsaw, PL, June 2015.
- [Zhang'11] J. Zhang, R. Li, H. Li, D. Rusanovskyy, and M. M. Hannuksela, *Ghost town fly 3DV sequence for purposes of 3DV standardization*, ISO/IEC JTC1/SC29/WG11, Geneva, Switzerland, Tech. Rec. M20027, March 2011.
- [Zhang'15] L. Zhang, J. Chen, J. Sole, M. Karczewicz, X. Xiu and J. -Z. Xu, *Adaptive Color-Space Transform for HEVC Screen Content Coding*, 2015 Data Compression Conference, Snowbird, UT, USA, 2015, pp. 233-242, doi: 10.1109/DCC.2015.33.
- [Zitnick'04] C.L. Zitnick, S. B. Kang, M. Uyttendaele, S. Winder and R. Szeliski, *High-quality video view interpolation using a layered representation*, ACM Transactions on Graphics, vol. 23, pp. 600-608, 2004

## PUBLICATIONS OF THE AUTHOR

### BOOK CHAPTERS

1. Kukolj, L. Bolecek, L. Polak, T. Kratochvil, O. Zach, J. Kufa, M. Slanina, T. Grajek, J. Samelak, M. Domański, D. Milovanovic, *3D Content Acquisition and Coding*, 3D Visual Content Creation, Coding and Delivery, Signals and Communication Technology: Springer International, 2019, pp. 41-95, ISBN: 978-3-319-77841-9, ISSN: 1860-4862

### INTERNATIONAL JOURNALS

1. J. Samelak, A. Dziembowski, D. Mieloch, *Advanced HEVC Screen Content Coding for MPEG Immersive Video*, Electronics, Vol. 11, No. 23, December 2022, ISSN: 2079-9292
2. O. Stankiewicz, M. Domański, A. Dziembowski, A. Grzelka, D. Mieloch, J. Samelak, *A free-viewpoint television system for horizontal virtual navigation*, IEEE Transactions on Multimedia, tom PP, nr 99, s. 1-1, 2018

### INTERNATIONAL CONFERENCES

1. D. Klóska, A. Dziembowski, J. Samelak, *Versatile input view selection for efficient immersive video transmission*, 31. International Conference in Central Europe on Computer Graphics, Visualization and Computer Vision, WSCG 2023, Pilsen, Czech Republic, 2023-05-15
2. J. Samelak, A. Dziembowski, D. Mieloch, M. Domański, M. Wawrzyniak, *Efficient Immersive Video Compression using Screen Content Coding*, 29th International Conference in Central Europe on Computer Graphics, Visualization and Computer Vision : WSCG 2021, WSCG 2021, Prague, Czech Republic, 17-20 May 2021
3. A. Dziembowski, J. Samelak, M. Domański, *View selection for virtual view synthesis in free navigation systems*, International Conference on Signals and Electronic Systems, ICSES 2018, Kraków, Poland, September 10-12 2018

4. J. Samelak, J. Stankowski, M. Domański, *Efficient frame-compatible stereoscopic video coding using HEVC Screen Content Coding*, IEEE International Conference on Systems, Signals and Image Processing IWSSIP 2017, Poznań, Poland, 22-24 May 2017,
5. M. Domański, M. Bartkowiak, A. Dziembowski, T. Grajek, A. Grzelka, A. Łuczak, D. Mieloch, J. Samelak, O. Stankiewicz, J. Stankowski, K. Wegner, *New results in free-viewpoint television systems for horizontal virtual navigation*, IEEE International Conference on Multimedia and Expo, ICME 2016, Seattle, USA, 11-15.07.2016
6. J. Samelak, J. Stankowski, M. Domański, *Adaptation of the 3D-HEVC coding tools to arbitrary locations of cameras*, International Conference on Signals and Electronic Systems, ICSES 2016, Kraków, Poland, September 5-7 2016,
7. M. Domański, A. Dziembowski, T. Grajek, A. Grzelka, Ł. Kowalski, M. Kurc, A. Łuczak, D. Mieloch, R. Ratajczak, J. Samelak, O. Stankiewicz, J. Stankowski, K. Wegner, *Methods of high efficiency compression for transmission of spatial representation of motion scenes*, IEEE International Conference on Multimedia and Expo, ICME 2015, Turin, Italy, 29.06-3.07.2015
8. J. Stankowski, Ł. Kowalski, J. Samelak, M. Domański, T. Grajek, K. Wegner, *3D-HEVC extension for circular camera arrangements*, 3DTV-Conference: The True Vision - Capture, Transmission and Display of 3D Video (3DTV-CON), Lisboa, Portugal, 8-10.07.2015

#### INTERNATIONAL CONFERENCES - STANDARDIZATION

1. A. Dziembowski, D. Mieloch, J. Samelak, *3D-HEVC in TMIV verification tests*, ISO/IEC JTC 1/SC 29/WG 4 MPEG 136, M57753, October 2021
2. M. Domański, J. Samelak, S. Rózek, T. Grajek, S. Maćkowiak, O. Stankiewicz, *[VCM] Stereoscopic and multiview video coding for machines*, MPEG130/m54407, Geneva, Switzerland, June 2020
3. J. Samelak, A. Dziembowski, D. Mieloch, M. Domański, *[MPEG-I Visual] Impact of HEVC profile on TMIV performance*, MPEG130/m53910, Alpbah, Austria, April 2020
4. J. Samelak, A. Dziembowski, D. Mieloch, M. Domański, *[MPEG-I Visual] HEVC-SCC in TMIV*, MPEG130/m53427, Alpbah, Austria, April 2020



5. M. Domański, J. Samelak, *Unified Screen Content and Multiview Video Coding - Experimental results*, Joint Video Exploration Team JVET of ITU-T SG 16 WP 3 and ISO/IEC JTC1/SC29/WG11, JVET-M0765, Marrakech, Morocco, 9-18 January 2019
6. M. Domański, A. Dziembowski, T. Grajek, A. Grzelka, D. Mieloch, R. Ratajczak, J. Samelak, O. Stankiewicz, J. Stankowski, K. Wegner, *Free-viewpoint television demonstration for sports events*, ISO/IEC JTC1/SC29/WG11 MPEG2018, M41994, Gwangju, South Korea, 22-26.01.2018
7. J. Samelak, O. Stankiewicz, M. Domański, *Do we need multiview profiles for future video coding generations?*, ISO/IEC JTC1/SC29/WG11 MPEG2017, M41699, Macao, China, October 2017
8. J. Samelak, O. Stankiewicz, M. Domański, *Do we need multiview profiles for future video coding generations?*, ISO/IEC JTC1/SC29/WG11 Joint Video Exploration Team (JVET), JVET\_H0044, Macao, China, October 2017
9. J. Samelak, J. Stankowski, M. Domański, *Experimental results for frame –compatible multiview video coding using HEVC SCC*, ISO/IEC JTC1/SC29/WG11 Joint Collaborative Team on Video Coding (JCT-VC), JCTVC-Z0041, Geneva, Switzerland, January 2017
10. M. Domański, A. Dziembowski, A. Grzelka, Ł. Kowalski, D. Mieloch, J. Samelak, J. Stankowski, O. Stankiewicz, K. Wegner, *Experimental video coding software for free navigation applications*, ISO/IEC JTC1/SC29/WG11 MPEG2016, M39527, Chengdu, China, 17-21.10.2016
11. M. Domański, A. Dziembowski, A. Grzelka, Ł. Kowalski, D. Mieloch, J. Samelak, J. Stankowski, O. Stankiewicz, K. Wegner, *Coding results for Poznan Fencing 2 and Poznan Blocks 2 test sequences in free navigation scenario*, ISO/IEC JTC1/SC29/WG11 MPEG2016, M39215, Chengdu, China, 17-21.10.2016
12. M. Domański, A. Dziembowski, A. Grzelka, Ł. Kowalski, D. Mieloch, J. Samelak, J. Stankowski, O. Stankiewicz, K. Wegner, *[FTV AHG] Extended results of Poznan University of Technology proposal for Call for Evidence on free-viewpoint television*, ISO/IEC JTC1/SC29/WG11 MPEG2016, M38246, Geneva, Switzerland, 30.05-3.06.2016

13. M. Domański, A. Dziembowski, A. Grzelka, Ł. Kowalski, D. Mieloch, J. Samelak, J. Stankowski, O. Stankiewicz, K. Wegner, *[FTV AHG] Technical Description of Poznan University of Technology proposal for Call for Evidence on free-viewpoint television*, ISO/IEC JTC1/SC29/WG11 MPEG2016, M37893, San Diego, USA, 22-26.02.2016
14. M. Domański, J. Samelak, O. Stankiewicz, J. Stankowski, K. Wegner, *[FTV AHG] 3D-HEVC extensions for free navigation*, ISO/IEC JTC1/SC29/WG11 MPEG2016, M38101, San Diego, USA, 22-26 February 2016

#### NATIONAL JOURNALS

1. J. Samelak, C. Korzeniewski, Ł. Kowalski, J. Stankowski, *Zoptymalizowana implementacja dekodera HEVC*, Przegląd Telekomunikacyjny, No. 6/2014, Warsaw, Poland, June 2014, pp. 583-586

#### PAPERS IN THE PROCESS OF PUBLICATION

1. J. Samelak, M. Domański, *Multiview Video Compression Using Advanced HEVC Screen Content Coding*, <https://arxiv.org/abs/2106.13574>
2. J. Samelak, M. Domański, *Circular Rectification of 3D Video and Efficient Modification of 3D-HEVC*, <https://arxiv.org/abs/2306.06285>

## APPENDIX: EXPERIMENTAL RESULTS

Table A.1. Circularly rectified camera parameters for ARC-HEVC (Section 4.4).

| Parameter | View | Ballet     | Breakdancers | BBB_Flowers | Poznan_Blocks |
|-----------|------|------------|--------------|-------------|---------------|
| $\alpha$  | 1    | -0,39495   | -0,45938     | 0,34034     | 0,64312       |
|           | 2    | -0,24341   | -0,28765     | 0,22689     | 0,45021       |
|           | 3    | -0,09630   | -0,12535     | 0,11345     | 0,26069       |
|           | 4    | 0,05464    | 0,04794      | 0,00000     | 0,08178       |
|           | 5    | 0,19954    | 0,21473      | -0,11345    | -0,12344      |
|           | 6    | 0,34641    | 0,38939      | -0,22689    | -0,29812      |
|           | 7    | 0,48447    | 0,55978      | -0,34034    | -0,48627      |
| $o_x$     | 1    | 226,44198  | 53,14096     | 645,86711   | 1133,54227    |
|           | 2    | 400,67535  | 234,18259    | 631,84719   | 1117,72118    |
|           | 3    | 518,14647  | 467,25264    | 631,80032   | 1111,15753    |
|           | 4    | 673,76843  | 694,48473    | 640,00000   | 1090,62062    |
|           | 5    | 776,87453  | 845,11840    | 648,19968   | 1080,48483    |
|           | 6    | 967,56713  | 1090,17933   | 648,15281   | 1057,95950    |
|           | 7    | 1110,30450 | 1306,68418   | 634,13289   | 1039,62190    |
| $o_y$     |      | 356,23763  | 374,51650    | 384,00000   | 562,05012     |
| $r$       |      | 26,28679   | 22,67017     | 1,05000     | 30,18157      |
| $f_x$     |      | 1914,95375 | 1882,34125   | 830,45711   | 1721,66111    |

Table A.2. PSNR [dB] values for the experiment evaluating ARC-HEVC in compression of multiview video (Section 4.6).

| Encoder         | QP | Ballet | Breakdancers | BBB_Flowers | Poznan_Blocks | average      |
|-----------------|----|--------|--------------|-------------|---------------|--------------|
| <b>3D-HEVC</b>  | 25 | 40.43  | 38.83        | 40.24       | 41.94         | <b>40.36</b> |
|                 | 30 | 38.71  | 37.25        | 37.36       | 39.34         | <b>38.17</b> |
|                 | 35 | 36.79  | 35.52        | 34.59       | 36.69         | <b>35.90</b> |
|                 | 40 | 34.70  | 33.56        | 31.85       | 33.99         | <b>33.53</b> |
| <b>ANY-HEVC</b> | 25 | 40.49  | 38.85        | 40.26       | 41.99         | <b>40.40</b> |
|                 | 30 | 38.79  | 37.30        | 37.39       | 39.40         | <b>38.22</b> |
|                 | 35 | 36.91  | 35.61        | 34.62       | 36.77         | <b>35.98</b> |
|                 | 40 | 34.86  | 33.67        | 31.90       | 34.07         | <b>33.63</b> |
| <b>ARC-HEVC</b> | 25 | 40.49  | 38.86        | 40.28       | 42.00         | <b>40.41</b> |
|                 | 30 | 38.79  | 37.30        | 37.41       | 39.42         | <b>38.23</b> |
|                 | 35 | 36.92  | 35.60        | 34.64       | 36.79         | <b>35.99</b> |
|                 | 40 | 34.87  | 33.67        | 31.92       | 34.09         | <b>33.64</b> |

Table A.3. Bitrate [kbps] values for the experiment evaluating ARC-HEVC in compression of multiview video (Section 4.6).

| Encoder         | QP | Ballet  | Breakdancers | BBB_Flowers | Poznan_Blocks | average        |
|-----------------|----|---------|--------------|-------------|---------------|----------------|
| <b>3D-HEVC</b>  | 25 | 2758.83 | 4835.11      | 6188.50     | 7844.20       | <b>5406.66</b> |
|                 | 30 | 1188.92 | 1944.54      | 3214.43     | 3911.95       | <b>2564.96</b> |
|                 | 35 | 574.86  | 972.50       | 1760.20     | 2076.74       | <b>1346.08</b> |
|                 | 40 | 304.42  | 513.94       | 969.19      | 1126.31       | <b>728.47</b>  |
| <b>ANY-HEVC</b> | 25 | 2694.10 | 4654.14      | 6099.87     | 7735.32       | <b>5295.86</b> |
|                 | 30 | 1147.64 | 1841.11      | 3161.51     | 3827.75       | <b>2494.50</b> |
|                 | 35 | 547.06  | 906.07       | 1721.46     | 2011.29       | <b>1296.47</b> |
|                 | 40 | 283.84  | 466.14       | 940.47      | 1075.03       | <b>691.37</b>  |
| <b>ARC-HEVC</b> | 25 | 2698.13 | 4683.97      | 6101.67     | 7739.86       | <b>5305.91</b> |
|                 | 30 | 1145.83 | 1857.88      | 3160.50     | 3834.07       | <b>2499.57</b> |
|                 | 35 | 547.89  | 913.64       | 1719.77     | 2012.46       | <b>1298.44</b> |
|                 | 40 | 283.07  | 468.27       | 937.40      | 1076.48       | <b>691.31</b>  |

Table A.4. PSNR [dB] values for the experiment comparing different view alignments (Section 5.3).

| View alignment | QP | Balloons | BBB_Butterfly | Kendo | Newspaper | Poznan_Hall2 | Poznan_Street | average      |
|----------------|----|----------|---------------|-------|-----------|--------------|---------------|--------------|
| 2×2            | 22 | 45.04    | 48.14         | 45.69 | 43.55     | 43.97        | 43.24         | <b>44.94</b> |
|                | 27 | 42.84    | 45.29         | 43.72 | 40.50     | 42.35        | 39.84         | <b>42.42</b> |
|                | 32 | 40.33    | 42.43         | 41.44 | 37.68     | 41.07        | 37.12         | <b>40.01</b> |
|                | 37 | 37.42    | 39.68         | 38.76 | 34.95     | 39.44        | 34.70         | <b>37.49</b> |
| 1×4            | 22 | 45.04    | 48.14         | 45.68 | 43.54     | 43.97        | 43.24         | <b>44.93</b> |
|                | 27 | 42.85    | 45.29         | 43.70 | 40.48     | 42.36        | 39.84         | <b>42.42</b> |
|                | 32 | 40.31    | 42.42         | 41.41 | 37.66     | 41.09        | 37.12         | <b>40.00</b> |
|                | 37 | 37.40    | 39.66         | 38.72 | 34.93     | 39.45        | 34.69         | <b>37.47</b> |
| 4×1            | 22 | 45.02    | 48.11         | 45.67 | 43.53     | 43.97        | 43.23         | <b>44.92</b> |
|                | 27 | 42.80    | 45.27         | 43.69 | 40.48     | 42.33        | 39.82         | <b>42.40</b> |
|                | 32 | 40.29    | 42.41         | 41.42 | 37.66     | 41.06        | 37.10         | <b>39.99</b> |
|                | 37 | 37.39    | 39.66         | 38.74 | 34.94     | 39.42        | 34.69         | <b>37.47</b> |

Table A.5. Bitrate [Mbps] values for the experiment comparing different view alignments (Section 5.3).

| View alignment | QP | Balloons | BBB_Butterfly | Kendo | Newspaper | Poznan_Hall2 | Poznan_Street | average      |
|----------------|----|----------|---------------|-------|-----------|--------------|---------------|--------------|
| 2×2            | 22 | 30.39    | 17.34         | 20.23 | 55.05     | 50.64        | 150.11        | <b>53.96</b> |
|                | 27 | 15.67    | 9.44          | 10.21 | 27.27     | 17.08        | 64.43         | <b>24.02</b> |
|                | 32 | 8.84     | 5.13          | 5.65  | 13.80     | 8.35         | 26.81         | <b>11.43</b> |
|                | 37 | 5.14     | 2.93          | 3.25  | 7.32      | 4.56         | 12.20         | <b>5.90</b>  |
| 1×4            | 22 | 30.49    | 17.54         | 20.09 | 54.79     | 50.87        | 149.38        | <b>53.86</b> |
|                | 27 | 16.03    | 9.42          | 10.08 | 26.57     | 17.79        | 64.73         | <b>24.10</b> |
|                | 32 | 8.94     | 5.08          | 5.50  | 13.30     | 8.85         | 26.59         | <b>11.38</b> |
|                | 37 | 5.25     | 2.83          | 3.10  | 7.05      | 4.84         | 11.77         | <b>5.81</b>  |
| 4×1            | 22 | 29.23    | 16.18         | 19.60 | 53.99     | 50.34        | 147.72        | <b>52.84</b> |
|                | 27 | 14.80    | 8.70          | 9.73  | 26.22     | 16.23        | 61.88         | <b>22.93</b> |
|                | 32 | 8.23     | 4.82          | 5.35  | 13.05     | 7.71         | 25.14         | <b>10.72</b> |
|                | 37 | 4.75     | 2.74          | 3.08  | 6.81      | 4.13         | 11.42         | <b>5.49</b>  |

Table A.6. Encoding time [s] values for the experiment comparing different view alignments (Section 5.3).

| View alignment | QP | Balloons | BBB_Butterfly | Kendo | Newspaper | Poznan_Hall2 | Poznan_Street | average      |
|----------------|----|----------|---------------|-------|-----------|--------------|---------------|--------------|
| 2×2            | 22 | 7955     | 5164          | 6362  | 11119     | 18720        | 30717         | <b>13340</b> |
|                | 27 | 6103     | 4273          | 4819  | 9060      | 11983        | 26219         | <b>10409</b> |
|                | 32 | 5658     | 3655          | 3971  | 6667      | 9576         | 16965         | <b>7749</b>  |
|                | 37 | 4563     | 3612          | 3718  | 4463      | 7998         | 9475          | <b>5638</b>  |
| 1×4            | 22 | 8892     | 5977          | 7473  | 12332     | 18178        | 36773         | <b>14937</b> |
|                | 27 | 6887     | 4572          | 4927  | 9310      | 12566        | 27667         | <b>10988</b> |
|                | 32 | 5324     | 3892          | 4363  | 6173      | 10123        | 18678         | <b>8092</b>  |
|                | 37 | 3752     | 3318          | 3629  | 4720      | 9292         | 9971          | <b>5780</b>  |
| 4×1            | 22 | 7820     | 5277          | 7114  | 11442     | 18704        | 37657         | <b>14669</b> |
|                | 27 | 6570     | 4185          | 5279  | 8608      | 11382        | 26721         | <b>10458</b> |
|                | 32 | 4557     | 3909          | 3823  | 6407      | 9000         | 16750         | <b>7408</b>  |
|                | 37 | 3979     | 3467          | 3631  | 4315      | 7870         | 8869          | <b>5355</b>  |

Table A.7. PSNR [dB] values for the experiment comparing SCC tools in compression of frame-compatible multiview video (Section 5.4).

| SCC configuration                  | QP | Balloons | BBB_Butterfly | Kendo | Newspaper | Poznan_Hall2 | Poznan_Street | average      |
|------------------------------------|----|----------|---------------|-------|-----------|--------------|---------------|--------------|
| configuration according to SCC CTC | 22 | 45.02    | 48.11         | 45.67 | 43.53     | 43.97        | 43.23         | <b>44.92</b> |
|                                    | 27 | 42.80    | 45.27         | 43.69 | 40.48     | 42.33        | 39.82         | <b>42.40</b> |
|                                    | 32 | 40.29    | 42.41         | 41.42 | 37.66     | 41.06        | 37.10         | <b>39.99</b> |
|                                    | 37 | 37.39    | 39.66         | 38.74 | 34.94     | 39.42        | 34.69         | <b>37.47</b> |
| Intra Boundary Filter (enabled)    | 22 | 45.02    | 48.11         | 45.67 | 43.53     | 43.97        | 43.23         | <b>44.92</b> |
|                                    | 27 | 42.81    | 45.27         | 43.70 | 40.48     | 42.33        | 39.82         | <b>42.40</b> |
|                                    | 32 | 40.30    | 42.41         | 41.42 | 37.67     | 41.05        | 37.11         | <b>39.99</b> |
|                                    | 37 | 37.40    | 39.66         | 38.74 | 34.94     | 39.43        | 34.70         | <b>37.48</b> |
| Hash-Based IBC Search (disabled)   | 22 | 45.02    | 48.11         | 45.67 | 43.53     | 43.97        | 43.23         | <b>44.92</b> |
|                                    | 27 | 42.80    | 45.27         | 43.69 | 40.48     | 42.33        | 39.82         | <b>42.40</b> |
|                                    | 32 | 40.29    | 42.41         | 41.42 | 37.66     | 41.06        | 37.10         | <b>39.99</b> |
|                                    | 37 | 37.39    | 39.66         | 38.74 | 34.94     | 39.42        | 34.69         | <b>37.47</b> |
| Palette Mode (disabled)            | 22 | 45.02    | 48.11         | 45.67 | 43.52     | 43.97        | 43.23         | <b>44.92</b> |
|                                    | 27 | 42.80    | 45.28         | 43.69 | 40.48     | 42.33        | 39.82         | <b>42.40</b> |
|                                    | 32 | 40.30    | 42.41         | 41.42 | 37.66     | 41.05        | 37.10         | <b>39.99</b> |
|                                    | 37 | 37.39    | 39.66         | 38.74 | 34.93     | 39.42        | 34.69         | <b>37.47</b> |
| all improvements                   | 22 | 45.02    | 48.10         | 45.67 | 43.53     | 43.97        | 43.23         | <b>44.92</b> |
|                                    | 27 | 42.81    | 45.27         | 43.69 | 40.48     | 42.33        | 39.82         | <b>42.40</b> |
|                                    | 32 | 40.30    | 42.41         | 41.42 | 37.67     | 41.05        | 37.11         | <b>39.99</b> |
|                                    | 37 | 37.40    | 39.66         | 38.74 | 34.94     | 39.43        | 34.70         | <b>37.48</b> |

Table A.8. Bitrate [Mbps] values for the experiment comparing SCC tools in compression of frame-compatible multiview video (Section 5.4).

| SCC configuration                  | QP | Balloons | BBB_Butterfly | Kendo | Newspaper | Poznan_Hall2 | Poznan_Street | average      |
|------------------------------------|----|----------|---------------|-------|-----------|--------------|---------------|--------------|
| configuration according to SCC CTC | 22 | 29.23    | 16.18         | 19.60 | 53.99     | 50.34        | 147.72        | <b>52.84</b> |
|                                    | 27 | 14.80    | 8.70          | 9.73  | 26.22     | 16.23        | 61.88         | <b>22.93</b> |
|                                    | 32 | 8.23     | 4.82          | 5.35  | 13.05     | 7.71         | 25.14         | <b>10.72</b> |
|                                    | 37 | 4.75     | 2.74          | 3.08  | 6.81      | 4.13         | 11.42         | <b>5.49</b>  |
| Intra Boundary Filter (enabled)    | 22 | 29.17    | 16.16         | 19.58 | 53.82     | 50.29        | 147.37        | <b>52.73</b> |
|                                    | 27 | 14.76    | 8.70          | 9.72  | 26.12     | 16.18        | 61.80         | <b>22.88</b> |
|                                    | 32 | 8.21     | 4.81          | 5.35  | 13.01     | 7.68         | 25.08         | <b>10.69</b> |
|                                    | 37 | 4.74     | 2.73          | 3.07  | 6.78      | 4.12         | 11.40         | <b>5.48</b>  |
| Hash-Based IBC Search (disabled)   | 22 | 29.23    | 16.18         | 19.60 | 53.99     | 50.34        | 147.72        | <b>52.84</b> |
|                                    | 27 | 14.80    | 8.70          | 9.73  | 26.22     | 16.23        | 61.88         | <b>22.93</b> |
|                                    | 32 | 8.23     | 4.82          | 5.35  | 13.05     | 7.71         | 25.14         | <b>10.72</b> |
|                                    | 37 | 4.75     | 2.74          | 3.08  | 6.81      | 4.13         | 11.42         | <b>5.49</b>  |
| Palette Mode (disabled)            | 22 | 29.23    | 16.18         | 19.61 | 53.93     | 50.32        | 147.72        | <b>52.83</b> |
|                                    | 27 | 14.79    | 8.70          | 9.73  | 26.19     | 16.22        | 61.90         | <b>22.92</b> |
|                                    | 32 | 8.23     | 4.82          | 5.35  | 13.04     | 7.69         | 25.14         | <b>10.71</b> |
|                                    | 37 | 4.75     | 2.76          | 3.07  | 6.80      | 4.13         | 11.42         | <b>5.49</b>  |
| all improvements                   | 22 | 29.17    | 16.17         | 19.58 | 53.77     | 50.28        | 147.34        | <b>52.72</b> |
|                                    | 27 | 14.75    | 8.69          | 9.72  | 26.12     | 16.18        | 61.77         | <b>22.87</b> |
|                                    | 32 | 8.21     | 4.80          | 5.34  | 13.01     | 7.68         | 25.08         | <b>10.69</b> |
|                                    | 37 | 4.74     | 2.77          | 3.07  | 6.78      | 4.12         | 11.39         | <b>5.48</b>  |

Table A.9. Encoding time [s] values for the experiment comparing SCC tools in compression of frame-compatible multiview video (Section 5.4).

| SCC configuration                  | QP | Balloons | BBB_Butterfly | Kendo | Newspaper | Poznan_Hall2 | Poznan_Street | average      |
|------------------------------------|----|----------|---------------|-------|-----------|--------------|---------------|--------------|
| configuration according to SCC CTC | 22 | 8085     | 5420          | 6309  | 11897     | 18940        | 33813         | <b>14077</b> |
|                                    | 27 | 6311     | 4241          | 5198  | 9026      | 11405        | 23135         | <b>9886</b>  |
|                                    | 32 | 4786     | 3885          | 4139  | 6282      | 8976         | 14313         | <b>7063</b>  |
|                                    | 37 | 3644     | 3475          | 3361  | 4608      | 7634         | 9387          | <b>5351</b>  |
| Intra Boundary Filter (enabled)    | 22 | 7915     | 5623          | 6213  | 11888     | 19207        | 33008         | <b>13976</b> |
|                                    | 27 | 6049     | 4402          | 5053  | 9156      | 10947        | 23089         | <b>9783</b>  |
|                                    | 32 | 4961     | 3798          | 3994  | 6420      | 8644         | 14725         | <b>7090</b>  |
|                                    | 37 | 4162     | 3420          | 3277  | 4631      | 8093         | 9781          | <b>5561</b>  |
| Hash-Based IBC Search (disabled)   | 22 | 8592     | 5343          | 6327  | 11513     | 18967        | 33015         | <b>13959</b> |
|                                    | 27 | 6022     | 4256          | 4928  | 8642      | 11852        | 22813         | <b>9752</b>  |
|                                    | 32 | 4691     | 3901          | 4035  | 6221      | 9309         | 14290         | <b>7075</b>  |
|                                    | 37 | 3671     | 3482          | 3289  | 4409      | 7874         | 9314          | <b>5340</b>  |
| Palette Mode (disabled)            | 22 | 6181     | 4033          | 4815  | 7706      | 14475        | 25425         | <b>10439</b> |
|                                    | 27 | 5074     | 3367          | 4029  | 6505      | 9147         | 19602         | <b>7954</b>  |
|                                    | 32 | 3989     | 3184          | 3240  | 4873      | 7634         | 12508         | <b>5905</b>  |
|                                    | 37 | 3541     | 2976          | 2776  | 3695      | 6404         | 8221          | <b>4602</b>  |
| all improvements                   | 22 | 6271     | 4015          | 4950  | 7812      | 14846        | 25316         | <b>10535</b> |
|                                    | 27 | 4924     | 3388          | 4079  | 6489      | 9181         | 19181         | <b>7874</b>  |
|                                    | 32 | 3864     | 3179          | 3293  | 5002      | 7229         | 12104         | <b>5779</b>  |
|                                    | 37 | 3010     | 2981          | 2762  | 3734      | 6224         | 7988          | <b>4450</b>  |

Table A.10. PSNR [dB] values for the experiment evaluating SCC in compression of stereoscopic video (Section 5.7.2).

|               | Encoder                | QP | Balloons | BBB_Butterfly | Kendo | Newspaper | Poznan_Hall2 | Poznan_Street | average      |
|---------------|------------------------|----|----------|---------------|-------|-----------|--------------|---------------|--------------|
| All Intra     | HEVC Main simulcast    | 22 | 45.20    | 48.41         | 45.93 | 43.56     | 44.92        | 43.17         | <b>45.20</b> |
|               |                        | 27 | 42.57    | 45.24         | 43.54 | 40.33     | 43.34        | 39.96         | <b>42.50</b> |
|               |                        | 32 | 39.59    | 42.17         | 40.82 | 37.33     | 41.44        | 37.11         | <b>39.74</b> |
|               |                        | 37 | 36.38    | 39.21         | 37.81 | 34.37     | 39.22        | 34.38         | <b>36.90</b> |
|               | HEVC Main side-by-side | 22 | 45.19    | 48.40         | 45.93 | 43.56     | 44.92        | 43.17         | <b>45.19</b> |
|               |                        | 27 | 42.57    | 45.23         | 43.53 | 40.33     | 43.33        | 39.95         | <b>42.49</b> |
|               |                        | 32 | 39.58    | 42.15         | 40.80 | 37.32     | 41.44        | 37.11         | <b>39.73</b> |
|               |                        | 37 | 36.36    | 39.20         | 37.79 | 34.36     | 39.21        | 34.37         | <b>36.88</b> |
|               | HEVC SCC simulcast     | 22 | 45.19    | 48.40         | 45.92 | 43.55     | 44.91        | 43.16         | <b>45.19</b> |
|               |                        | 27 | 42.56    | 45.24         | 43.53 | 40.33     | 43.33        | 39.94         | <b>42.49</b> |
|               |                        | 32 | 39.57    | 42.16         | 40.81 | 37.32     | 41.44        | 37.09         | <b>39.73</b> |
|               |                        | 37 | 36.37    | 39.20         | 37.79 | 34.36     | 39.22        | 34.37         | <b>36.88</b> |
|               | HEVC SCC side-by-side  | 22 | 45.01    | 48.22         | 45.80 | 43.43     | 44.87        | 43.06         | <b>45.07</b> |
|               |                        | 27 | 42.32    | 45.06         | 43.34 | 40.20     | 43.26        | 39.80         | <b>42.33</b> |
|               |                        | 32 | 39.29    | 41.97         | 40.55 | 37.17     | 41.35        | 36.92         | <b>39.54</b> |
|               |                        | 37 | 36.03    | 38.96         | 37.49 | 34.17     | 39.13        | 34.16         | <b>36.65</b> |
| Random Access | HEVC Main simulcast    | 22 | 44.06    | 47.41         | 44.72 | 42.99     | 44.10        | 41.80         | <b>44.18</b> |
|               |                        | 27 | 41.70    | 44.19         | 42.33 | 40.24     | 42.88        | 39.39         | <b>41.79</b> |
|               |                        | 32 | 38.84    | 41.07         | 39.54 | 37.40     | 41.22        | 36.94         | <b>39.17</b> |
|               |                        | 37 | 35.88    | 38.23         | 36.70 | 34.58     | 39.18        | 34.51         | <b>36.51</b> |
|               | HEVC Main side-by-side | 22 | 44.05    | 47.40         | 44.71 | 42.99     | 44.10        | 41.81         | <b>44.17</b> |
|               |                        | 27 | 41.68    | 44.17         | 42.30 | 40.24     | 42.87        | 39.39         | <b>41.77</b> |
|               |                        | 32 | 38.82    | 41.05         | 39.50 | 37.39     | 41.18        | 36.94         | <b>39.15</b> |
|               |                        | 37 | 35.84    | 38.21         | 36.65 | 34.57     | 39.14        | 34.51         | <b>36.49</b> |
|               | HEVC SCC simulcast     | 22 | 44.03    | 47.39         | 44.70 | 42.97     | 44.09        | 41.79         | <b>44.16</b> |
|               |                        | 27 | 41.66    | 44.18         | 42.31 | 40.22     | 42.88        | 39.38         | <b>41.77</b> |
|               |                        | 32 | 38.81    | 41.04         | 39.53 | 37.38     | 41.20        | 36.93         | <b>39.15</b> |
|               |                        | 37 | 35.84    | 38.20         | 36.70 | 34.56     | 39.16        | 34.52         | <b>36.50</b> |
|               | HEVC SCC side-by-side  | 22 | 44.00    | 47.34         | 44.66 | 42.97     | 44.09        | 41.79         | <b>44.14</b> |
|               |                        | 27 | 41.59    | 44.09         | 42.23 | 40.22     | 42.87        | 39.38         | <b>41.73</b> |
|               |                        | 32 | 38.71    | 40.96         | 39.37 | 37.38     | 41.19        | 36.89         | <b>39.08</b> |
|               |                        | 37 | 35.69    | 38.09         | 36.48 | 34.52     | 39.14        | 34.45         | <b>36.39</b> |



Table A.11.Bitrate [kbps] values for the experiment evaluating SCC in compression of stereoscopic video (Section 5.7.2).

|                      | Encoder                       | QP | Balloons | BBB_Butterfly | Kendo   | Newspaper | Poznan_Hall2 | Poznan_Street | average         |
|----------------------|-------------------------------|----|----------|---------------|---------|-----------|--------------|---------------|-----------------|
| <b>All Intra</b>     | <b>HEVC Main simulcast</b>    | 22 | 12544.53 | 7964.31       | 8512.40 | 18411.66  | 11750.48     | 42779.69      | <b>16993.84</b> |
|                      |                               | 27 | 7836.23  | 4721.33       | 5227.89 | 10680.18  | 6107.82      | 23191.02      | <b>9627.41</b>  |
|                      |                               | 32 | 4963.24  | 2791.18       | 3285.59 | 6304.77   | 3393.94      | 12585.00      | <b>5553.95</b>  |
|                      |                               | 37 | 3149.78  | 1699.81       | 2070.70 | 3778.06   | 1960.07      | 6972.65       | <b>3271.84</b>  |
|                      | <b>HEVC Main side-by-side</b> | 22 | 12542.57 | 7947.78       | 8503.68 | 18411.24  | 11744.76     | 42775.63      | <b>16987.61</b> |
|                      |                               | 27 | 7832.67  | 4709.75       | 5221.36 | 10673.15  | 6102.39      | 23187.73      | <b>9621.17</b>  |
|                      |                               | 32 | 4955.36  | 2782.11       | 3278.47 | 6298.27   | 3388.10      | 12583.93      | <b>5547.71</b>  |
|                      |                               | 37 | 3141.87  | 1691.49       | 2063.78 | 3774.14   | 1950.69      | 6971.66       | <b>3265.61</b>  |
|                      | <b>HEVC SCC simulcast</b>     | 22 | 12540.04 | 7970.06       | 8516.49 | 18406.82  | 11680.41     | 42500.74      | <b>16935.76</b> |
|                      |                               | 27 | 7840.10  | 4727.75       | 5230.35 | 10677.97  | 6033.65      | 22932.12      | <b>9573.66</b>  |
|                      |                               | 32 | 4966.89  | 2798.03       | 3289.51 | 6309.37   | 3365.31      | 12405.49      | <b>5522.43</b>  |
|                      |                               | 37 | 3155.65  | 1704.58       | 2070.48 | 3779.54   | 1957.20      | 6880.40       | <b>3257.97</b>  |
|                      | <b>HEVC SCC side-by-side</b>  | 22 | 10234.71 | 5899.91       | 6936.42 | 16047.12  | 10931.90     | 37107.11      | <b>14526.20</b> |
|                      |                               | 27 | 6006.02  | 3413.30       | 3965.15 | 8747.86   | 5217.57      | 18319.68      | <b>7611.60</b>  |
|                      |                               | 32 | 3616.03  | 1991.70       | 2345.14 | 4903.66   | 2776.71      | 9194.73       | <b>4138.00</b>  |
|                      |                               | 37 | 2182.50  | 1176.29       | 1403.45 | 2796.51   | 1568.48      | 4733.79       | <b>2310.17</b>  |
| <b>Random Access</b> | <b>HEVC Main simulcast</b>    | 22 | 1763.97  | 1408.72       | 1620.03 | 1763.16   | 1726.55      | 5079.73       | <b>2227.03</b>  |
|                      |                               | 27 | 950.37   | 754.06        | 855.64  | 949.53    | 733.34       | 2219.61       | <b>1077.09</b>  |
|                      |                               | 32 | 542.91   | 413.79        | 485.13  | 537.60    | 382.54       | 1090.32       | <b>575.38</b>   |
|                      |                               | 37 | 323.83   | 242.77        | 290.27  | 316.95    | 214.71       | 573.51        | <b>327.00</b>   |
|                      | <b>HEVC Main side-by-side</b> | 22 | 1769.75  | 1398.84       | 1616.50 | 1762.79   | 1730.83      | 5077.29       | <b>2226.00</b>  |
|                      |                               | 27 | 950.84   | 748.02        | 854.01  | 946.64    | 737.23       | 2216.78       | <b>1075.59</b>  |
|                      |                               | 32 | 541.94   | 409.15        | 482.55  | 534.12    | 381.78       | 1088.20       | <b>572.96</b>   |
|                      |                               | 37 | 321.57   | 239.00        | 288.65  | 314.34    | 212.94       | 571.56        | <b>324.68</b>   |
|                      | <b>HEVC SCC simulcast</b>     | 22 | 1761.44  | 1402.42       | 1609.67 | 1762.95   | 1707.61      | 5054.18       | <b>2216.38</b>  |
|                      |                               | 27 | 947.04   | 750.23        | 850.81  | 948.29    | 727.50       | 2204.37       | <b>1071.37</b>  |
|                      |                               | 32 | 541.91   | 411.72        | 481.74  | 536.33    | 378.04       | 1079.25       | <b>571.50</b>   |
|                      |                               | 37 | 322.86   | 242.22        | 288.95  | 316.07    | 213.31       | 568.23        | <b>325.27</b>   |
|                      | <b>HEVC SCC side-by-side</b>  | 22 | 1605.55  | 1146.92       | 1432.18 | 1623.63   | 1677.24      | 4715.10       | <b>2033.44</b>  |
|                      |                               | 27 | 820.00   | 596.28        | 717.64  | 831.35    | 680.71       | 1908.83       | <b>925.80</b>   |
|                      |                               | 32 | 448.59   | 320.60        | 387.24  | 448.60    | 341.90       | 871.08        | <b>469.67</b>   |
|                      |                               | 37 | 255.27   | 185.50        | 219.52  | 254.52    | 186.40       | 431.39        | <b>255.43</b>   |

Table A.12. Encoding time [s] values for the experiment evaluating SCC in compression of stereoscopic video (Section 5.7.2).

|                      | Encoder                       | QP | Balloons | BBB_Butterfly | Kendo | Newspaper | Poznan_Hall2 | Poznan_Street | average     |
|----------------------|-------------------------------|----|----------|---------------|-------|-----------|--------------|---------------|-------------|
| <b>All Intra</b>     | <b>HEVC Main simulcast</b>    | 22 | 805      | 852           | 812   | 837       | 1772         | 2203          | <b>1213</b> |
|                      |                               | 27 | 687      | 828           | 658   | 697       | 1574         | 1904          | <b>1058</b> |
|                      |                               | 32 | 604      | 834           | 569   | 663       | 1474         | 1673          | <b>969</b>  |
|                      |                               | 37 | 632      | 727           | 582   | 623       | 1448         | 1569          | <b>930</b>  |
|                      | <b>HEVC Main side-by-side</b> | 22 | 792      | 814           | 764   | 868       | 1765         | 2202          | <b>1201</b> |
|                      |                               | 27 | 710      | 847           | 671   | 765       | 1590         | 1847          | <b>1072</b> |
|                      |                               | 32 | 644      | 837           | 661   | 664       | 1526         | 1679          | <b>1002</b> |
|                      |                               | 37 | 598      | 678           | 579   | 605       | 1478         | 1543          | <b>914</b>  |
|                      | <b>HEVC SCC simulcast</b>     | 22 | 1537     | 1325          | 1108  | 1811      | 2732         | 5043          | <b>2259</b> |
|                      |                               | 27 | 1241     | 1194          | 1102  | 1697      | 2094         | 4209          | <b>1923</b> |
|                      |                               | 32 | 1185     | 1106          | 1059  | 1454      | 2117         | 3548          | <b>1745</b> |
|                      |                               | 37 | 1001     | 1135          | 875   | 1228      | 1865         | 2738          | <b>1474</b> |
|                      | <b>HEVC SCC side-by-side</b>  | 22 | 1474     | 1060          | 1270  | 1918      | 2777         | 5187          | <b>2281</b> |
|                      |                               | 27 | 1344     | 918           | 1075  | 1627      | 2186         | 4230          | <b>1897</b> |
|                      |                               | 32 | 1118     | 975           | 868   | 1331      | 1813         | 3124          | <b>1538</b> |
|                      |                               | 37 | 889      | 806           | 772   | 1013      | 1664         | 2289          | <b>1239</b> |
| <b>Random Access</b> | <b>HEVC Main simulcast</b>    | 22 | 2297     | 2242          | 2110  | 1859      | 5117         | 5037          | <b>3110</b> |
|                      |                               | 27 | 2050     | 2118          | 1886  | 1621      | 4512         | 4300          | <b>2748</b> |
|                      |                               | 32 | 1906     | 2263          | 1810  | 1552      | 4552         | 4027          | <b>2685</b> |
|                      |                               | 37 | 1678     | 2199          | 1755  | 1530      | 4262         | 4080          | <b>2584</b> |
|                      | <b>HEVC Main side-by-side</b> | 22 | 2199     | 2477          | 2375  | 1791      | 4871         | 4765          | <b>3080</b> |
|                      |                               | 27 | 1963     | 2427          | 1920  | 1636      | 4383         | 4167          | <b>2749</b> |
|                      |                               | 32 | 1771     | 2316          | 2049  | 1836      | 4184         | 3919          | <b>2679</b> |
|                      |                               | 37 | 1662     | 1952          | 1679  | 1719      | 4038         | 3818          | <b>2478</b> |
|                      | <b>HEVC SCC simulcast</b>     | 22 | 3098     | 2729          | 3161  | 2093      | 5141         | 5215          | <b>3573</b> |
|                      |                               | 27 | 2308     | 2308          | 2424  | 1754      | 3781         | 3843          | <b>2736</b> |
|                      |                               | 32 | 1738     | 2009          | 1963  | 1343      | 3051         | 3109          | <b>2202</b> |
|                      |                               | 37 | 1462     | 1731          | 1717  | 1234      | 2733         | 2685          | <b>1927</b> |
|                      | <b>HEVC SCC side-by-side</b>  | 22 | 2920     | 2574          | 3089  | 2093      | 4770         | 5099          | <b>3424</b> |
|                      |                               | 27 | 2204     | 2223          | 2382  | 1711      | 3615         | 3665          | <b>2633</b> |
|                      |                               | 32 | 1680     | 1842          | 1808  | 1373      | 2933         | 2943          | <b>2096</b> |
|                      |                               | 37 | 1450     | 1650          | 1465  | 1230      | 2485         | 2530          | <b>1802</b> |

Table A.13. PSNR [dB] values for the experiment evaluating SCC in compression of multiview video (Section 5.7.3).

|                       | Encoder                       | QP    | Balloons | BBB_Butterfly | Kendo | Newspaper | Poznan_Hall2 | Poznan_Street | average      |
|-----------------------|-------------------------------|-------|----------|---------------|-------|-----------|--------------|---------------|--------------|
| <b>All Intra</b>      | <b>HEVC Main simulcast</b>    | 22    | 45.20    | 48.33         | 45.82 | 43.68     | 43.98        | 43.29         | <b>45.05</b> |
|                       |                               | 27    | 43.14    | 45.51         | 43.95 | 40.70     | 42.40        | 39.99         | <b>42.62</b> |
|                       |                               | 32    | 40.70    | 42.67         | 41.76 | 37.93     | 41.16        | 37.37         | <b>40.27</b> |
|                       |                               | 37    | 37.83    | 39.97         | 39.15 | 35.24     | 39.56        | 35.00         | <b>37.79</b> |
|                       | <b>HEVC Main side-by-side</b> | 22    | 45.20    | 48.33         | 45.81 | 43.67     | 43.98        | 43.29         | <b>45.05</b> |
|                       |                               | 27    | 43.13    | 45.49         | 43.94 | 40.68     | 42.39        | 39.99         | <b>42.60</b> |
|                       |                               | 32    | 40.69    | 42.66         | 41.75 | 37.91     | 41.15        | 37.36         | <b>40.25</b> |
|                       |                               | 37    | 37.82    | 39.95         | 39.14 | 35.20     | 39.55        | 34.99         | <b>37.78</b> |
|                       | <b>HEVC SCC simulcast</b>     | 22    | 45.20    | 48.33         | 45.82 | 43.68     | 43.97        | 43.29         | <b>45.05</b> |
|                       |                               | 27    | 43.13    | 45.50         | 43.94 | 40.69     | 42.39        | 39.98         | <b>42.61</b> |
|                       |                               | 32    | 40.68    | 42.67         | 41.75 | 37.93     | 41.16        | 37.35         | <b>40.26</b> |
|                       |                               | 37    | 37.82    | 39.95         | 39.14 | 35.23     | 39.56        | 34.98         | <b>37.78</b> |
|                       | <b>HEVC SCC side-by-side</b>  | 22    | 45.02    | 48.10         | 45.67 | 43.53     | 43.97        | 43.23         | <b>44.92</b> |
|                       |                               | 27    | 42.81    | 45.27         | 43.69 | 40.48     | 42.33        | 39.82         | <b>42.40</b> |
|                       |                               | 32    | 40.30    | 42.41         | 41.42 | 37.67     | 41.05        | 37.11         | <b>39.99</b> |
|                       |                               | 37    | 37.40    | 39.66         | 38.74 | 34.94     | 39.43        | 34.70         | <b>37.48</b> |
| <b>Multiview HEVC</b> | 22                            | 45.25 | 48.42    | 45.89         | 43.81 | 44.27     | 43.52        | <b>45.19</b>  |              |
|                       | 27                            | 43.12 | 45.65    | 43.97         | 40.82 | 42.44     | 40.13        | <b>42.69</b>  |              |
|                       | 32                            | 40.76 | 42.84    | 41.82         | 38.07 | 41.24     | 37.47        | <b>40.37</b>  |              |
|                       | 37                            | 37.96 | 40.13    | 39.25         | 35.37 | 39.71     | 35.14        | <b>37.93</b>  |              |
| <b>Random Access</b>  | <b>HEVC Main simulcast</b>    | 22    | 43.98    | 47.37         | 44.67 | 42.90     | 42.66        | 40.85         | <b>43.74</b> |
|                       |                               | 27    | 42.23    | 44.49         | 42.87 | 40.50     | 41.88        | 39.02         | <b>41.83</b> |
|                       |                               | 32    | 39.93    | 41.64         | 40.60 | 37.99     | 40.84        | 36.99         | <b>39.67</b> |
|                       |                               | 37    | 37.26    | 39.02         | 38.06 | 35.44     | 39.41        | 34.97         | <b>37.36</b> |
|                       | <b>HEVC Main side-by-side</b> | 22    | 43.97    | 47.37         | 44.66 | 42.89     | 42.66        | 40.85         | <b>43.73</b> |
|                       |                               | 27    | 42.22    | 44.47         | 42.85 | 40.48     | 41.87        | 39.02         | <b>41.82</b> |
|                       |                               | 32    | 39.91    | 41.63         | 40.57 | 37.97     | 40.83        | 36.98         | <b>39.65</b> |
|                       |                               | 37    | 37.23    | 39.02         | 38.02 | 35.40     | 39.39        | 34.96         | <b>37.34</b> |
|                       | <b>HEVC SCC simulcast</b>     | 22    | 43.96    | 47.36         | 44.66 | 42.89     | 42.65        | 40.84         | <b>43.73</b> |
|                       |                               | 27    | 42.21    | 44.49         | 42.87 | 40.49     | 41.88        | 39.01         | <b>41.83</b> |
|                       |                               | 32    | 39.90    | 41.64         | 40.59 | 37.98     | 40.84        | 36.98         | <b>39.66</b> |
|                       |                               | 37    | 37.23    | 39.01         | 38.05 | 35.43     | 39.39        | 34.96         | <b>37.35</b> |
|                       | <b>HEVC SCC side-by-side</b>  | 22    | 43.94    | 47.29         | 44.61 | 42.87     | 42.65        | 40.83         | <b>43.70</b> |
|                       |                               | 27    | 42.16    | 44.39         | 42.77 | 40.46     | 41.88        | 39.01         | <b>41.78</b> |
|                       |                               | 32    | 39.82    | 41.53         | 40.42 | 37.92     | 40.84        | 36.97         | <b>39.58</b> |
|                       |                               | 37    | 37.11    | 38.87         | 37.83 | 35.34     | 39.38        | 34.90         | <b>37.24</b> |
| <b>Multiview HEVC</b> | 22                            | 43.50 | 46.70    | 44.17         | 42.40 | 42.39     | 40.34        | <b>43.25</b>  |              |
|                       | 27                            | 41.71 | 43.89    | 42.33         | 40.07 | 41.66     | 38.74        | <b>41.40</b>  |              |
|                       | 32                            | 39.34 | 41.13    | 40.05         | 37.58 | 40.57     | 36.79        | <b>39.24</b>  |              |
|                       | 37                            | 36.69 | 38.54    | 37.54         | 35.04 | 39.07     | 34.78        | <b>36.94</b>  |              |

Table A.14. Bitrate [Mbps] values for the experiment evaluating SCC in compression of multiview video (Section 5.7.3).

|                | Encoder                | QP    | Balloons | BBB_Butterfly | Kendo | Newspaper | Poznan_Hall2 | Poznan_Street | average      |
|----------------|------------------------|-------|----------|---------------|-------|-----------|--------------|---------------|--------------|
| All Intra      | HEVC Main simulcast    | 22    | 37.12    | 26.23         | 25.17 | 61.98     | 51.26        | 158.91        | <b>60.11</b> |
|                |                        | 27    | 22.14    | 14.92         | 14.66 | 34.31     | 18.95        | 79.07         | <b>30.67</b> |
|                |                        | 32    | 13.81    | 8.41          | 9.07  | 19.36     | 10.10        | 39.79         | <b>16.76</b> |
|                |                        | 37    | 8.76     | 4.90          | 5.71  | 11.23     | 5.71         | 21.25         | <b>9.59</b>  |
|                | HEVC Main side-by-side | 22    | 37.12    | 26.20         | 25.14 | 61.99     | 51.30        | 158.94        | <b>60.12</b> |
|                |                        | 27    | 22.12    | 14.89         | 14.63 | 34.30     | 18.92        | 79.07         | <b>30.66</b> |
|                |                        | 32    | 13.78    | 8.37          | 9.04  | 19.34     | 10.07        | 39.77         | <b>16.73</b> |
|                |                        | 37    | 8.74     | 4.86          | 5.68  | 11.20     | 5.67         | 21.22         | <b>9.56</b>  |
|                | HEVC SCC simulcast     | 22    | 37.10    | 26.22         | 25.17 | 61.95     | 51.17        | 158.29        | <b>59.98</b> |
|                |                        | 27    | 22.14    | 14.93         | 14.66 | 34.29     | 18.78        | 78.34         | <b>30.52</b> |
|                |                        | 32    | 13.82    | 8.41          | 9.07  | 19.36     | 9.99         | 39.17         | <b>16.64</b> |
|                |                        | 37    | 8.77     | 4.90          | 5.71  | 11.23     | 5.67         | 20.95         | <b>9.54</b>  |
|                | HEVC SCC side-by-side  | 22    | 29.17    | 16.17         | 19.58 | 53.77     | 50.28        | 147.34        | <b>52.72</b> |
|                |                        | 27    | 14.75    | 8.69          | 9.72  | 26.12     | 16.18        | 61.77         | <b>22.87</b> |
|                |                        | 32    | 8.21     | 4.80          | 5.34  | 13.01     | 7.68         | 25.08         | <b>10.69</b> |
|                |                        | 37    | 4.74     | 2.77          | 3.07  | 6.78      | 4.12         | 11.39         | <b>5.48</b>  |
| Multiview HEVC | 22                     | 28.18 | 15.69    | 18.86         | 53.25 | 57.20     | 146.10       | <b>53.21</b>  |              |
|                | 27                     | 13.54 | 8.56     | 8.73          | 25.57 | 15.34     | 58.69        | <b>21.74</b>  |              |
|                | 32                     | 7.51  | 4.68     | 4.71          | 12.78 | 7.02      | 23.02        | <b>9.95</b>   |              |
|                | 37                     | 4.42  | 2.63     | 2.73          | 6.72  | 3.73      | 10.38        | <b>5.10</b>   |              |
| Random Access  | HEVC Main simulcast    | 22    | 5.56     | 4.63          | 4.89  | 6.18      | 9.56         | 24.64         | <b>9.24</b>  |
|                |                        | 27    | 2.74     | 2.37          | 2.42  | 3.04      | 2.43         | 8.45          | <b>3.57</b>  |
|                |                        | 32    | 1.55     | 1.26          | 1.35  | 1.64      | 1.16         | 3.61          | <b>1.76</b>  |
|                |                        | 37    | 0.92     | 0.72          | 0.81  | 0.93      | 0.63         | 1.81          | <b>0.97</b>  |
|                | HEVC Main side-by-side | 22    | 5.56     | 4.61          | 4.88  | 6.18      | 9.58         | 24.65         | <b>9.24</b>  |
|                |                        | 27    | 2.74     | 2.35          | 2.41  | 3.03      | 2.44         | 8.45          | <b>3.57</b>  |
|                |                        | 32    | 1.55     | 1.24          | 1.35  | 1.63      | 1.16         | 3.61          | <b>1.75</b>  |
|                |                        | 37    | 0.92     | 0.71          | 0.80  | 0.92      | 0.63         | 1.80          | <b>0.96</b>  |
|                | HEVC SCC simulcast     | 22    | 5.53     | 4.62          | 4.86  | 6.17      | 9.46         | 24.53         | <b>9.20</b>  |
|                |                        | 27    | 2.73     | 2.36          | 2.41  | 3.03      | 2.41         | 8.40          | <b>3.56</b>  |
|                |                        | 32    | 1.54     | 1.25          | 1.35  | 1.64      | 1.15         | 3.58          | <b>1.75</b>  |
|                |                        | 37    | 0.92     | 0.72          | 0.81  | 0.93      | 0.63         | 1.79          | <b>0.97</b>  |
|                | HEVC SCC side-by-side  | 22    | 5.03     | 3.39          | 4.26  | 5.74      | 9.44         | 23.76         | <b>8.60</b>  |
|                |                        | 27    | 2.23     | 1.65          | 1.89  | 2.57      | 2.29         | 7.40          | <b>3.01</b>  |
|                |                        | 32    | 1.15     | 0.85          | 0.97  | 1.26      | 1.01         | 2.70          | <b>1.32</b>  |
|                |                        | 37    | 0.64     | 0.48          | 0.54  | 0.66      | 0.53         | 1.19          | <b>0.67</b>  |
| Multiview HEVC | 22                     | 3.43  | 2.42     | 2.82          | 4.29  | 6.06      | 14.69        | <b>5.62</b>   |              |
|                | 27                     | 1.56  | 1.23     | 1.27          | 1.96  | 1.60      | 4.84         | <b>2.07</b>   |              |
|                | 32                     | 0.82  | 0.65     | 0.66          | 0.97  | 0.73      | 1.82         | <b>0.94</b>   |              |
|                | 37                     | 0.46  | 0.37     | 0.38          | 0.52  | 0.39      | 0.82         | <b>0.49</b>   |              |

Table A.15. Encoding time [s] values for the experiment evaluating SCC in compression of multiview video (Section 5.7.3).

|                      | Encoder                       | QP | Balloons | BBB_Butterfly | Kendo | Newspaper | Poznan_Hall2 | Poznan_Street | average      |
|----------------------|-------------------------------|----|----------|---------------|-------|-----------|--------------|---------------|--------------|
| <b>All Intra</b>     | <b>HEVC Main simulcast</b>    | 22 | 3193     | 3263          | 2632  | 3984      | 7635         | 9546          | <b>5042</b>  |
|                      |                               | 27 | 2994     | 2928          | 2478  | 3013      | 6234         | 8189          | <b>4306</b>  |
|                      |                               | 32 | 2744     | 2965          | 2425  | 2824      | 6061         | 7669          | <b>4115</b>  |
|                      |                               | 37 | 2385     | 2613          | 2313  | 2625      | 5847         | 6940          | <b>3787</b>  |
|                      | <b>HEVC Main side-by-side</b> | 22 | 2760     | 3228          | 2597  | 3147      | 6785         | 8814          | <b>4555</b>  |
|                      |                               | 27 | 2852     | 2793          | 2779  | 2787      | 6122         | 7542          | <b>4146</b>  |
|                      |                               | 32 | 2914     | 2659          | 2472  | 2575      | 5874         | 6715          | <b>3868</b>  |
|                      |                               | 37 | 2442     | 2831          | 2147  | 2317      | 5833         | 5971          | <b>3590</b>  |
|                      | <b>HEVC SCC simulcast</b>     | 22 | 4984     | 4966          | 4363  | 7470      | 11820        | 19263         | <b>8811</b>  |
|                      |                               | 27 | 4307     | 4350          | 4073  | 6196      | 8681         | 15930         | <b>7256</b>  |
|                      |                               | 32 | 3830     | 3867          | 3838  | 5069      | 7644         | 12338         | <b>6097</b>  |
|                      |                               | 37 | 3349     | 3603          | 3279  | 4390      | 7283         | 10532         | <b>5406</b>  |
|                      | <b>HEVC SCC side-by-side</b>  | 22 | 6165     | 3849          | 5777  | 7646      | 15177        | 26032         | <b>10774</b> |
|                      |                               | 27 | 4931     | 3259          | 4802  | 6232      | 9269         | 19778         | <b>8045</b>  |
|                      |                               | 32 | 3875     | 3056          | 3829  | 5387      | 7349         | 13063         | <b>6093</b>  |
|                      |                               | 37 | 3021     | 3593          | 3227  | 3544      | 6093         | 8387          | <b>4644</b>  |
|                      | <b>Multiview HEVC</b>         | 22 | 8750     | 5647          | 8285  | 10773     | 21965        | 25064         | <b>13414</b> |
|                      |                               | 27 | 7131     | 4708          | 6821  | 8495      | 15332        | 18754         | <b>10207</b> |
|                      |                               | 32 | 5736     | 4135          | 5758  | 6746      | 11893        | 13644         | <b>7985</b>  |
|                      |                               | 37 | 4548     | 3906          | 4982  | 6254      | 10401        | 10180         | <b>6712</b>  |
| <b>Random Access</b> | <b>HEVC Main simulcast</b>    | 22 | 9358     | 9083          | 8856  | 7550      | 21438        | 21861         | <b>13024</b> |
|                      |                               | 27 | 9020     | 8476          | 7793  | 6774      | 18021        | 17973         | <b>11343</b> |
|                      |                               | 32 | 7906     | 8263          | 7343  | 6376      | 17305        | 16804         | <b>10666</b> |
|                      |                               | 37 | 7458     | 7998          | 6937  | 6180      | 16713        | 16205         | <b>10249</b> |
|                      | <b>HEVC Main side-by-side</b> | 22 | 9001     | 8796          | 8545  | 7536      | 22950        | 23336         | <b>13361</b> |
|                      |                               | 27 | 8080     | 8432          | 7932  | 6909      | 19447        | 18755         | <b>11592</b> |
|                      |                               | 32 | 7195     | 7939          | 7384  | 6366      | 17861        | 17944         | <b>10782</b> |
|                      |                               | 37 | 7002     | 7713          | 6834  | 6140      | 17722        | 17188         | <b>10433</b> |
|                      | <b>HEVC SCC simulcast</b>     | 22 | 11833    | 9955          | 11570 | 8170      | 25699        | 27950         | <b>15863</b> |
|                      |                               | 27 | 8502     | 8248          | 8623  | 6340      | 15306        | 16229         | <b>10541</b> |
|                      |                               | 32 | 7093     | 7178          | 6902  | 5051      | 11931        | 13032         | <b>8531</b>  |
|                      |                               | 37 | 5138     | 6148          | 5738  | 4680      | 10835        | 11029         | <b>7261</b>  |
|                      | <b>HEVC SCC side-by-side</b>  | 22 | 11473    | 10284         | 11680 | 8804      | 25265        | 27346         | <b>15809</b> |
|                      |                               | 27 | 8720     | 8608          | 9448  | 6840      | 14388        | 16532         | <b>10756</b> |
|                      |                               | 32 | 6866     | 7224          | 6815  | 5096      | 12529        | 12862         | <b>8565</b>  |
|                      |                               | 37 | 5143     | 6154          | 5603  | 4720      | 10352        | 11286         | <b>7210</b>  |
|                      | <b>Multiview HEVC</b>         | 22 | 8910     | 9848          | 9157  | 8135      | 21681        | 21003         | <b>13122</b> |
|                      |                               | 27 | 8402     | 9348          | 8426  | 7679      | 19217        | 18473         | <b>11924</b> |
|                      |                               | 32 | 7555     | 9120          | 7929  | 7191      | 18667        | 17780         | <b>11374</b> |
|                      |                               | 37 | 7577     | 8786          | 7513  | 6882      | 17648        | 17039         | <b>10907</b> |

Table A.16. PSNR [dB] values for the experiment evaluating ASCC in compression of multiview video (Section 6.4.2).

|                      | Encoder               | QP | Balloons | Shark | Kendo | Newspaper | Poznan_Hall2 | Poznan_Street | Dancer | GT_Fly | average      |
|----------------------|-----------------------|----|----------|-------|-------|-----------|--------------|---------------|--------|--------|--------------|
| <b>All Intra</b>     | <b>HEVC</b>           | 25 | 44.15    | 43.46 | 44.88 | 41.96     | 42.80        | 41.21         | 40.32  | 41.86  | <b>42.58</b> |
|                      |                       | 30 | 41.90    | 40.26 | 42.87 | 39.17     | 41.58        | 38.40         | 36.83  | 39.16  | <b>40.02</b> |
|                      |                       | 35 | 39.15    | 37.18 | 40.41 | 36.42     | 40.05        | 35.96         | 33.76  | 36.50  | <b>37.43</b> |
|                      |                       | 40 | 36.09    | 34.36 | 37.64 | 33.71     | 38.19        | 33.58         | 31.22  | 33.94  | <b>34.84</b> |
|                      | <b>SCC</b>            | 25 | 43.90    | 42.89 | 44.74 | 41.72     | 42.75        | 41.13         | 40.22  | 41.88  | <b>42.40</b> |
|                      |                       | 30 | 41.56    | 39.70 | 42.65 | 38.87     | 41.48        | 38.21         | 36.74  | 39.12  | <b>39.79</b> |
|                      |                       | 35 | 38.78    | 36.66 | 40.14 | 36.10     | 39.94        | 35.71         | 33.67  | 36.40  | <b>37.18</b> |
|                      |                       | 40 | 35.67    | 33.94 | 37.32 | 33.33     | 38.05        | 33.26         | 31.12  | 33.83  | <b>34.57</b> |
|                      | <b>ASCC</b>           | 25 | 42.70    | 42.37 | 43.62 | 40.12     | 42.05        | 39.23         | 39.14  | 41.18  | <b>41.30</b> |
|                      |                       | 30 | 40.42    | 39.43 | 41.56 | 37.69     | 40.98        | 37.22         | 36.14  | 38.64  | <b>39.01</b> |
|                      |                       | 35 | 37.74    | 36.54 | 39.14 | 35.20     | 39.42        | 35.16         | 33.34  | 36.13  | <b>36.58</b> |
|                      |                       | 40 | 34.84    | 33.90 | 36.47 | 32.64     | 37.50        | 32.99         | 30.91  | 33.69  | <b>34.12</b> |
|                      | <b>Multiview HEVC</b> | 25 | 43.39    | 42.69 | 44.25 | 40.95     | 42.40        | 40.20         | 39.69  | 41.60  | <b>41.90</b> |
|                      |                       | 30 | 41.15    | 39.68 | 42.20 | 38.36     | 41.28        | 37.71         | 36.47  | 38.94  | <b>39.47</b> |
|                      |                       | 35 | 38.43    | 36.73 | 39.76 | 35.75     | 39.77        | 35.49         | 33.58  | 36.32  | <b>36.98</b> |
|                      |                       | 40 | 35.44    | 34.05 | 37.07 | 33.13     | 37.91        | 33.23         | 31.09  | 33.82  | <b>34.47</b> |
| <b>Random Access</b> | <b>HEVC</b>           | 25 | 43.08    | 41.67 | 43.66 | 41.44     | 42.10        | 39.83         | 38.77  | 40.12  | <b>41.33</b> |
|                      |                       | 30 | 40.96    | 38.65 | 41.47 | 39.01     | 41.16        | 37.85         | 35.88  | 37.78  | <b>39.10</b> |
|                      |                       | 35 | 38.33    | 35.79 | 38.95 | 36.43     | 39.79        | 35.82         | 33.34  | 35.66  | <b>36.76</b> |
|                      |                       | 40 | 35.49    | 33.25 | 36.27 | 33.84     | 38.07        | 33.73         | 31.05  | 33.53  | <b>34.40</b> |
|                      | <b>SCC</b>            | 25 | 43.04    | 41.41 | 43.53 | 41.32     | 42.10        | 39.83         | 38.84  | 40.17  | <b>41.28</b> |
|                      |                       | 30 | 40.89    | 38.36 | 41.30 | 38.90     | 41.17        | 37.85         | 35.95  | 37.75  | <b>39.02</b> |
|                      |                       | 35 | 38.24    | 35.51 | 38.76 | 36.30     | 39.79        | 35.75         | 33.35  | 35.55  | <b>36.66</b> |
|                      |                       | 40 | 35.37    | 33.07 | 36.10 | 33.67     | 38.05        | 33.58         | 31.01  | 33.41  | <b>34.28</b> |
|                      | <b>ASCC</b>           | 25 | 42.31    | 41.01 | 42.78 | 40.44     | 41.85        | 39.20         | 38.24  | 39.76  | <b>40.70</b> |
|                      |                       | 30 | 40.02    | 38.11 | 40.50 | 38.06     | 40.88        | 37.26         | 35.54  | 37.43  | <b>38.48</b> |
|                      |                       | 35 | 37.40    | 35.37 | 38.04 | 35.58     | 39.45        | 35.30         | 33.09  | 35.30  | <b>36.19</b> |
|                      |                       | 40 | 34.61    | 32.92 | 35.44 | 33.07     | 37.64        | 33.26         | 30.83  | 33.16  | <b>33.87</b> |
|                      | <b>Multiview HEVC</b> | 25 | 42.35    | 41.03 | 42.83 | 40.49     | 41.87        | 39.22         | 38.25  | 39.79  | <b>40.73</b> |
|                      |                       | 30 | 40.07    | 38.11 | 40.54 | 38.11     | 40.88        | 37.28         | 35.53  | 37.44  | <b>38.50</b> |
|                      |                       | 35 | 37.45    | 35.37 | 38.09 | 35.62     | 39.45        | 35.31         | 33.09  | 35.31  | <b>36.21</b> |
|                      |                       | 40 | 34.66    | 32.93 | 35.48 | 33.10     | 37.66        | 33.28         | 30.83  | 33.16  | <b>33.89</b> |

Table A.17. Bitrate [kbps] values for the experiment evaluating ASCC in compression of multiview video (Section 6.4.2).

|                      | Encoder               | QP | Balloons | Shark | Kendo | Newspaper | Poznan_Hall2 | Poznan_Street | Dancer | GT_Fly | average      |
|----------------------|-----------------------|----|----------|-------|-------|-----------|--------------|---------------|--------|--------|--------------|
| <b>All Intra</b>     | <b>HEVC</b>           | 25 | 16662    | 54222 | 10780 | 26113     | 16978        | 65074         | 104764 | 55531  | <b>43765</b> |
|                      |                       | 30 | 10420    | 30623 | 6629  | 14820     | 8635         | 32526         | 54049  | 29010  | <b>23339</b> |
|                      |                       | 35 | 6418     | 16033 | 4050  | 8381      | 4616         | 16678         | 24675  | 14321  | <b>11896</b> |
|                      |                       | 40 | 4011     | 8000  | 2538  | 4890      | 2588         | 8998          | 10379  | 6843   | <b>6031</b>  |
|                      | <b>SCC</b>            | 25 | 12594    | 27959 | 8588  | 21205     | 15310        | 56125         | 60370  | 29744  | <b>28987</b> |
|                      |                       | 30 | 7106     | 14131 | 4834  | 10705     | 6746         | 23378         | 28367  | 14537  | <b>13726</b> |
|                      |                       | 35 | 4052     | 6770  | 2742  | 5545      | 3350         | 10362         | 11989  | 6660   | <b>6434</b>  |
|                      |                       | 40 | 2389     | 3197  | 1627  | 3012      | 1841         | 4956          | 5128   | 2996   | <b>3143</b>  |
|                      | <b>ASCC</b>           | 25 | 8154     | 20780 | 5376  | 12799     | 8168         | 28069         | 40730  | 21317  | <b>18174</b> |
|                      |                       | 30 | 4763     | 11316 | 3077  | 6772      | 4024         | 12914         | 20424  | 10767  | <b>9257</b>  |
|                      |                       | 35 | 2801     | 5712  | 1803  | 3726      | 2097         | 6389          | 9357   | 5245   | <b>4641</b>  |
|                      |                       | 40 | 1688     | 2756  | 1090  | 2129      | 1153         | 3387          | 4037   | 2509   | <b>2343</b>  |
|                      | <b>Multiview HEVC</b> | 25 | 9508     | 22273 | 6318  | 15440     | 10193        | 37110         | 45658  | 23906  | <b>21301</b> |
|                      |                       | 30 | 5468     | 12007 | 3539  | 7945      | 4698         | 15283         | 22292  | 11831  | <b>10383</b> |
|                      |                       | 35 | 3214     | 6062  | 2062  | 4285      | 2460         | 7288          | 10159  | 5655   | <b>5148</b>  |
|                      |                       | 40 | 1940     | 2943  | 1254  | 2441      | 1359         | 3789          | 4407   | 2706   | <b>2605</b>  |
| <b>Random Access</b> | <b>HEVC</b>           | 25 | 2209     | 10391 | 2076  | 2426      | 2373         | 7265          | 13833  | 10425  | <b>6375</b>  |
|                      |                       | 30 | 1219     | 5269  | 1125  | 1287      | 1004         | 2837          | 5961   | 4450   | <b>2894</b>  |
|                      |                       | 35 | 702      | 2645  | 647   | 708       | 517          | 1349          | 2707   | 2078   | <b>1419</b>  |
|                      |                       | 40 | 422      | 1300  | 391   | 410       | 287          | 700           | 1251   | 999    | <b>720</b>   |
|                      | <b>SCC</b>            | 25 | 1963     | 6482  | 1897  | 2128      | 2278         | 6901          | 10078  | 7258   | <b>4873</b>  |
|                      |                       | 30 | 1003     | 2978  | 958   | 1026      | 893          | 2371          | 4037   | 3008   | <b>2034</b>  |
|                      |                       | 35 | 548      | 1404  | 520   | 525       | 436          | 1009          | 1721   | 1356   | <b>940</b>   |
|                      |                       | 40 | 317      | 689   | 302   | 288       | 234          | 481           | 789    | 660    | <b>470</b>   |
|                      | <b>ASCC</b>           | 25 | 1362     | 4582  | 1314  | 1418      | 1376         | 3957          | 6677   | 4994   | <b>3210</b>  |
|                      |                       | 30 | 706      | 2244  | 667   | 699       | 579          | 1408          | 2796   | 2105   | <b>1400</b>  |
|                      |                       | 35 | 395      | 1103  | 372   | 375       | 301          | 642           | 1281   | 977    | <b>681</b>   |
|                      |                       | 40 | 226      | 532   | 215   | 211       | 166          | 323           | 609    | 471    | <b>344</b>   |
|                      | <b>Multiview HEVC</b> | 25 | 1368     | 4592  | 1319  | 1421      | 1381         | 3946          | 6640   | 5003   | <b>3209</b>  |
|                      |                       | 30 | 710      | 2249  | 670   | 702       | 582          | 1409          | 2789   | 2112   | <b>1403</b>  |
|                      |                       | 35 | 399      | 1108  | 375   | 378       | 304          | 645           | 1284   | 983    | <b>684</b>   |
|                      |                       | 40 | 229      | 536   | 218   | 214       | 170          | 326           | 611    | 474    | <b>347</b>   |

Table A.18. Encoding time [s] values for the experiment evaluating ASCC in compression of multiview video (Section 6.4.2).

|               | Encoder        | QP | Balloons | Shark | Kendo | Newspaper | Poznan_Hall2 | Poznan_Street | Dancer | GT_Fly | average      |
|---------------|----------------|----|----------|-------|-------|-----------|--------------|---------------|--------|--------|--------------|
| All Intra     | HEVC           | 25 | 4526     | 12083 | 4277  | 5002      | 10593        | 13259         | 14047  | 12277  | <b>9508</b>  |
|               |                | 30 | 4210     | 11170 | 4132  | 4443      | 10240        | 11344         | 12310  | 11008  | <b>8607</b>  |
|               |                | 35 | 3786     | 10088 | 3642  | 4120      | 9742         | 10218         | 10853  | 10111  | <b>7820</b>  |
|               |                | 40 | 3774     | 9498  | 3641  | 3802      | 9260         | 10129         | 10066  | 9543   | <b>7464</b>  |
|               | SCC            | 25 | 18491    | 43969 | 14727 | 25417     | 23865        | 62212         | 81485  | 39415  | <b>38698</b> |
|               |                | 30 | 14445    | 29217 | 11820 | 17835     | 16588        | 39359         | 61752  | 29648  | <b>27583</b> |
|               |                | 35 | 11155    | 21613 | 10030 | 13135     | 14483        | 24314         | 37925  | 20479  | <b>19142</b> |
|               |                | 40 | 8641     | 15916 | 8607  | 9665      | 12135        | 16721         | 30617  | 14133  | <b>14554</b> |
|               | ASCC           | 25 | 15523    | 17924 | 14233 | 17437     | 19081        | 29521         | 22295  | 15339  | <b>18919</b> |
|               |                | 30 | 11694    | 14551 | 11362 | 12886     | 13870        | 18192         | 16161  | 11831  | <b>13818</b> |
|               |                | 35 | 8718     | 11789 | 8386  | 8922      | 10125        | 13160         | 13534  | 9924   | <b>10570</b> |
|               |                | 40 | 6476     | 10893 | 6483  | 6897      | 8216         | 10592         | 11312  | 8363   | <b>8654</b>  |
|               | Multiview HEVC | 25 | 14961    | 17890 | 14282 | 16945     | 20237        | 33479         | 24286  | 16093  | <b>19772</b> |
|               |                | 30 | 11410    | 14761 | 11089 | 13092     | 14371        | 21639         | 17684  | 12012  | <b>14507</b> |
|               |                | 35 | 9195     | 12371 | 8875  | 9664      | 10420        | 14924         | 13963  | 9857   | <b>11159</b> |
|               |                | 40 | 7036     | 11101 | 7040  | 7704      | 7646         | 11804         | 11464  | 8978   | <b>9097</b>  |
| Random Access | HEVC           | 25 | 9502     | 27869 | 9436  | 7089      | 17351        | 18395         | 24685  | 28859  | <b>17898</b> |
|               |                | 30 | 7722     | 22826 | 7933  | 6288      | 14765        | 14204         | 19938  | 21248  | <b>14366</b> |
|               |                | 35 | 6444     | 18589 | 6810  | 5594      | 13411        | 13102         | 16897  | 17833  | <b>12335</b> |
|               |                | 40 | 5790     | 16565 | 6257  | 5222      | 12760        | 12400         | 15251  | 15062  | <b>11163</b> |
|               | SCC            | 25 | 29092    | 72791 | 26395 | 23422     | 35499        | 46779         | 75575  | 68570  | <b>47265</b> |
|               |                | 30 | 21933    | 56102 | 18991 | 18467     | 26441        | 36431         | 59128  | 53902  | <b>36424</b> |
|               |                | 35 | 17785    | 38555 | 14269 | 15574     | 23112        | 29613         | 44991  | 42820  | <b>28340</b> |
|               |                | 40 | 15411    | 30665 | 11853 | 13547     | 19728        | 28009         | 36396  | 35678  | <b>23911</b> |
|               | ASCC           | 25 | 13905    | 34794 | 14319 | 11131     | 17047        | 22235         | 29536  | 28310  | <b>21410</b> |
|               |                | 30 | 11303    | 28407 | 11761 | 9345      | 14328        | 17502         | 23217  | 22486  | <b>17294</b> |
|               |                | 35 | 9450     | 24326 | 10024 | 8147      | 13398        | 16398         | 19250  | 19805  | <b>15100</b> |
|               |                | 40 | 8233     | 21956 | 8913  | 7680      | 12205        | 15145         | 18036  | 17313  | <b>13685</b> |
|               | Multiview HEVC | 25 | 13757    | 33077 | 14276 | 11059     | 17162        | 22183         | 28630  | 29970  | <b>21264</b> |
|               |                | 30 | 11409    | 29961 | 11407 | 9247      | 14646        | 17978         | 23100  | 23444  | <b>17649</b> |
|               |                | 35 | 9948     | 25034 | 10083 | 8237      | 13060        | 16107         | 20614  | 19779  | <b>15358</b> |
|               |                | 40 | 8261     | 21383 | 8745  | 7710      | 12392        | 14022         | 16866  | 16474  | <b>13232</b> |



Table A.19. PSNR [dB] values for the experiment evaluating ASCC in compression of screen content video (Section 6.4.3).

| Encoder             | QP | All Intra |       | Random Access |       |
|---------------------|----|-----------|-------|---------------|-------|
|                     |    | SCC       | ASCC  | SCC           | ASCC  |
| ChineseEditing      | 25 | 47.10     | 47.17 | 48.23         | 48.39 |
|                     | 30 | 42.95     | 43.08 | 44.08         | 44.24 |
|                     | 35 | 38.59     | 38.75 | 39.72         | 39.94 |
|                     | 40 | 33.98     | 34.22 | 35.17         | 35.42 |
| MissionControlClip3 | 25 | 47.00     | 47.01 | 47.45         | 47.47 |
|                     | 30 | 43.19     | 43.20 | 43.89         | 43.91 |
|                     | 35 | 39.22     | 39.23 | 40.14         | 40.17 |
|                     | 40 | 35.12     | 35.16 | 36.22         | 36.24 |
| sc_console          | 25 | 54.98     | 55.11 | 54.44         | 54.54 |
|                     | 30 | 49.89     | 49.96 | 49.07         | 49.13 |
|                     | 35 | 44.60     | 44.72 | 43.54         | 43.67 |
|                     | 40 | 38.69     | 39.10 | 38.05         | 38.28 |
| sc_desktop          | 25 | 51.44     | 51.73 | 52.71         | 52.98 |
|                     | 30 | 47.06     | 47.20 | 48.30         | 48.51 |
|                     | 35 | 42.09     | 42.26 | 43.50         | 43.78 |
|                     | 40 | 37.00     | 37.17 | 38.23         | 38.46 |
| sc_flyingGraphics   | 25 | 49.01     | 48.83 | 44.56         | 44.51 |
|                     | 30 | 44.22     | 44.10 | 39.48         | 39.45 |
|                     | 35 | 39.50     | 39.49 | 35.07         | 35.07 |
|                     | 40 | 34.87     | 34.92 | 31.35         | 31.38 |
| sc_map              | 25 | 47.72     | 47.71 | 48.64         | 48.68 |
|                     | 30 | 43.01     | 43.02 | 43.95         | 44.02 |
|                     | 35 | 38.58     | 38.63 | 39.39         | 39.47 |
|                     | 40 | 34.78     | 34.81 | 35.49         | 35.55 |
| sc_programming      | 25 | 48.47     | 48.51 | 47.98         | 48.00 |
|                     | 30 | 44.41     | 44.47 | 43.66         | 43.70 |
|                     | 35 | 40.26     | 40.32 | 39.51         | 39.55 |
|                     | 40 | 35.93     | 36.03 | 35.74         | 35.81 |
| sc_robot            | 25 | 42.52     | 42.52 | 40.96         | 40.96 |
|                     | 30 | 38.62     | 38.62 | 37.70         | 37.70 |
|                     | 35 | 35.62     | 35.62 | 35.14         | 35.14 |
|                     | 40 | 33.14     | 33.15 | 32.97         | 32.97 |
| sc_web_browsing     | 25 | 50.95     | 51.22 | 52.03         | 52.27 |
|                     | 30 | 46.52     | 46.62 | 47.59         | 47.86 |
|                     | 35 | 41.89     | 41.95 | 43.24         | 43.45 |
|                     | 40 | 37.03     | 37.17 | 38.38         | 38.56 |
| Basketball_Screen   | 25 | 46.41     | 46.40 | 46.64         | 46.66 |
|                     | 30 | 42.84     | 42.86 | 43.33         | 43.36 |
|                     | 35 | 39.18     | 39.20 | 39.88         | 39.91 |
|                     | 40 | 35.42     | 35.44 | 36.28         | 36.35 |
| ChinaSpeed          | 25 | 45.21     | 45.22 | 42.74         | 42.74 |
|                     | 30 | 41.37     | 41.37 | 38.96         | 38.95 |
|                     | 35 | 37.75     | 37.76 | 35.41         | 35.41 |
|                     | 40 | 34.33     | 34.33 | 32.32         | 32.33 |
| MissionControlClip2 | 25 | 46.22     | 46.20 | 46.36         | 46.36 |
|                     | 30 | 42.85     | 42.84 | 43.06         | 43.05 |
|                     | 35 | 39.44     | 39.42 | 39.71         | 39.71 |
|                     | 40 | 35.97     | 35.97 | 36.52         | 36.56 |
| SlideShow           | 25 | 50.97     | 50.96 | 50.31         | 50.33 |
|                     | 30 | 47.39     | 47.38 | 46.63         | 46.63 |
|                     | 35 | 43.85     | 43.83 | 43.08         | 43.09 |
|                     | 40 | 39.97     | 40.02 | 39.55         | 39.58 |

Table A.20.Bitrate [kbps] values for the experiment evaluating ASCC in compression of screen content video (Section 6.4.3).

| Encoder             | QP | All Intra |        | Random Access |       |
|---------------------|----|-----------|--------|---------------|-------|
|                     |    | SCC       | ASCC   | SCC           | ASCC  |
| ChineseEditing      | 25 | 112008    | 117355 | 7117          | 7487  |
|                     | 30 | 85120     | 88979  | 5419          | 5660  |
|                     | 35 | 66106     | 69394  | 4113          | 4310  |
|                     | 40 | 49926     | 52969  | 3065          | 3242  |
| MissionControlClip3 | 25 | 56212     | 57692  | 3838          | 3914  |
|                     | 30 | 39270     | 40307  | 2467          | 2521  |
|                     | 35 | 27227     | 28119  | 1628          | 1674  |
|                     | 40 | 18667     | 19555  | 1096          | 1138  |
| sc_console          | 25 | 32477     | 41177  | 5314          | 5978  |
|                     | 30 | 26265     | 30077  | 4105          | 4467  |
|                     | 35 | 21109     | 24081  | 3151          | 3407  |
|                     | 40 | 16401     | 18883  | 2441          | 2645  |
| sc_desktop          | 25 | 36047     | 42440  | 2865          | 3265  |
|                     | 30 | 28573     | 32240  | 2273          | 2480  |
|                     | 35 | 23252     | 26495  | 1864          | 2040  |
|                     | 40 | 19181     | 22374  | 1551          | 1717  |
| sc_flyingGraphics   | 25 | 58146     | 63313  | 26891         | 28452 |
|                     | 30 | 43029     | 46115  | 15769         | 16537 |
|                     | 35 | 31799     | 34625  | 9375          | 9855  |
|                     | 40 | 23246     | 26034  | 5842          | 6192  |
| sc_map              | 25 | 36522     | 37298  | 2779          | 2819  |
|                     | 30 | 24950     | 25477  | 1846          | 1878  |
|                     | 35 | 15860     | 16362  | 1161          | 1191  |
|                     | 40 | 10052     | 10391  | 720           | 742   |
| sc_programming      | 25 | 25668     | 26790  | 4067          | 4135  |
|                     | 30 | 18499     | 19326  | 2364          | 2409  |
|                     | 35 | 13690     | 14435  | 1356          | 1393  |
|                     | 40 | 10096     | 10764  | 836           | 873   |
| sc_robot            | 25 | 27780     | 27783  | 4067          | 4070  |
|                     | 30 | 13956     | 13973  | 1621          | 1621  |
|                     | 35 | 6753      | 6785   | 677           | 678   |
|                     | 40 | 3366      | 3398   | 318           | 320   |
| sc_web_browsing     | 25 | 6394      | 7200   | 369           | 415   |
|                     | 30 | 4596      | 5207   | 268           | 296   |
|                     | 35 | 3448      | 4035   | 201           | 228   |
|                     | 40 | 2638      | 3287   | 153           | 182   |
| Basketball_Screen   | 25 | 100573    | 103824 | 7705          | 7870  |
|                     | 30 | 68156     | 70545  | 4693          | 4816  |
|                     | 35 | 47387     | 49382  | 3036          | 3134  |
|                     | 40 | 33322     | 35274  | 2040          | 2128  |
| ChinaSpeed          | 25 | 19399     | 19474  | 4900          | 4909  |
|                     | 30 | 12645     | 12708  | 2496          | 2502  |
|                     | 35 | 8171      | 8231   | 1275          | 1279  |
|                     | 40 | 5252      | 5310   | 671           | 676   |
| MissionControlClip2 | 25 | 84664     | 84940  | 7972          | 7992  |
|                     | 30 | 56706     | 56890  | 4747          | 4755  |
|                     | 35 | 36662     | 36742  | 2816          | 2829  |
|                     | 40 | 23182     | 23424  | 1721          | 1741  |
| SlideShow           | 25 | 4138      | 4116   | 631           | 629   |
|                     | 30 | 2656      | 2604   | 372           | 369   |
|                     | 35 | 1744      | 1727   | 229           | 227   |
|                     | 40 | 1135      | 1143   | 149           | 149   |

Table A.21. Encoding time [s] values for the experiment evaluating ASCC in compression of screen content video (Section 6.4.3).

| Encoder             | QP | All Intra |       | Random Access |       |
|---------------------|----|-----------|-------|---------------|-------|
|                     |    | SCC       | ASCC  | SCC           | ASCC  |
| ChineseEditing      | 25 | 55785     | 62980 | 9287          | 10712 |
|                     | 30 | 51116     | 58577 | 9123          | 9955  |
|                     | 35 | 48530     | 55544 | 8096          | 9208  |
|                     | 40 | 43745     | 47907 | 7807          | 8635  |
| MissionControlClip3 | 25 | 37169     | 45036 | 14322         | 15525 |
|                     | 30 | 33742     | 40537 | 11940         | 13117 |
|                     | 35 | 28259     | 34715 | 10160         | 10788 |
|                     | 40 | 25898     | 29968 | 8582          | 9769  |
| sc_console          | 25 | 26271     | 36459 | 27086         | 31521 |
|                     | 30 | 25583     | 31907 | 25757         | 29603 |
|                     | 35 | 23542     | 31301 | 23342         | 26069 |
|                     | 40 | 21821     | 27187 | 20704         | 24273 |
| sc_desktop          | 25 | 33875     | 39601 | 11076         | 11867 |
|                     | 30 | 32097     | 40465 | 10747         | 11782 |
|                     | 35 | 30909     | 38506 | 9373          | 11177 |
|                     | 40 | 26667     | 33770 | 9038          | 10449 |
| sc_flyingGraphics   | 25 | 21177     | 25763 | 46738         | 67792 |
|                     | 30 | 19925     | 23876 | 38783         | 54058 |
|                     | 35 | 17959     | 21347 | 33632         | 40124 |
|                     | 40 | 16093     | 19133 | 27840         | 33675 |
| sc_map              | 25 | 19102     | 22423 | 5474          | 6199  |
|                     | 30 | 17085     | 20318 | 4951          | 5452  |
|                     | 35 | 15177     | 17539 | 4296          | 4766  |
|                     | 40 | 13099     | 14938 | 3610          | 3833  |
| sc_programming      | 25 | 15632     | 18492 | 13528         | 15575 |
|                     | 30 | 13907     | 15487 | 11680         | 13006 |
|                     | 35 | 13029     | 15965 | 9285          | 10583 |
|                     | 40 | 11842     | 14340 | 7948          | 8993  |
| sc_robot            | 25 | 12599     | 14157 | 13857         | 17015 |
|                     | 30 | 10374     | 11623 | 10385         | 10865 |
|                     | 35 | 8065      | 9152  | 6482          | 8432  |
|                     | 40 | 6067      | 7027  | 5573          | 6982  |
| sc_web_browsing     | 25 | 5893      | 8148  | 968           | 1083  |
|                     | 30 | 5633      | 7313  | 902           | 1070  |
|                     | 35 | 5035      | 5959  | 846           | 999   |
|                     | 40 | 4701      | 5563  | 684           | 858   |
| Basketball_Screen   | 25 | 35544     | 43427 | 12642         | 13614 |
|                     | 30 | 30693     | 38875 | 10104         | 11270 |
|                     | 35 | 27711     | 33262 | 7921          | 9096  |
|                     | 40 | 25387     | 30288 | 7146          | 7702  |
| ChinaSpeed          | 25 | 15617     | 17423 | 33372         | 45562 |
|                     | 30 | 13882     | 15464 | 26384         | 33689 |
|                     | 35 | 11058     | 13228 | 19784         | 24109 |
|                     | 40 | 10130     | 11621 | 15439         | 16471 |
| MissionControlClip2 | 25 | 33742     | 39817 | 14712         | 17158 |
|                     | 30 | 27923     | 34056 | 12746         | 14187 |
|                     | 35 | 24777     | 29968 | 11019         | 11644 |
|                     | 40 | 22373     | 25580 | 9259          | 9857  |
| SlideShow           | 25 | 7995      | 10361 | 8765          | 9769  |
|                     | 30 | 7525      | 8630  | 6109          | 8600  |
|                     | 35 | 6974      | 8686  | 5502          | 7469  |
|                     | 40 | 5968      | 7396  | 4411          | 6472  |

Table A.22. PSNR [dB] values for the experiment evaluating ASCC in compression of immersive video, part 1 of 2 (Section 6.4.4).

| Sequence           | QP | SCC   | ASCC  |   |                   |   |   |                                       |
|--------------------|----|-------|---|---|-------------------|---|---|---------------------------------------|
|                    |    |       | QPel IBC accuracy for views. FPel for depth | QPel IBC accuracy for depth. FPel for views | QPel IBC accuracy | QPel + tile-based IBC for first views atlas | QPel + tile-based IBC for all views atlases | QPel + tile-based IBC for all atlases |
| ClassroomVideo     | 25 | 34.40 | 34.40                                       | 34.40                                       | 34.40             | 34.38                                       | 34.38                                       | 34.38                                 |
|                    | 27 | 34.36 | 34.36                                       | 34.36                                       | 34.36             | 34.35                                       | 34.35                                       | 34.35                                 |
|                    | 30 | 33.41 | 33.41                                       | 33.41                                       | 33.41             | 33.39                                       | 33.38                                       | 33.38                                 |
|                    | 33 | 31.70 | 31.70                                       | 31.70                                       | 31.70             | 31.64                                       | 31.63                                       | 31.63                                 |
| TechnicolorMuseum  | 21 | 32.06 | 32.06                                       | 32.06                                       | 32.06             | 32.06                                       | 32.06                                       | 32.05                                 |
|                    | 27 | 31.49 | 31.49                                       | 31.49                                       | 31.49             | 31.49                                       | 31.49                                       | 31.49                                 |
|                    | 33 | 29.73 | 29.73                                       | 29.73                                       | 29.73             | 29.72                                       | 29.72                                       | 29.71                                 |
|                    | 37 | 27.22 | 27.21                                       | 27.22                                       | 27.21             | 27.22                                       | 27.22                                       | 27.20                                 |
| Fan                | 30 | 28.70 | 28.70                                       | 28.70                                       | 28.70             | 28.70                                       | 28.70                                       | 28.69                                 |
|                    | 38 | 28.50 | 28.50                                       | 28.50                                       | 28.50             | 28.51                                       | 28.51                                       | 28.51                                 |
|                    | 45 | 27.96 | 27.96                                       | 27.95                                       | 27.96             | 27.96                                       | 27.95                                       | 27.94                                 |
|                    | 48 | 26.70 | 26.70                                       | 26.69                                       | 26.69             | 26.68                                       | 26.67                                       | 26.65                                 |
| OrangeKitchen      | 14 | 33.28 | 33.28                                       | 33.28                                       | 33.28             | 33.29                                       | 33.28                                       | 33.28                                 |
|                    | 21 | 32.87 | 32.87                                       | 32.87                                       | 32.87             | 32.87                                       | 32.87                                       | 32.86                                 |
|                    | 27 | 31.73 | 31.73                                       | 31.72                                       | 31.72             | 31.73                                       | 31.73                                       | 31.71                                 |
|                    | 33 | 29.69 | 29.69                                       | 29.68                                       | 29.69             | 29.67                                       | 29.65                                       | 29.63                                 |
| TechnicolorPainter | 22 | 37.75 | 37.75                                       | 37.75                                       | 37.75             | 37.76                                       | 37.76                                       | 37.76                                 |
|                    | 28 | 36.94 | 36.94                                       | 36.94                                       | 36.94             | 36.93                                       | 36.93                                       | 36.93                                 |
|                    | 35 | 35.07 | 35.07                                       | 35.08                                       | 35.08             | 35.05                                       | 35.05                                       | 35.04                                 |
|                    | 44 | 31.98 | 31.97                                       | 31.98                                       | 31.97             | 31.94                                       | 31.93                                       | 31.93                                 |
| IntelFrog          | 30 | 30.86 | 30.86                                       | 30.86                                       | 30.86             | 30.84                                       | 30.84                                       | 30.84                                 |
|                    | 36 | 30.28 | 30.28                                       | 30.27                                       | 30.27             | 30.27                                       | 30.27                                       | 30.28                                 |
|                    | 43 | 29.07 | 29.07                                       | 29.07                                       | 29.06             | 29.07                                       | 29.07                                       | 29.05                                 |
|                    | 47 | 26.57 | 26.57                                       | 26.57                                       | 26.57             | 26.55                                       | 26.54                                       | 26.53                                 |
| Poznan_Carpark     | 22 | 36.34 | 36.35                                       | 36.34                                       | 36.35             | 36.36                                       | 36.36                                       | 36.35                                 |
|                    | 26 | 35.48 | 35.48                                       | 35.48                                       | 35.48             | 35.51                                       | 35.51                                       | 35.50                                 |
|                    | 32 | 33.51 | 33.52                                       | 33.51                                       | 33.51             | 33.54                                       | 33.54                                       | 33.54                                 |
|                    | 39 | 30.42 | 30.40                                       | 30.41                                       | 30.40             | 30.40                                       | 30.40                                       | 30.39                                 |
| Chess              | 11 | 36.50 | 36.50                                       | 36.49                                       | 36.50             | 36.49                                       | 36.49                                       | 36.49                                 |
|                    | 18 | 35.92 | 35.92                                       | 35.92                                       | 35.92             | 35.91                                       | 35.90                                       | 35.90                                 |
|                    | 25 | 34.49 | 34.50                                       | 34.50                                       | 34.51             | 34.50                                       | 34.49                                       | 34.47                                 |
|                    | 31 | 32.29 | 32.30                                       | 32.28                                       | 32.28             | 32.26                                       | 32.24                                       | 32.23                                 |
| Group              | 24 | 30.53 | 30.53                                       | 30.53                                       | 30.53             | 30.53                                       | 30.53                                       | 30.51                                 |
|                    | 30 | 29.81 | 29.81                                       | 29.80                                       | 29.80             | 29.80                                       | 29.80                                       | 29.76                                 |
|                    | 35 | 28.09 | 28.09                                       | 28.09                                       | 28.09             | 28.08                                       | 28.08                                       | 28.03                                 |
|                    | 40 | 26.25 | 26.24                                       | 26.24                                       | 26.23             | 26.22                                       | 26.22                                       | 26.18                                 |
| Poznan_Fencing2    | 22 | 35.14 | 35.14                                       | 35.14                                       | 35.14             | 35.13                                       | 35.12                                       | 35.12                                 |
|                    | 25 | 34.72 | 34.72                                       | 34.72                                       | 34.72             | 34.72                                       | 34.72                                       | 34.72                                 |
|                    | 32 | 33.67 | 33.68                                       | 33.67                                       | 33.68             | 33.67                                       | 33.67                                       | 33.68                                 |
|                    | 41 | 31.48 | 31.47                                       | 31.49                                       | 31.48             | 31.47                                       | 31.47                                       | 31.46                                 |
| Poznan_Hall2       | 15 | 41.02 | 41.01                                       | 41.01                                       | 41.01             | 41.01                                       | 41.01                                       | 41.02                                 |
|                    | 23 | 40.46 | 40.46                                       | 40.45                                       | 40.45             | 40.46                                       | 40.46                                       | 40.44                                 |
|                    | 31 | 39.01 | 38.99                                       | 39.00                                       | 38.98             | 39.00                                       | 38.99                                       | 38.98                                 |
|                    | 40 | 36.17 | 36.16                                       | 36.17                                       | 36.16             | 36.16                                       | 36.15                                       | 36.15                                 |
| Poznan_Street      | 20 | 36.55 | 36.55                                       | 36.55                                       | 36.55             | 36.54                                       | 36.54                                       | 36.55                                 |
|                    | 24 | 35.68 | 35.67                                       | 35.67                                       | 35.67             | 35.69                                       | 35.69                                       | 35.69                                 |
|                    | 29 | 33.90 | 33.92                                       | 33.90                                       | 33.92             | 33.91                                       | 33.91                                       | 33.91                                 |
|                    | 34 | 31.18 | 31.20                                       | 31.17                                       | 31.19             | 31.16                                       | 31.16                                       | 31.17                                 |

Table A.23. PSNR [dB] values for the experiment evaluating ASCC in compression of immersive video, part 2 of 2 (Section 6.4.4).

| Sequence          | QP | SCC   | ASCC  |   |                   |   |   |                                       |
|-------------------|----|-------|---|---|-------------------|---|---|---------------------------------------|
|                   |    |       | QPel IBC accuracy for views, FPel for depth | QPel IBC accuracy for depth, FPel for views | QPel IBC accuracy | QPel + tile-based IBC for first views atlas | QPel + tile-based IBC for all views atlases | QPel + tile-based IBC for all atlases |
| ChessPieces       | 4  | 36.47 | 36.47                                       | 36.47                                       | 36.47             | 36.47                                       | 36.47                                       | 36.46                                 |
|                   | 11 | 36.13 | 36.13                                       | 36.11                                       | 36.11             | 36.11                                       | 36.11                                       | 36.09                                 |
|                   | 18 | 34.99 | 34.99                                       | 35.04                                       | 35.04             | 35.04                                       | 35.04                                       | 35.01                                 |
|                   | 26 | 33.09 | 33.08                                       | 33.08                                       | 33.07             | 33.08                                       | 33.05                                       | 33.03                                 |
| TechnicolorHijack | 16 | 39.66 | 39.66                                       | 39.66                                       | 39.66             | 39.66                                       | 39.66                                       | 39.66                                 |
|                   | 22 | 39.04 | 39.05                                       | 39.04                                       | 39.04             | 39.04                                       | 39.03                                       | 39.01                                 |
|                   | 29 | 37.43 | 37.44                                       | 37.41                                       | 37.42             | 37.40                                       | 37.39                                       | 37.38                                 |
|                   | 38 | 34.77 | 34.77                                       | 34.77                                       | 34.77             | 34.74                                       | 34.72                                       | 34.70                                 |
| Mirror            | 25 | 30.22 | 30.22                                       | 30.22                                       | 30.22             | 30.22                                       | 30.22                                       | 30.22                                 |
|                   | 30 | 30.01 | 30.01                                       | 30.01                                       | 30.01             | 30.01                                       | 30.01                                       | 30.01                                 |
|                   | 35 | 29.39 | 29.39                                       | 29.39                                       | 29.39             | 29.40                                       | 29.40                                       | 29.40                                 |
|                   | 40 | 27.98 | 27.98                                       | 27.98                                       | 27.97             | 27.99                                       | 27.98                                       | 27.98                                 |

Table A.24. Bitrate [kbps] values for the experiment evaluating ASCC in compression of immersive video, part 1 of 2 (Section 6.4.4).

| Sequence           | QP | SCC    | ASCC  |   |                   |   |   |                                       |
|--------------------|----|--------|---|---|-------------------|---|---|---------------------------------------|
|                    |    |        | QPel IBC accuracy for views, FPel for depth | QPel IBC accuracy for depth, FPel for views | QPel IBC accuracy | QPel + tile-based IBC for first views atlas | QPel + tile-based IBC for all views atlases | QPel + tile-based IBC for all atlases |
| ClassroomVideo     | 25 | 185613 | 185624                                      | 185601                                      | 185612            | 185832                                      | 186142                                      | 186937                                |
|                    | 27 | 19563  | 19504                                       | 19530                                       | 19471             | 19478                                       | 19553                                       | 19886                                 |
|                    | 30 | 4477   | 4498  | 4462  | 4483              | 4510  | 4550  | 4765                                  |
|                    | 33 | 2194   | 2200  | 2194  | 2199              | 2202  | 2224  | 2355                                  |
| TechnicolorMuseum  | 21 | 43378  | 43225                                       | 43294                                       | 43141             | 43581                                       | 43725                                       | 44251                                 |
|                    | 27 | 19583  | 19617                                       | 19556                                       | 19591             | 19745                                       | 19815                                       | 20008                                 |
|                    | 33 | 7063   | 7110  | 7056  | 7103              | 7142  | 7196  | 7310                                  |
|                    | 37 | 2386   | 2388  | 2384  | 2386              | 2403  | 2446  | 2516                                  |
| Fan                | 30 | 157168 | 156570                                      | 157267                                      | 156669            | 157566                                      | 159508                                      | 162667                                |
|                    | 38 | 64315  | 64346                                       | 64354                                       | 64385             | 64799                                       | 65554                                       | 68060                                 |
|                    | 45 | 30687  | 30825                                       | 30740                                       | 30878             | 30996                                       | 31226                                       | 32707                                 |
|                    | 48 | 17312  | 17346                                       | 17389                                       | 17423             | 17456                                       | 17530                                       | 18214                                 |
| OrangeKitchen      | 14 | 21130  | 20152                                       | 21127                                       | 20149             | 21687                                       | 22062                                       | 22746                                 |
|                    | 21 | 9702   | 9529  | 9668  | 9495              | 10033                                       | 10174                                       | 10424                                 |
|                    | 27 | 4496   | 4550  | 4482  | 4536              | 4588  | 4671  | 4833                                  |
|                    | 33 | 2398   | 2413  | 2387  | 2401              | 2396  | 2450  | 2562                                  |
| TechnicolorPainter | 22 | 75286  | 74699                                       | 73764                                       | 73178             | 72291                                       | 72314                                       | 75150                                 |
|                    | 28 | 25897  | 25562                                       | 25338                                       | 25002             | 24710                                       | 24785                                       | 25742                                 |
|                    | 35 | 11696  | 11687                                       | 11558                                       | 11550             | 11366                                       | 11420                                       | 11886                                 |
|                    | 44 | 6390   | 6393  | 6378  | 6381              | 6300  | 6335  | 6564                                  |
| IntelFrog          | 30 | 311619 | 311276                                      | 308184                                      | 307841            | 308431                                      | 310012                                      | 315711                                |
|                    | 36 | 76344  | 76446                                       | 74892                                       | 74994             | 74812                                       | 75170                                       | 76916                                 |
|                    | 43 | 25700  | 25999                                       | 25431                                       | 25730             | 25515                                       | 25627                                       | 26429                                 |
|                    | 47 | 12098  | 12124                                       | 12053                                       | 12079             | 11872                                       | 11922                                       | 12312                                 |

Table A.25. Bitrate [kbps] values for the experiment evaluating ASCC in compression of immersive video, part 2 of 2 (Section 6.4.4).

| Sequence          | QP | SCC   | ASCC  |   |                   |   |   |                                       |
|-------------------|----|-------|---|---|-------------------|---|---|---------------------------------------|
|                   |    |       | QPel IBC accuracy for views, FPel for depth | QPel IBC accuracy for depth, FPel for views | QPel IBC accuracy | QPel + tile-based IBC for first views atlas | QPel + tile-based IBC for all views atlases | QPel + tile-based IBC for all atlases |
| Poznan_Carpark    | 22 | 77999 | 77612                                       | 76352                                       | 75965             | 75864                                       | 75980                                       | 78312                                 |
|                   | 26 | 21371 | 21359                                       | 20758                                       | 20745             | 20196                                       | 20233                                       | 20774                                 |
|                   | 32 | 8294  | 8352  | 8176  | 8234              | 7863  | 7896  | 8144                                  |
|                   | 39 | 4081  | 4091  | 4048  | 4059              | 3904  | 3931  | 4038                                  |
| Chess             | 11 | 20060 | 19305                                       | 20028                                       | 19273             | 19700                                       | 20204                                       | 20780                                 |
|                   | 18 | 8715  | 8653  | 8688  | 8625              | 8669  | 8788  | 9075                                  |
|                   | 25 | 3941  | 3947  | 3938  | 3944              | 3956  | 4005  | 4193                                  |
|                   | 31 | 2141  | 2143  | 2147  | 2149              | 2154  | 2173  | 2296                                  |
| Group             | 24 | 68574 | 68515                                       | 68532                                       | 68473             | 68396                                       | 68630                                       | 69906                                 |
|                   | 30 | 28205 | 28223                                       | 28181                                       | 28199             | 28156                                       | 28287                                       | 28712                                 |
|                   | 35 | 9972  | 9994  | 9963  | 9986              | 9988  | 10083                                       | 10354                                 |
|                   | 40 | 4425  | 4425  | 4434  | 4434              | 4441  | 4485  | 4655                                  |
| Poznan_Fencing2   | 22 | 83128 | 82837                                       | 81939                                       | 81648             | 81670                                       | 81918                                       | 83994                                 |
|                   | 25 | 20678 | 20679                                       | 20044                                       | 20045             | 20054                                       | 20182                                       | 21131                                 |
|                   | 32 | 9067  | 9091  | 8868  | 8893              | 8902  | 8967  | 9492                                  |
|                   | 41 | 4886  | 4893  | 4833  | 4839              | 4852  | 4893  | 5164                                  |
| Poznan_Hall2      | 15 | 48358 | 47633                                       | 45107                                       | 44382             | 44812                                       | 45021                                       | 49872                                 |
|                   | 23 | 22427 | 22361                                       | 20174                                       | 20108             | 20080                                       | 20151                                       | 22640                                 |
|                   | 31 | 9861  | 9871  | 9144  | 9154              | 9100  | 9141  | 10167                                 |
|                   | 40 | 5279  | 5278  | 5087  | 5086              | 5066  | 5095  | 5421                                  |
| Poznan_Street     | 20 | 67442 | 67137                                       | 65780                                       | 65476             | 64919                                       | 65000                                       | 67207                                 |
|                   | 24 | 16351 | 16285                                       | 15435                                       | 15369             | 14681                                       | 14717                                       | 15427                                 |
|                   | 29 | 5715  | 5874  | 5437  | 5595              | 5091  | 5119  | 5364                                  |
|                   | 34 | 2614  | 2688  | 2531  | 2606              | 2360  | 2382  | 2429                                  |
| ChessPieces       | 4  | 12769 | 12311                                       | 12733                                       | 12275             | 12529                                       | 12885                                       | 13428                                 |
|                   | 11 | 6322  | 6285  | 6299  | 6262              | 6303  | 6421  | 6690                                  |
|                   | 18 | 3393  | 3394  | 3389  | 3391              | 3409  | 3476  | 3643                                  |
|                   | 26 | 2073  | 2074  | 2070  | 2071              | 2080  | 2113  | 2236                                  |
| TechnicolorHijack | 16 | 27186 | 26762                                       | 27179                                       | 26754             | 27016                                       | 27492                                       | 28642                                 |
|                   | 22 | 12634 | 12611                                       | 12618                                       | 12595             | 12650                                       | 12798                                       | 13455                                 |
|                   | 29 | 6975  | 6984  | 6961  | 6971              | 6984  | 7050  | 7485                                  |
|                   | 38 | 4509  | 4512  | 4496  | 4499              | 4510  | 4531  | 4832                                  |
| Mirror            | 25 | 62769 | 61034                                       | 62662                                       | 60927             | 62669                                       | 64939                                       | 65598                                 |
|                   | 30 | 23476 | 22988                                       | 23423                                       | 22935             | 23929                                       | 24901                                       | 25216                                 |
|                   | 35 | 9305  | 9465  | 9285  | 9445              | 9762  | 9892  | 10138                                 |
|                   | 40 | 4113  | 4139  | 4110  | 4137              | 4191  | 4208  | 4367                                  |

Table A.26. Encoding time [s] values for the experiment evaluating ASCC in compression of immersive video, part 1 of 2 (Section 6.4.4).

| Sequence           | QP | SCC   | ASCC  |   |                   |   |   |                                       |
|--------------------|----|-------|---|---|-------------------|---|---|---------------------------------------|
|                    |    |       | QPel IBC accuracy for views, FPel for depth | QPel IBC accuracy for depth, FPel for views | QPel IBC accuracy | QPel + tile-based IBC for first views atlas | QPel + tile-based IBC for all views atlases | QPel + tile-based IBC for all atlases |
| ClassroomVideo     | 25 | 17290 | 18284                                       | 17314                                       | 18308             | 7418  | 5577  | 5715                                  |
|                    | 27 | 6556  | 6982  | 6577  | 7002              | 3699  | 2586  | 2732                                  |
|                    | 30 | 4228  | 4596  | 4248  | 4617              | 2916  | 1972  | 2130                                  |
|                    | 33 | 3580  | 3868  | 3599  | 3887              | 2599  | 1752  | 1913                                  |
| TechnicolorMuseum  | 21 | 5130  | 5512  | 5150  | 5531              | 3847  | 2213  | 2381                                  |
|                    | 27 | 4480  | 4909  | 4498  | 4928              | 3511  | 1996  | 2169                                  |
|                    | 33 | 4238  | 4652  | 4257  | 4671              | 3293  | 1843  | 2013                                  |
|                    | 37 | 4012  | 4417  | 4031  | 4435              | 3092  | 1702  | 1869                                  |
| Fan                | 30 | 13835 | 14452                                       | 13948                                       | 14564             | 10500                                       | 5952  | 5121                                  |
|                    | 38 | 10048 | 10525                                       | 10155                                       | 10631             | 8079  | 4821  | 3999                                  |
|                    | 45 | 7047  | 7422  | 7144  | 7519              | 6085  | 4022  | 3250                                  |
|                    | 48 | 5226  | 5544  | 5322  | 5640              | 4783  | 3450  | 2717                                  |
| OrangeKitchen      | 14 | 3751  | 4094  | 3768  | 4110              | 3365  | 2094  | 2301                                  |
|                    | 21 | 3385  | 3717  | 3402  | 3733              | 3122  | 1939  | 2141                                  |
|                    | 27 | 3102  | 3415  | 3118  | 3431              | 2948  | 1802  | 2010                                  |
|                    | 33 | 2860  | 3182  | 2876  | 3198              | 2756  | 1676  | 1884                                  |
| TechnicolorPainter | 22 | 12775 | 13852                                       | 12914                                       | 13991             | 11378                                       | 6579  | 5018                                  |
|                    | 28 | 9040  | 9967  | 9179  | 10106             | 8843  | 4804  | 3489                                  |
|                    | 35 | 7517  | 8394  | 7666  | 8544              | 7685  | 4030  | 2869                                  |
|                    | 44 | 6602  | 7417  | 6746  | 7560              | 6885  | 3502  | 2452                                  |
| IntelFrog          | 30 | 32319 | 34095                                       | 32463                                       | 34239             | 20970                                       | 12611                                       | 9754                                  |
|                    | 36 | 19712 | 20945                                       | 19812                                       | 21046             | 14791                                       | 8257  | 6069                                  |
|                    | 43 | 13491 | 14544                                       | 13628                                       | 14681             | 11491                                       | 6271  | 4540                                  |
|                    | 47 | 10217 | 11186                                       | 10365                                       | 11334             | 9417  | 5150  | 3636                                  |
| Poznan_Carpark     | 22 | 10298 | 10805                                       | 10351                                       | 10857             | 6365  | 5303  | 4604                                  |
|                    | 26 | 5447  | 5743  | 5503  | 5799              | 4136  | 3381  | 2872                                  |
|                    | 32 | 4041  | 4316  | 4103  | 4378              | 3368  | 2758  | 2349                                  |
|                    | 39 | 3374  | 3626  | 3427  | 3679              | 2929  | 2405  | 2064                                  |
| Chess              | 11 | 4244  | 4533  | 4269  | 4558              | 3849  | 2352  | 2499                                  |
|                    | 18 | 3735  | 3993  | 3759  | 4016              | 3472  | 2115  | 2260                                  |
|                    | 25 | 3397  | 3660  | 3415  | 3677              | 3214  | 1944  | 2095                                  |
|                    | 31 | 3173  | 3411  | 3196  | 3433              | 3002  | 1796  | 1948                                  |
| Group              | 24 | 7880  | 8310  | 7921  | 8351              | 5978  | 3397  | 3347                                  |
|                    | 30 | 6509  | 6921  | 6553  | 6965              | 4943  | 2838  | 2785                                  |
|                    | 35 | 5830  | 6193  | 5866  | 6229              | 4334  | 2515  | 2467                                  |
|                    | 40 | 5268  | 5655  | 5307  | 5694              | 3898  | 2236  | 2187                                  |
| Poznan_Fencing2    | 22 | 16191 | 17174                                       | 16293                                       | 17276             | 11844                                       | 7378  | 6318                                  |
|                    | 25 | 8498  | 9058  | 8583  | 9143              | 7301  | 4744  | 3857                                  |
|                    | 32 | 6363  | 6829  | 6444  | 6910              | 5782  | 3827  | 3067                                  |
|                    | 41 | 5159  | 5551  | 5241  | 5634              | 4840  | 3257  | 2567                                  |
| Poznan_Hall2       | 15 | 8772  | 9080  | 8809  | 9117              | 7455  | 5891  | 4238                                  |
|                    | 23 | 6760  | 7116  | 6726  | 7082              | 6030  | 4734  | 3439                                  |
|                    | 31 | 5371  | 5709  | 5386  | 5724              | 4960  | 3839  | 2856                                  |
|                    | 40 | 4473  | 4769  | 4536  | 4832              | 4221  | 3223  | 2455                                  |

Table A.27. Encoding time [s] values for the experiment evaluating ASCC in compression of immersive video, part 2 of 2 (Section 6.4.4).

| Sequence          | QP | SCC  | ASCC  |   |                   |   |   |                                       |
|-------------------|----|------|---|---|-------------------|---|---|---------------------------------------|
|                   |    |      | QPel IBC accuracy for views, FPel for depth | QPel IBC accuracy for depth, FPel for views | QPel IBC accuracy | QPel + tile-based IBC for first views atlas | QPel + tile-based IBC for all views atlases | QPel + tile-based IBC for all atlases |
| Poznan_Street     | 20 | 8548 | 9373  | 8563  | 9389              | 5664  | 4940  | 4300                                  |
|                   | 24 | 4820 | 5156  | 4836  | 5172              | 3723  | 3145  | 2676                                  |
|                   | 29 | 3658 | 3933  | 3679  | 3954              | 3028  | 2531  | 2193                                  |
|                   | 34 | 3065 | 3350  | 3097  | 3382              | 2641  | 2172  | 1912                                  |
| ChessPieces       | 4  | 4426 | 4784  | 4447  | 4805              | 4056  | 2319  | 2468                                  |
|                   | 11 | 3917 | 4282  | 3938  | 4303              | 3683  | 2110  | 2256                                  |
|                   | 18 | 3624 | 3967  | 3648  | 3992              | 3448  | 1960  | 2108                                  |
|                   | 26 | 3423 | 3767  | 3442  | 3786              | 3244  | 1822  | 1973                                  |
| TechnicolorHijack | 16 | 6225 | 6899  | 6291  | 6965              | 6704  | 3353  | 3129                                  |
|                   | 22 | 5326 | 5998  | 5395  | 6068              | 6037  | 2985  | 2744                                  |
|                   | 29 | 4689 | 5357  | 4752  | 5419              | 5507  | 2696  | 2458                                  |
|                   | 38 | 4238 | 4860  | 4291  | 4913              | 5082  | 2461  | 2237                                  |
| Mirror            | 25 | 8294 | 8503  | 8327  | 8536              | 7418  | 3849  | 3688                                  |
|                   | 30 | 5604 | 5700  | 5625  | 5721              | 5111  | 3012  | 2907                                  |
|                   | 35 | 4211 | 4296  | 4230  | 4314              | 3973  | 2573  | 2499                                  |
|                   | 40 | 3455 | 3534  | 3471  | 3549              | 3309  | 2250  | 2189                                  |